LONG-CHAIN BRANCHING IN ETHYLENE POLYMERIZATION USING COMBINED METALLOCENE CATALYST SYSTEMS

by

Daryoosh Beigzadeh

A thesis

presented to the University of Waterloo

in the fulfillment of the

thesis requirement for the degree of

Doctor of Philosophy

in

Chemical Engineering

Waterloo, Ontario, Canada, 2000

ABSTRACT

The development of homogeneous and supported metallocene catalysts has revolutionized the polyolefin industry. These single-site catalysts produce ethylene homo- and copolymers with properties that are different from the ones of traditional polyethylenes synthesized with free radical initiators or Ziegler-Natta catalysts. With the advent of monocyclopentadienyl metallocenes (constrained geometry catalysts, CGC), the production of polyolefins with long-chain branches became possible. These catalyst systems can produce polyethylenes with both excellent physical properties and improved melt behavior. The improved processability is believed to be the result of significant amounts of long-chain branching in the polymer.

The concept of combining two metallocene catalysts to manipulate long-chain branching (LCB) in ethylene polymerization was introduced. Using mathematical modeling the feasibility of the idea was investigated and the characteristics of an efficient system were predicted. Polymerization experiments were performed to evaluate the model predictions and to examine the effects of different reaction components on the microstructure of the synthesized polymer. Excellent agreement between experimental data and model predictions was observed. The structure of the branches in CGC polymerization systems was also investigated using a Monte-Carlo model.

The precipitation mechanism in Crystallization Analysis Fractionation (CRYSTAF) was investigated and a mechanism for the separation was proposed. Copolymer chains were simulated using a Monte-Carlo model and the precipitation was simulated according to the proposed mechanism. Good agreement between experimental

and simulated CRYSTAF curves verifies the validity of the proposed fractionation mechanism.

A general model for the polymerization of vinylic monomers with free-radical initiators was developed. In this model transfer to polymer as the source of branching with the potential of gelation was considered. The results of this simulation provided information about the distribution of branching and time variations of average molecular weights as well as amounts and molecular weights of chains with different branching contents before, during, and after gelation.

ACKNOWLEDGMENTS

The completion of this thesis is a result of contributions from many people to all of whom I am grateful.

First, I would like to thank my supervisor, Professor Joao Soares, for his invaluable and continuous guidance, direction and above all, friendship during the course of this work.

I would like to express my gratitude and appreciation to Professor Thomas Duever, my supervisor, for his support and encouragement throughout the course of my research.

My special thanks are due to Professor Archie Hamielec, my supervisor, for his mentorship and guidance. It was certainly a great privilege for me to have access to his "vast sea of knowledge".

Many thanks to my friends in the polymer group, Luigi, Jung Dae, William, Deborah, Catherine, Loui, Karen, Leonardo, Gifford, and particularly Colin for their continuous support and friendship.

I would also like to thank the technical staff of the Department of Chemical Engineering particularly Mr. Bert Habicher, Mr. Tim Campbell, and Mr. Rick Hecktus for providing technical support in setting up of my reactor system and also Ms. Jan Venne for helping me with NMR analysis.

I would like to express my special appreciation to my parents for their encouragement and support during my entire academic life.

Finally, and most importantly, I would like to thank my wife, Afrooz, for her never-ending love and patience throughout the months of computer work, experimentation and writing, and to our son, Keon, whose arrival provided the inspiration to complete the final details of this work.

To My Wife, Afrooz

TABLE OF CONTENTS

LIST OF TABLES

LIST OF FIGURES

Chapter 1

Introduction

1-1- Background

In spite of the simple structure of ethylene, the field of polyethylene production is a complex one with a very wide range of resin types and many different manufacturing processes. From a comparatively late start (in the 60's), polyethylene production has increased rapidly to make polyethylene the major tonnage plastics material world-wide.

With the application of metallocene catalysts for polymerization, the production of polyethylene experienced a revolution. Particularly, the advent of Constrained Geometry Catalyst (CGC) systems (monocyclopentadienyl metallocene catalysts) promises to have a remarkable impact on olefin polymerization. In general, a narrow molecular weight and comonomer distribution (in the case of copolymerization with α-olefins) would be expected to improve physical properties at the expense of processability. However, using CGC systems, polyethylenes with both excellent physical

properties and improved processability can be synthesized. This attractive behavior is due to the formation of long chain branches (LCB) during the polymerization of ethylene with CGC.

Lai et al. (1993, 1997) were the first to employ CGC to incorporate macromonomers, formed in-situ, into the polymer backbone and synthesize polyethylenes with long-chain branches. These macromonomers are dead polymer chains with terminal double bonds formed via β-hydride elimination reaction. The presence of long-chain branching in polyethylene samples, synthesized by this catalyst system, has also been reported in the literature by other research groups.

CGC systems have also been used to copolymerize ethylene with linear and branched α-olefins. Generally in CGC polymerization systems ethylene has reactivity ratios with α-olefins that are sufficiently low to obtain substantial incorporation of α-olefins.

1-2- Research Objectives

Although in CGC polymerization systems the existence of long-chain branching is evident, the branching level is somehow limited and higher branching degrees can not be achieved, as shown in the literature. The objective of this research was to seek ways to obtain higher degrees of LCB and control the molecular weight, polydispersity index, and cumulative copolymer composition (in the case of copolymerization with α-olefins) of ethylene/α-olefin copolymers made with metallocene catalysts.

In this investigation a novel technique for the control of long-chain branching is proposed. The feasibility of the proposed technique was first demonstrated with

mathematical modeling. Based on the simulation results, polymerization experiments were designed and performed. The synthesized polymers were then analyzed with ^{13}C-NMR and GPC for their LCB degree, molecular weight distribution (MWD), and comonomer content.

1-3- Thesis Outline

Chapter 1 provides background information on long-chain branching in olefin polymerization using metallocene catalysts.

Chapter 2 reviews the literature on long-chain branching for polyolefins . Then, based on the information gathered, a technique for controlling long-chain branching in polyethylenes made with metallocene catalysts has been proposed.

Chapter 3 investigates the feasibility and versatility of the proposed technique using mathematical modeling. In this chapter mechanisms for olefin homo- and copolymerization and LCB formation have been proposed. Based on the proposed polymerization mechanism, a mathematical model has been developed and the effects of different catalysts systems and process conditions on polymer microstructure have been investigated.

Chapter 4 discusses the techniques employed to characterize the synthesized polymer samples. This chapter explains how carbon-13 nuclear magnetic resonance spectroscopy (^{13}C-NMR) can be used to estimate LCB degree of homopolyethylene and to determine comonomer content of ethylene/α-olefin copolymer samples. Gel permeation chromatography (GPC) is another characterization technique described in this chapter. This instrument is used to determine molecular weight distribution of polymer

samples. It has also been explained how LCB degree can be estimated using multi-detector GPC instruments.

Chapter 5 evaluates the proposed technique for controlling long-chain branching and the predictions made by mathematical modeling in a set of carefully designed polymerization experiments. It first describes the experimental methods for polymerization and polymer characterization. Then homopolymerization of ethylene with combined catalyst systems is investigated. Next, the effects of cocatalyst type and amount on chain microstructure have been investigated. Copolymerization of ethylene with other α-olefins is also performed to gain more information about ethylene homopolymerization and also to estimate polymerization kinetic constants.

Chapter 6 is devoted to the investigation of the fractionation mechanism in crystallization analysis fractionation (CRYSTAF). In this chapter a mechanism for polymer precipitation in CRYSTAF has been proposed. Based on the considered mechanism a Monte Carlo model was developed to simulate CRYSTAF curves. Conclusions on the accuracy of the proposed fractionation mechanism were made based on the agreement between simulated and actual CRYSTAF curves.

Chapter 7 presents the most significant contributions of this research and makes some recommendations for future work.

Appendices A-D provide supplementary information for the subjects discussed in Chapters 1-7. Appendix E presents a general model for the polymerization of vinylic monomers using free-radical initiator with transfer to polymer and the potential of gelation. This model looks at some chain structures that are not possible to characterize experimentally.

Chapter 2

Literature Review and Research Objectives

2-1- Literature Review

The development of homogeneous and supported single-site catalysts is one of the most exciting areas in the polyolefin industry. These single-site catalysts produce ethylene/α-olefin copolymers with properties that are different from the ones of traditional linear low-density polyethylene (LLDPE) and low-density polyethylene (LDPE) synthesized with Ziegler-Natta catalysts and free radical initiators, respectively. With the aid of constrained geometry catalyst (CGC) systems, production of ethylene/α-olefin copolymers, and ethylene polymers having long-chain branches (LCB) has become possible. Unlike conventional metallocene catalysts, the active site (the metal) in CGC catalysts is attached to only one cyclopentadienyl ring (Figure 2-1), resulting in less steric

hindrance, which makes it possible for bulky monomers to incorporate into the polymer backbone.

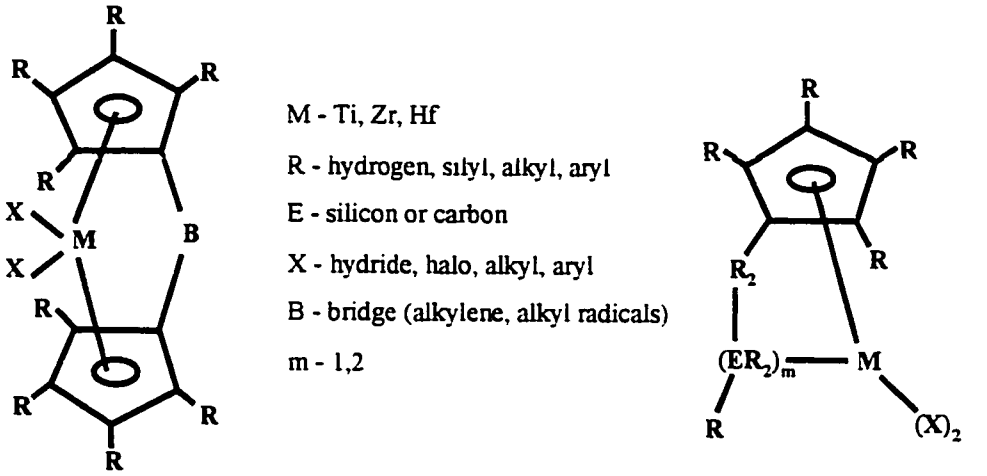

Figure 2-1- Schematic of the structures of CGC and conventional metallocene catalysts.

These catalyst systems can produce polyethylenes with both excellent physical properties and improved melt behavior. The improved processability is believed to be the result of significant amounts of long-chain branching in the polymer.

Chum et al. (1995) investigated the effect of long-chain branching on physical and rheological properties of different polyolefin thermoplastics and elastomers synthesized with CGC. They showed that by increasing LCB per 10000 carbon atoms from 0.07 to 2.56 (for polyolefin thermoplastics) the I_{10}/I_2 ratio (the melt index ratio using 10 and 2.16 kg weights, respectively) increased from 6.9 to 12.3, while the Young's modulus and tensile strength remained almost constant. This indicates that long-chain branching improves processability without sacrificing physical properties.

Lai et al. (1993, 1997) were the first to use a CGC system to synthesize polyethylenes with long-chain branches (LCB). They named their product "Substantially Linear Olefin Polymer". The polymerization reaction was carried out in a CSTR operated at steady-state at a pressure of about 490 psig and temperatures in the range of 140 to 200 °C. They used an aliphatic solvent in a solution polymerization process in order to maximize the degree of long-chain branching. A suitable cocatalyst specified by these researchers is tris(pentafluorophenyl)borane. According to the information provided in their patent, the homopolyethylene synthesized under the mentioned polymerization conditions had long-chain branching frequencies in the range of 0.01 to 3 LCB's per 1000 carbon atoms (especially from about 0.3 to 1 LCB per 1000 carbon atoms), measured by ^{13}C-NMR using the methodology proposed by Randall (1989).

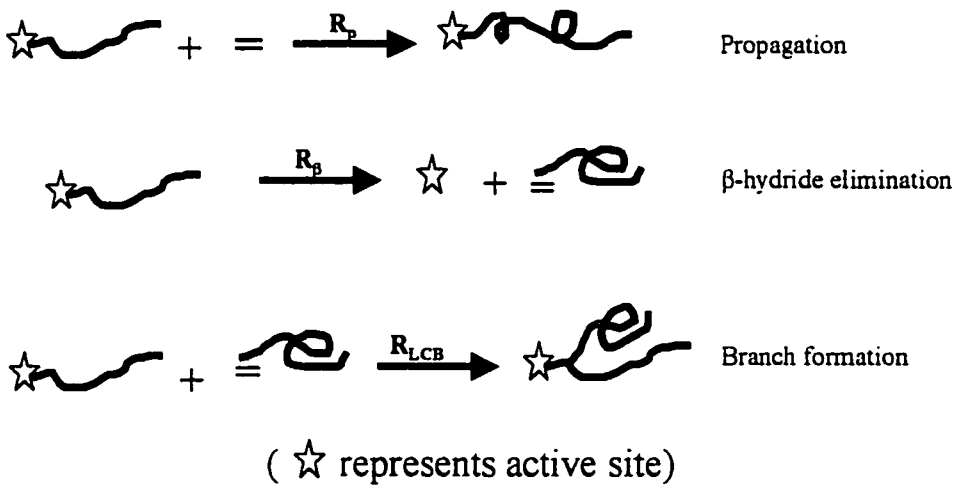

Figure 2-2- Schematic of the polymerization mechanism for CGC systems.

They proposed that the formation of macromonomers (dead polymer chains with terminal double bonds) via facile b-hydride elimination and reinsertion of these

macromonomers into the polymer backbone is the main mechanism for the formation of long chain branches. (Figure 2-2). Lai et al. (1993, 1997) also presented some interesting data on the properties of their polymer. Superior physical and mechanical properties and, at the same time, remarkable processability (shear thinning, delayed melt fracture) are properties that had not been observed before in polyethylenes produced by classical Ziegler-Natta catalysts or even by other metallocene catalyst systems. These outstanding characteristics were attributed to LCB in these polymers.

Knight and Lai (1993) also compared the ability of CGC to incorporate higher α-olefins with conventional Ziegler-Natta catalysts. They showed that higher α-olefins would have much higher reactivity ratios when they were polymerized with CGC systems.

Swogger and Kao (1993) used the catalyst system and polymerization procedure recommended by Lai et al. (1993, 1997) to synthesize four homopolyethylenes with LCB frequencies of 0.2, 0.44, 0.53 and 0.66 LCB per polymer molecule as measured by ^{13}C-NMR and GPC. They developed a mathematical model for a CSTR which predicted long-chain branching frequencies, density of ethylene-1-octene copolymers, melt index, and finally I_{10}/I_2 ratios. Unfortunately very little detail was given about the mathematical model.

Sugawara (1994) prepared a calibration curve to relate the branching degree to CSTR operating conditions using the data obtained by Lai et al. (1993). Based on this calibration curve, two polymers with very low and moderate levels of LCB were produced. These polymers were compared with a conventional LLDPE (made by Ziegler-Natta catalyst system) and a high pressure LDPE in terms of impact strength,

processability, blown film processability, stability, and MD/TD (machine direction/transverse direction) balance of tear strength. Based on these tests, Sugawara provided a summary of properties which shows the position of metallocene copolymers of ethylene-α-olefins in the balance of strength versus processability.

Brant et al. (1995) used CGC systems to copolymerize ethylene with branched α-olefins. They used different branched α-olefins containing up to 30 carbon atoms (preferably 8 to 12 carbon atoms). They found that ethylene had reactivity ratios with α-olefins which were sufficiently low to obtain substantial incorporation of α-olefins when these catalyst systems were employed. The polymerization was carried out in a 1-liter autoclave reactor (semibatch operation) at 80 °C and at constant pressure of ethylene. The resulting copolymer had 1 to 5 mole percent of branched α-olefins with a substantially uniform copolymer composition with CDBI (composition distribution breadth index) of about 50 percent. This means that 50% or more of the copolymer chains had an α-olefin content within 50 percent (molar) of the mean copolymer composition. This is in contrast to LLDPE prepared using conventional Ziegler-Natta catalysts, where CDBI's are on the order of 30 to 40 percent. The copolymers made with CGC had weight average molecular weights in the range of 80,000 to 500,000 and polydispersity indices of 2 to 4.

Brant and Canich (1995) also copolymerized ethylene with higher linear α-olefins with CGC systems. The employed α-olefins had 10 to 100 carbon atoms (preferably 12 to 30 carbon atoms). Despite the large molecular dimensions of higher α-olefins, they had polymerization rates high enough to be sufficiently incorporated in the copolymer chain. The polymerization was carried out in a 1-liter autoclave reactor in semibatch operation at 80 °C and at constant pressure of ethylene. The resulting copolymer had 1 to 50 mole

percent (preferably 4 to 30 mole percent) of higher α-olefins with a substantially uniform copolymer composition with CDBI of about 70 percent. These copolymers had weight average molecular weights in the range of 30,000 to 1,000,000 and polydispersity indices of 2 to 4, even for copolymers of very high molecular weight.

Shiono et al. (1995, 1997) compared the capability of a titanium-based CGC (CGC-Ti) with other metallocene systems in copolymerizing ethylene with polypropylene macromonomers (polypropylene chains with number average molecular weight of $M_n \approx 710$ and terminal double bond generated via β-hydride elimination). They used zirconocene/MAO systems in a batch operation to synthesize atactic polypropylene macromonomers (PPM). The polymerization was carried out at room temperature for 12 hours. They copolymerized ethylene with the synthesized PPM in a semi-batch reactor under atmospheric pressure of ethylene at 40 °C using four different metallocene catalyst systems including CGC-Ti. They used methylaluminoxane (MAO) as cocatalyst for all of the employed catalyst systems. The synthesized polymers were analyzed by proton nuclear magnetic resonance spectroscopy (^{1}H-NMR), ^{13}C-NMR, GPC, and differential scanning calorimetry (DSC). It was found that the addition of PPM to the CGC-Ti catalyst system caused a marked increase in catalytic activity, whereas the activities of other metallocene catalysts decreased by addition of PPM. They found that the ability of incorporating PPM into the copolymer, as measured by ^{13}C-NMR and ^{1}H-NMR, increased in the following order:

$$Cp_2ZrCl_2 << Cp_2TiCl_2 < Et[IndH_4]ZrCl_2 << \text{CGC-Ti}$$

where:

Cp_2ZrCl_2	bis(cyclopentadienyl)zirconium dichloride
Cp_2TiCl_2	bis(cyclopentadienyl)titanium dichloride
$Et[IndH_4]ZrCl_2$	ethylenebis(tetrahydroindenyl)zirconium dichloride
CGC-Ti	(t-butylamido)dimethyl(tetramethyl-η^5-cyclopentadienyl)zirconium

This was in good agreement with what they observed for melting points of the polymers measured by DSC.

Soga et al. (1996) copolymerized ethylene and oligoethylene (low-molecular weight polyethylene) having terminal double bonds with a titanium-based CGC (CGC-Ti). They used MAO and $(C_6H_5)_3C{\cdot}B(C_6F_5)_4$ as cocatlaysts. The oligoethylene macromonomers were synthesized with Cp_2ZrCl_2/MAO. Significant amount of long-side-chain oligoethylene in the synthesized polyethylene samples was observed from the ^{13}C-NMR analysis.

Malmberg et al. (1998) studied the polymerization of ethylene using homogeneous $Et[Ind]_2ZrCl_2$/MAO and $Et[IndH_4]_2ZrCl_2$/MAO in a slurry process. They analyzed the synthesized samples with ^{13}C-NMR and reported the existence of long-chain branches. They also performed some rheological tests and observed improved melt behavior in long-chain branched samples as compared to linear ones. Unfortunately no information was reported in their paper on the long-chain branching degrees of the synthesized samples.

Wang et al. (1999a) employed CGC-Ti to copolymerize ethylene with1-octene. They used a CSTR at 140 °C and 500 psi operating at steady-state with a mean residence time of 4 minutes. The samples were analyzed with ^{13}C-NMR for their comonomer

content. They observed that CGC had a significantly higher reactivity ratio for incorporating 1-octene as compared to other conventional metallocene catalysts. They also used the same reactor system to study the LCB formation in ethylene polymerization using a combined CGC-Ti/Cp_2ZrCl_2 catalyst system (Wang et al. 1999b). They investigated the effect of catalyst and cocatalyst types and ratios on activity, molecular weight distribution, and on long-chain branching degree. They reported lower branching degrees for the samples synthesized with the combined catalyst as compared to the ones synthesized with CGC alone.

Soares and Hamielec (1996) proposed a comprehensive model for the polymerization of ethylene/α-olefins with long-chain branch formation using metallocenes. They obtained an analytical solution for the chain length distribution of the populations containing different number of long-chain branches per molecule for a CSTR operating at steady-state. Their model was developed based on a kinetic model involving propagation, long-chain branch formation, transfer to chain transfer agent, and β-hydride elimination. They showed that the distribution of chain length for populations containing n LCB/chain could be represented by the general expression:

$$P_{r,n} = \frac{1}{(n+1)\prod_{i=0}^{n-1}(n-i)^2} A^{r-1-n} B^n P_{1,0}^{n+1} r^{2n} \qquad (2\text{-}1)$$

and that the frequency distribution of chain length for polymer populations with n long chain branches per chain is as follows:

$$f(r,n) = \frac{1}{(2n)!} r^{2n} \tau^{2n+1} \exp(-\tau r) \qquad (2\text{-}2)$$

where, A and B in Equation (2-1) are lumped kinetic parameters, r represents chain length and τ is given by:

$$\tau = \frac{R_\beta}{R_p} + \frac{R_{CTA}}{R_p} + \frac{R_{LCB}}{R_p} \tag{2-3}$$

where R_β is the rate of β-hydride elimination, R_p is the rate of monomer propagation, R_{CTA} is the rate of transfer to chain transfer agent, and R_{LCB} is the rate of macromonomer propagation or long-chain branch formation.

They also presented an analytical expression for the weight distribution of copolymer composition with chain length r, and n long-chain branches per chain:

$$w(r,y,n)drdy = \frac{1}{(2n+1)!} r^{2n+1} \tau^{2n+2} \exp(-r\tau)dr \times \frac{1}{\sqrt{2\pi\beta/r}} \exp\left(-\frac{y^2 r}{2\beta}\right)dy \tag{2-4}$$

where y is the deviation from the average mole fraction of monomer type 1 in the copolymer, F_1, and:

$$\beta = F_1(1-F_1)K \tag{2-5}$$

$$K = [1 + 4F_1(1-F_1)(r_1 r_2 - 1)]^{0.5} \tag{2-6}$$

and r_1 and r_2 are reactivity ratios for copolymerization.

Zhu and Li (1997) attempted to model the polymerization of ethylene using combined CGC and a conventional metallocene catalyst. They assumed that all macromonomers are generated only by the second catalyst and that only CGC could incorporate these macromonomers. They presented an analytical expression for the distribution of branched polymer chains synthesized with the combined catalyst system:

$$\phi_{r,m,2} = (-1)^m (a_2 - \lambda_2)\left[\frac{a_1\lambda_2}{(a_1 - a_2)^2}\right]^m [f_m(r)\exp(-a_2 r) - g_m(r)\exp(-a_1 r)] \tag{2-7}$$

where $\phi_{r,\,m,\,2}$ is the mole fraction of active site 2 (CGC active sites) with chain length r and m number of branches, a_1 and a_2 are the ratios of the rates of consumption of active sites (transfer, deactivation etc.) to the propagation rate for catalysts type 1 and 2, respectively. The parameter λ_i is the ratio of LCB formation to the propagation rate for catalyst type i and

$$f_m(r) = \sum_{n=0}^{m} \frac{(m-1+n)!\left[(a_1 - a_2)r\right]^{m-n}}{n!(m-1)!(m-n)!} \tag{2-8}$$

$$g_m(r) = \sum_{n=0}^{m-1} \frac{(m+n)!\left[(a_1 - a_2)r\right]^{m-n-1}}{n!m!(m-n-1)!} \tag{2-9}$$

However, their analytical expression is applicable only to the branched chains and no information was given about the distribution of unreacted linear macromonomers (formed by the linear catalysts).

2-2- Research Objective and Proposal

The objective of this work is to seek ways to obtain higher degrees of LCB and control the molecular weight, polydispersity index, and cumulative copolymer composition (in the case of copolymerization with α-olefins) of polyolefins made with CGC and other metallocene ctalysts.

As proposed by Lai et al. (1993, 1997), the main mechanism for long-chain branch formation in olefin polymerization with metallocene catalysts is terminal branching. This mechanism has been known in free radical polymerization for many years (Hamielec et al., 1987). In free radical polymerization, dead chains with terminal double bonds (macromonomers) are produced via chain transfer to monomer or via

termination by disproportionation. In metallocene catalyst polymerization systems, the β-hydride elimination and transfer to monomer are the main mechanisms for in-situ macromonomer formation. These macromonomers, which usually contain terminal unsaturations, can add to the active sites and form long chain branches (Figure 2-2). According to the polymerization mechanism proposed by Soares and Hamielec (1996, 1997), the rate of LCB formation is proportional to the concentration of macromonomers in the reaction mixture. Therefore, any increase in macromonomer concentration will accelerate the rate of LCB formation. Soares et al. (1997) showed how combined catalyst systems were efficient in tailor-making molecular weight and molecular weight distribution in ethylene polymerization. The same idea can be employed to control long-chain branching. For example, if a conventional metallocene catalyst (which can only produce linear chains) with higher β-hydride elimination rate constant than CGC is added to the polymerization system of Lai et al. (1993, 1997), the overall rate of β-hydride elimination reaction will be higher and more macromonomers will be produced. Hence, the rate of LCB formation will increase. In such a system, by changing the amount and/or type of the added metallocene catalyst (linear catalyst), the LCB degree can be controlled. The feasibility and efficiency of the proposed technique will be discussed and evaluated in detail in the following chapters.

Chapter 3

Mathematical Modeling

3-1- A General Model for Olefin Polymerization Using Combined Catalyst Systems.

The main mechanism for long-chain branch formation in olefin polymerization with metallocene catalysts is terminal branching (incorporation of macromonmers). In these polymerization systems, the β-hydride elimination and transfer to monomer are the main mechanisms for in-situ macromonomer formation. According to the proposed polymerization mechanism, the rate of LCB formation is proportional to the concentration of macromonomers in the reaction mixture. Therefore, any increase in macromonomer concentration will accelerate the rate of LCB formation. As discussed in Chapter 2, combined catalyst systems could be used to achieve this purpose. The

feasibility of this idea is investigated in detail in this chapter using mathematical modeling.

3-1-1- Reaction Mechanism and Kinetics

Olefin copolymerization with long chain branch (LCB) formation includes steps of initiation, propagation, addition of dead polymer chains with terminal double-bonds to active centers (LCB formation), transfer to chain transfer agent (formation of dead polymer chains with saturated chain-ends), β-hydride elimination (formation of dead polymer chains with terminal double-bonds), and catalyst deactivation. In the proposed model the combination of two catalyst types has been considered. Catalyst type 1 (LCB catalyst) is capable of polymerizing both monomers and macromonomers, whereas catalyst type 2 (linear catalyst) can only polymerize monomers (unable to incorporate macromonomers).

Initiation:

$$C_1+M_1 \rightarrow P_{1,0} \qquad k_{i,11}$$

$$C_1+M_2 \rightarrow S_{1,0} \qquad k_{i,12}$$

$$C_2+M_1 \rightarrow Q_1 \qquad k_{i,21}$$

$$C_2+M_2 \rightarrow T_1 \qquad k_{i,22}$$

Propagation:

$$P_{r,1} + M_1 \rightarrow P_{r+1,1} \qquad k_{1,11}$$

$$P_{r,1} + M_2 \rightarrow S_{r+1,1} \qquad k_{1,12}$$

$$S_{r,1} + M_1 \rightarrow P_{r+1,1} \qquad k_{1,21}$$

$$S_{r,1} + M_2 \rightarrow S_{r+1,1} \qquad k_{1,22}$$

$$Q_r + M_1 \rightarrow Q_{r+1} \qquad k_{2,11}$$

$$Q_r + M_2 \rightarrow T_{r+1} \qquad k_{2,12}$$

$$T_r + M_1 \rightarrow Q_{r+1} \qquad k_{2,21}$$

$$T_r + M_2 \rightarrow T_{r+1} \qquad k_{2,22}$$

Long-chain branching:

$$P_{r,1} + D^{=}_{1,q,J} \rightarrow P_{r+q,1+J+1} \qquad k_{LCB,11}$$

$$S_{r,1} + D^{=}_{1,q,J} \rightarrow P_{r+q,1+J+1} \qquad k_{LCB,21}$$

$$P_{r,1} + D^{=}_{2,q,J} \rightarrow S_{r+q,1+J+1} \qquad k_{LCB,12}$$

$$S_{r,1} + D^{=}_{2,q,J} \rightarrow S_{r+q,1+J+1} \qquad k_{LCB,22}$$

Transfer:

$$P_{r,1} + CTA \rightarrow D_{r,1} + C_1 \qquad k_{CTA,11}$$

$$S_{r,1} + CTA \rightarrow D_{r,1} + C_1 \qquad k_{CTA,12}$$

$$Q_r + CTA \rightarrow D_{r,0} + C_2 \qquad k_{CTA,21}$$

$$T_r + CTA \rightarrow D_{r,0} + C_2 \qquad k_{CTA,22}$$

β-hydride elimination:

$$P_{r,i} \rightarrow D^{=}_{1,r,i} + C_1 \qquad k_{\beta,11}$$

$$S_{r,i} \rightarrow D^{=}_{2,r,i} + C_1 \qquad k_{\beta,12}$$

$$Q_r \rightarrow D^{=}_{1,r,0} + C_2 \qquad k_{\beta,21}$$

$$T_r \rightarrow D^{=}_{2,r,0} + C_2 \qquad k_{\beta,22}$$

Deactivation:

$$C_1 \rightarrow DC \qquad k_{da,1}$$

$$C_2 \rightarrow DC \qquad k_{da,2}$$

$$P_{r,i} \rightarrow D_{r,i} \qquad k_{da,1}$$

$$S_{r,i} \rightarrow D_{r,i} \qquad k_{da,2}$$

$$Q_r \rightarrow D_{r,0} \qquad k_{da,2}$$

$$T_r \rightarrow D_{r,0} \qquad k_{da,2}$$

where:

$D^{=}_{m,r,i}$ dead polymer of chain length r containing i long chain branches and terminal unsaturation, ended with monomer m (m = 1 or 2).

$D_{r,i}$ dead polymer of chain length r containing i long chain branches and a saturated chain-end.

$P_{r,i}$ living polymer of chain length r containing i long chain branches made on catalyst site type 1 ending with monomer 1.

Q_r linear living polymer of chain length r made on catalyst site type 2 ending with monomer 1.

$S_{r,i}$ living polymer of chain length r containing i long chain branches made on catalyst site type 1 ending with monomer 2.

T_r linear living polymer of chain length r made on catalyst site type 2 ending with monomer 2.

C_i catalyst site type i.

DC dead catalyst site (or inactive).

M_1, M_2 monomers 1 and 2.

CTA chain transfer agent.

$k_{i,jq}$ initiation rate constant for catalyst site type j reacting with monomer q.

$k_{j,mq}$ propagation rate constant for incorporation of monomer q to a chain made on catalyst site type j ended with monomer m.

$k_{LCB,jm}$ propagation rate constant for incorporation of macromonomers ended with monomer m to a living chain ended with monomer j.

$k_{CTA,jq}$ transfer rate constant for a living chain made on catalyst site type j ended with monomer q.

$k_{\beta,jq}$ β-hydride elimination rate constant of a living chains made on catalyst site type j ended with monomer q.

$k_{da,j}$ deactivation rate constant for catalyst site type j.

3-1-2- Population Balances

Based on the above reaction mechanism, balances for different populations can be derived as follows:

Catalysts:

$$\frac{dC_1}{dt} = s(C_{1,in} - C_1) - (k_{i,11}M_1 + k_{i,12}M_2 + k_{da,1})C_1 + CTA(k_{CTA,11}\eta_0 + k_{CTA,12}\psi_0) + (k_{\beta,11}\eta_0 + k_{\beta,12}\psi_0) \quad (3\text{-}1)$$

$$\frac{dC_2}{dt} = s(C_{2,in} - C_2) - (k_{i,21}M_1 + k_{i,22}M_2 + k_{da,2})C_2 + CTA(k_{CTA,21}\gamma_0 + k_{CTA,22}\tau_0) + (k_{\beta,21}\gamma_0 + k_{\beta,22}\tau_0) \quad (3\text{-}2)$$

where s is the reciprocal of the mean residence time in the reactor

Monomers:

$$\frac{dM_1}{dt} = s(M_{1,in} - M_1) - (k_{1,11}\eta_0 + k_{1,21}\psi_0 + k_{2,11}\gamma_0 + k_{2,21}\tau_0)M_1 \quad (3\text{-}3)$$

$$\frac{dM_2}{dt} = s(M_{2,in} - M_2) - (k_{1,12}\eta_0 + k_{1,22}\psi_0 + k_{2,12}\gamma_0 + k_{2,22}\tau_0)M_2 \quad (3\text{-}4)$$

Dead Polymer Chains:

$$\frac{dD^{=}_{1,r,0}}{dt} = k_{\beta,11}P_{r,0} + k_{\beta,21}Q_r - (k_{LCB,11}\eta_0 + k_{LCB,21}\psi_0 + s)D^{=}_{1,r,0} \qquad (i=0) \quad (3\text{-}5)$$

$$\frac{dD^{=}_{1,r,i}}{dt} = k_{\beta,11}P_{r,i} - (k_{LCB,11}\eta_0 + k_{LCB,21}\psi_0 + s)D^{=}_{1,r,i} \qquad (i>0) \quad (3\text{-}6)$$

$$\frac{dD^{=}_{2,r,0}}{dt} = k_{\beta,12}S_{r,0} + k_{\beta,22}T_r - (k_{LCB,12}\eta_0 + k_{LCB,22}\psi_0 + s)D^{=}_{2,r,0} \qquad (i=0) \quad (3\text{-}7)$$

$$\frac{dD^{=}_{2,r,i}}{dt} = k_{\beta,12}S_{r,i} - (k_{LCB,12}\eta_0 + k_{LCB,22}\psi_0 + s)D^{=}_{2,r,i} \qquad (i>0) \qquad (3\text{-}8)$$

$$\frac{dD_{r,0}}{dt} = (k_{CTA,11}P_{r,0} + k_{CTA,12}S_{r,0} + k_{CTA,21}Q_r + k_{CTA,22}T_r)CTA + k_{da,1}(P_{r,0} + S_{r,0}) + k_{da,2}(Q_r + T_r) - sD_{r,0} \qquad (i=0) \qquad (3\text{-}9)$$

$$\frac{dD_{r,i}}{dt} = (k_{CTA,11}P_{r,i} + k_{CTA,12}S_{r,i})CTA + k_{da,1}(P_{r,i} + S_{r,i}) - sD_{r,i} \qquad (i>0) \qquad (3\text{-}10)$$

Living Polymer Chains:

$$\frac{dP_{1,0}}{dt} = k_{i,11}C_1M_1 - (k_{1,11}M_1 + k_{1,12}M_2 + k_{LCB,11}\lambda_0 + k_{LCB,12}\sigma_0)P_{1,0} - (k_{CTA,11}CTA + k_{\beta,11} + k_{da,1} + s)P_{1,0} \qquad (3\text{-}11)$$

$$\frac{dP_{r,i}}{dt} = k_{1,11}M_1(P_{r-1,i} - P_{r,i}) + k_{1,21}M_1S_{r-1,i} - k_{1,12}M_2P_{r,i} - (k_{LCB,11}\lambda_0 + k_{LCB,12}\sigma_0)P_{r,i} + k_{LCB,11}\sum_{s=1}^{r-1}\sum_{j=0}^{i-1}P_{r-s,j}D^{=}_{1,s,i-1-j} + k_{LCB,21}\sum_{s=1}^{r-1}\sum_{j=0}^{i-1}S_{r-s,j}D^{=}_{1,s,i-1-j} - (k_{CTA,11}CTA + k_{\beta,11} + k_{da,1} + s)P_{r,i} \qquad (3\text{-}12)$$

$$\frac{dS_{1,0}}{dt} = k_{i,12}C_1M_2 - (k_{1,21}M_1 + k_{1,22}M_2 + k_{LCB,21}\lambda_0 + k_{LCB,22}\sigma_0)S_{1,0} - (k_{CTA,12}CTA + k_{\beta,12} + k_{da,1} + s)S_{1,0} \qquad (3\text{-}13)$$

$$\frac{dS_{r,i}}{dt} = k_{1,22}M_2(S_{r-1,i} - S_{r,i}) + k_{1,12}M_2P_{r-1,i} - k_{1,21}M_1S_{r,i} - (k_{LCB,21}\lambda_0 + k_{LCB,22}\sigma_0)S_{r,i} + k_{LCB,12}\sum_{s=1}^{r-1}\sum_{j=0}^{i-1}P_{r-s,j}D^{=}_{2,s,i-1-j} + k_{LCB,22}\sum_{s=1}^{r-1}\sum_{j=0}^{i-1}S_{r-s,j}D^{=}_{2,s,i-1-j} - (k_{CTA,12}CTA + k_{\beta,12} + k_{da,1} + s)S_{r,i} \qquad (3\text{-}14)$$

$$\frac{dQ_1}{dt} = k_{i,21}M_1C_2 - (k_{2,11}M_1 + k_{2,12}M_2)Q_1 - (k_{CTA,21}CTA + k_{\beta,21} + k_{da,2} + s)Q_1 \qquad (3\text{-}15)$$

$$\frac{dQ_r}{dt} = k_{2,11}M_1(Q_{r-1} - Q_r) - k_{2,12}M_2Q_r + k_{2,21}M_1T_{r-1} - (k_{CTA,21}CTA + k_{\beta,21} + k_{da,2} + s)Q_r \quad (3\text{-}16)$$

$$\frac{dT_1}{dt} = k_{i,22}M_2C_2 - (k_{2,21}M_1 + k_{2,22}M_2)T_1 - (k_{CTA,22}CTA + k_{\beta,22} + k_{da,2} + s)T_1 \quad (3\text{-}17)$$

$$\frac{dT_r}{dt} = k_{2,22}M_2(T_{r-1} - T_r) + k_{2,12}M_2Q_{r-1} - k_{2,21}M_1T_r - (k_{CTA,22}CTA + k_{\beta,22} + k_{da,2} + s)T_r \quad (3\text{-}18)$$

In the above equations, the Greek letters stand for the moments of different populations, defined as follows:

λ_j *j*th moment of the dead polymers with terminal double-bond ended with monomer 1.

σ_j *j*th moment of the dead polymers with terminal double-bond ended with monomer 2.

μ_j *j*th moment of the dead polymers with saturated chain-end.

η_j *j*th moment of the living polymer chains made on the LCB catalyst ended with monomer 1.

ψ_j *j*th moment of the living polymer chains made on the LCB catalyst ended with monomer 2.

γ_j *j*th moment of living polymer chains made on the linear catalyst, ended with monomer 1.

τ_j jth moment of living polymer chains made on the linear catalyst, ended with monomer 2.

where these moments are defined by the following equations:

$$\lambda_j = \sum_{r=1}^{\infty}\sum_{i=0}^{\infty}(r.i)^j D^{=}_{1,r,i} \tag{3-19}$$

$$\sigma_j = \sum_{r=1}^{\infty}\sum_{i=0}^{\infty}(r.i)^j D^{=}_{2,r,i} \tag{3-20}$$

$$\mu_j = \sum_{r=1}^{\infty}\sum_{i=0}^{\infty}(r.i)^j D_{r,i} \tag{3-21}$$

$$\eta_j = \sum_{r=1}^{\infty}\sum_{i=0}^{\infty}(r.i)^j P_{r,i} \tag{3-22}$$

$$\psi_j = \sum_{r=1}^{\infty}\sum_{i=0}^{\infty}(r.i)^j S_{r,i} \tag{3-23}$$

$$\gamma_j = \sum_{r=1}^{\infty} r^j Q_r \tag{3-24}$$

$$\tau_j = \sum_{r=1}^{\infty} r^j T_r \tag{3-25}$$

Moment Equations and Chain-Length Averages

Chain length averages, X_n, X_w, and polydispersity indices for different chain populations, calculated by the method of moments, can be stated as follows:

$$X_n = \frac{FirstMoment}{ZerothMoment} \tag{3-26}$$

$$X_w = \frac{SecondMoment}{FirstMoment} \tag{3-27}$$

$$PDI = \frac{\bar{r}_w}{\bar{r}_n} \tag{3-28}$$

Average values for instantaneous long-chain branching frequency can also be easily obtained by noticing that:

$$B_n = \frac{R_{LCB}}{R_{cf}} = \frac{R_{LCB}}{R_\beta + R_{da} + R_{CTA} - R_{LCB}} \tag{3-29}$$

where:

B_n average number of LCB per polymer chain

R_{LCB} rate of macromonomer propagation

R_{cf} net rate of dead polymer chain formation

R_β rate of β-hydride elimination reaction

R_{da} rate of deactivation reaction

R_{CTA} rate of transfer reaction

The instantaneous number of branching points per 1000 carbon atoms (λ_n) can also be easily calculated:

$$\lambda_n = 500\frac{R_{LCB}}{R_p} \tag{3-30}$$

where R_p is the rate of monomer propagation.

3-1-3- Dynamic Simulation Results and Discussion

According to the definition of moments and population balances of different species in the reaction mixture, the zeroth, the first, and the second moments for different polymer chains can be calculated. Considering the seven types of polymer chains mentioned above, there will be a system of 21 differential equations for moments (shown in Appendix A) for the dynamic operation of CSTR. To find different moments, these 21 equations and the balance equations for monomers, catalysts, and chain transfer agent (total of 26 ordinary differential) should be solved simultaneously. The method of Range-Kutta of order 6 (Gerald, 1994) were used to solve the obtained system of differential equations

In this simulation, homo- and copolymerization of ethylene using two site-type metallocene catalysts were studied. Typical values for ethylene homo- and co-polymerization kinetic rate constants were used in the computer simulation (Appendix B). Values of reactivity ratios were taken from the data obtained by Knight and Lai (1993). By varying rate constants, one can simulate the effect of combining different linear catalysts with an LCB catalyst on polymer characteristics. Along with the effect of reaction parameters, the influence of some process parameters, such as residence time of the reactor, were also investigated (Beigzadeh et al., 1997).

Tables 3-1 and 3-2 show the initial conditions used in computer simulations for homo- and copolymerization of ethylene, respectively.

Table 3-1- Initial conditions used in ethylene homopolymerization simulation.

Reactor residence time (min)	5
Catalyst 1 concentration in feed (mol/L)	1E-6
Catalyst 2 concentration in feed (mol/L)	1E-6
Ethylene concentration in feed (mol/L)	0.02
Chain transfer agent concentration in feed (mol/L)	0
Initial concentration of catalysts and monomers in reactor	0 (pure solvent-full reactor)

Table 3-2- Initial conditions used in ethylene copolymerization simulation.

Reactor residence time (min)	5
Catalyst 1 concentration in feed (mol/L)	1E-6
Catalyst 2 concentration in feed (mol/L)	1E-6
Ethylene concentration in feed (mol/L)	0.02
1-octene concentration in feed (mol/L)	0.003
Chain transfer agent concentration in feed (mol/L)	0
Initial concentration of catalysts and monomers in reactor	0 (pure solvent-full reactor)

In all of the computer runs, the effects of process conditions were investigated by changing their values after reaching the steady state. For example, in Figure 3-1, the number of branching points per 1000 carbon atoms (λ_n) after about 25 minutes ($t \approx 25$ min) reaches its steady state value. At $t = 45$ min (after 9 residence times), by changing the ratio of the LCB catalyst to the linear catalyst, the value of λ_n changes and reaches a new steady state value corresponding to the new reaction operation conditions.

Figures 3-1 to 3-6 illustrate the effects of catalyst system characteristics at different process conditions on polymer chain microstructure for the homopolymerization of ethylene with combined catalyst systems, while Figures 3-7 to 3-11 discuss the effects of catalyst deactivation for the copolymerization of ethylene with 1-octene.

Figure 3-1 compares the number of branching points per 1000 carbon atoms (λ_n) for different values of the propagation rate constant of the linear catalyst at different process conditions. Higher propagation rate constant values for this catalyst favor the formation of linear chains (versus branched chains), therefore lowering the number of branching points per 1000 carbon atoms (λ_n) is obtained.

Since higher ratios of the LCB/linear catalyst imply higher rates of LCB formation, by changing the ratio of the two catalysts (at t = 45 min), an increase in the number of LCB per 1000 carbon atoms (λ_n) is observed. Increasing the monomer concentration (at t = 90 min) increases the propagation rate and production of linear chains, therefore the number of branching points per 1000 carbon atoms (λ_n) decreases. These conclusions can be easily understood by inspection of Equation (3-30).

Higher residence time for the same reaction volume means lower feed flow rate. Therefore, at higher residence times the monomer concentration in the reaction mixture will decrease, hence lower propagation rates will be obtained. On the other hand, at higher residence times, the concentration of polymer (and of the macromonomers) increases, which accelerates the formation of LCB. This effect is shown by changing the residence time of the reactor for reaction times of t = 135 min and t = 180 min. Shorter residence times decrease λ_n and longer residence times increase λ_n.

According to the model developed here, the use of a chain transfer agent does not change the number of active sites in the reaction mixture, therefore the rate of LCB and polymer mass formation will not be affected by the introduction of chain transfer agent. This means no variation in λ_n, as is also illustrated in Figure 3-1.

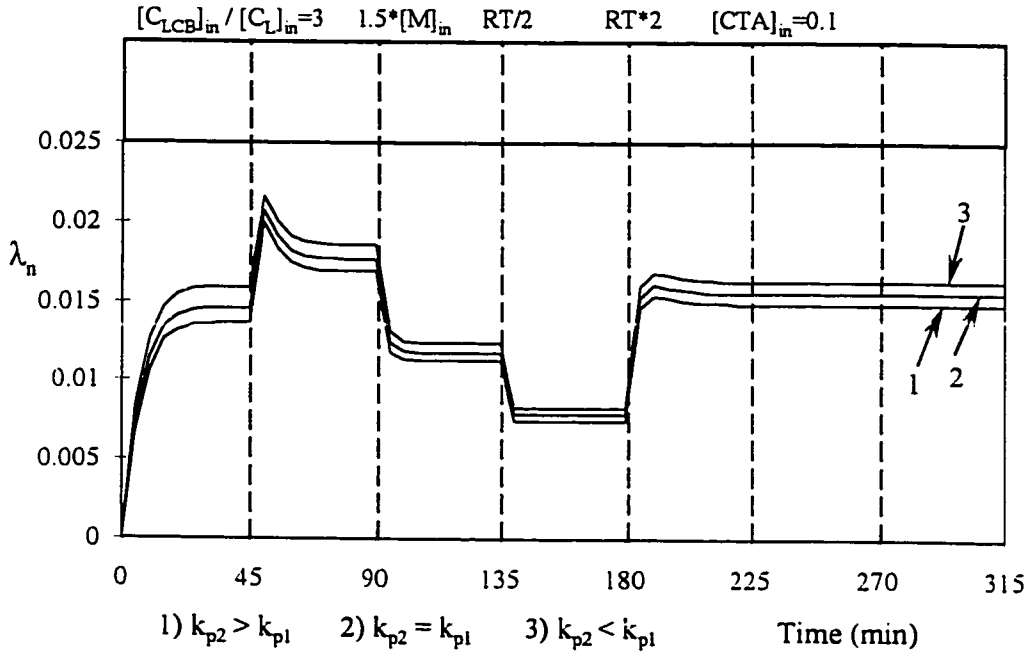

Figure 3-1- Variations in the number of branching points per 1000 carbon atoms (λ_n) for different process conditions for catalyst systems with different k_{p2} values. Values of k_{p2} for lines 1, 2, and 3 are 5000, 4000, and 3000 L/mol.s, respectively. k_{p1} = 4000 L/mol.s.

Figure 3-2 illustrates the effect of the propagation rate constant of the linear catalyst on the weight-average molecular weight (M_w). As expected, higher propagation rates for the linear catalyst lead to the production of polymer with higher molecular weights. At higher monomer concentrations in the feed rate, monomer concentration in the reactor and consequently the propagation rate increase, which causes the formation of longer chains and consequently higher M_w values.

As previuosly discussed, at higher reactor residence times the rate of LCB formation is higher. Higher rates of LCB formation will evidently increase the molecular weight. This fact is shown in Figure 3-2 for t = 135 min and t = 180 min, where the

molecular weight increases at longer reactor residence times and decreases when the residence time is shorter.

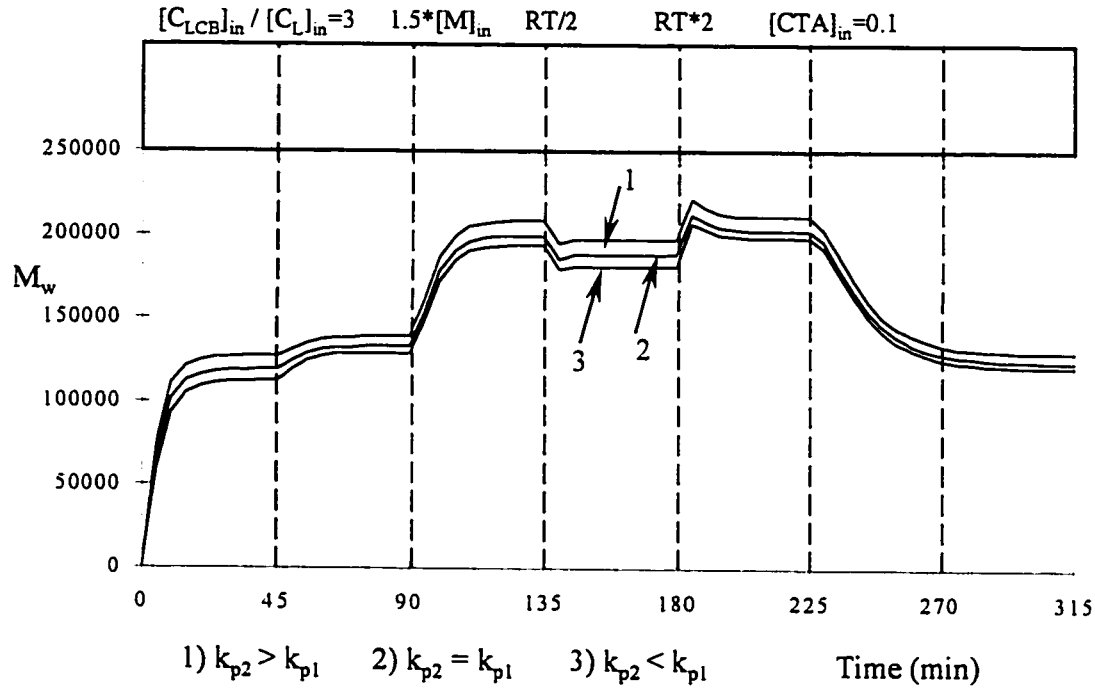

Figure 3-2- Variations in weight average molecular weight (M_w) for different process conditions for catalyst systems with different k_{p2} values. Values of k_{p2} for lines 1, 2, and 3 are 5000, 4000, and 3000 L/mol.s, respectively. k_{p1} = 4000 L/mol.s.

As expected, introduction of a chain transfer agent reduces the molecular weight. This is due to the reaction between growing chains and chain transfer agent and production of dead polymer with saturated chain ends.

Figure 3-3 shows the effect of process conditions on the number of LCB points per 1000 carbon atoms (λ_n) for different values of $k_{\beta,2}$.

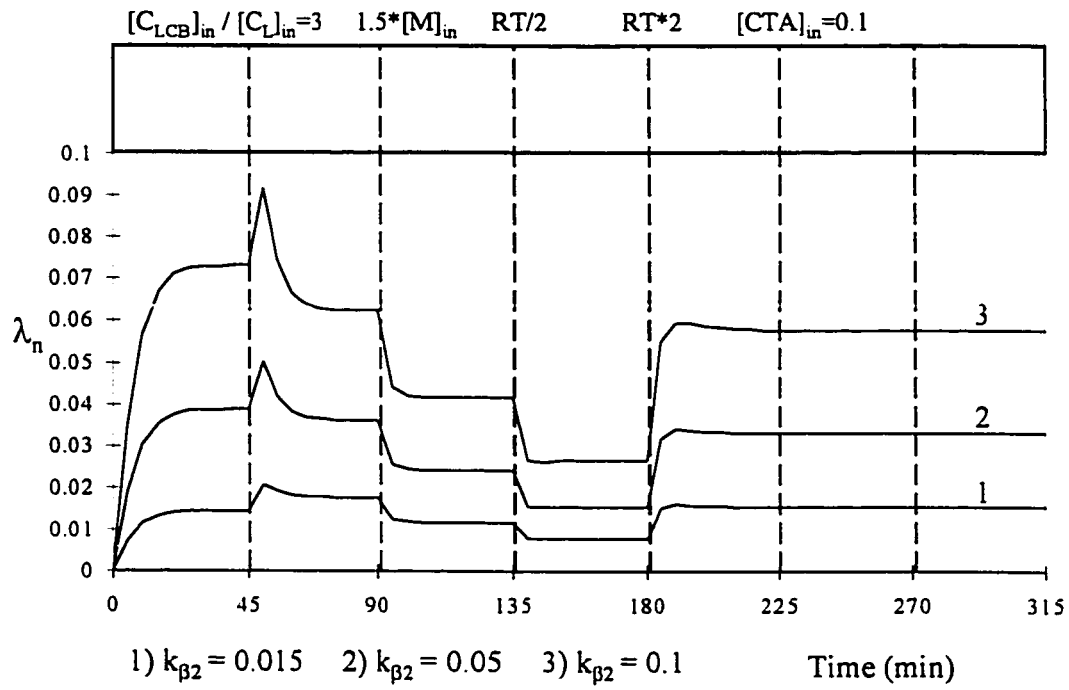

Figure 3-3- Variations in the number of branching points per 1000 carbon atoms (λ_n) for different process conditions for catalyst systems with different $k_{\beta 2}$ values. The values of $k_{\beta 2}$ are in s^{-1}.

According to the proposed reaction mechanism, the rate of formation of branching points is proportional to the concentration of active sites on the LCB catalyst and to the concentration of macromonomer. Higher $k_{\beta 2}$ values for the linear catalyst increase the concentration of macromonomers and higher λ_n values are therefore obtained. Increasing the ratio of the LCB/linear catalyst (t = 45 min) increases the concentration of branching active sites; however, this also reduces the concentration of linear active sites and consequently the concentration of macromonomer. For catalyst systems with high $k_{\beta 2}$ values, an increases in LCB/linear catalyst ratio can actually decrease λ_n, as clearly

indicated in case 3 in Figure 3-3. Depending on the $k_{\beta,2}$ values of the linear catalyst, changing the ratio of the two catalysts might increase or decrease the number of branching points per 1000 carbon atoms. This is a very important design factor when selecting catalysts for the production of polyolefins with LCBs.

The effect of the $k_{\beta,2}$ values on B_n (average number of LCB per polymer chain) is shown in Figure 3-4. Again, similar to the results seen in Figure 3-1, higher $k_{\beta,2}$ values lead to higher macromonomer concentration and higher B_n values are obtained.

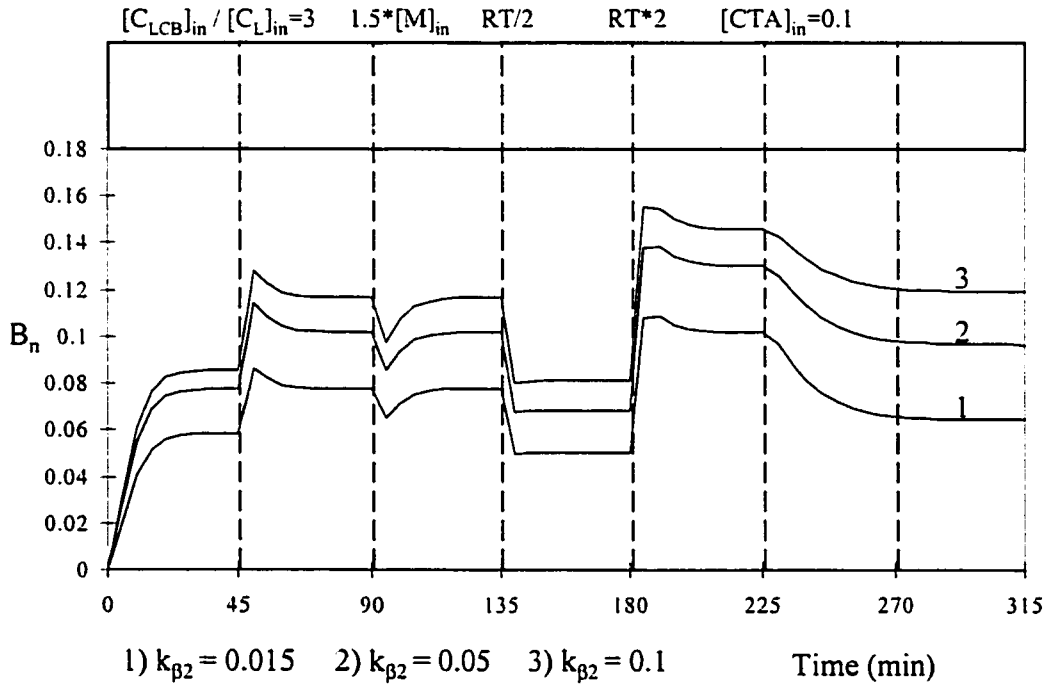

Figure 3-4- Variations in the number of branching points per polymer chain (B_n) for different process conditions for catalyst systems with different $k_{\beta 2}$ values. The values of $k_{\beta 2}$ are in s^{-1}.

The dependency of B_n on the ratio of the two catalysts is not similar to that observed for λ_n. The variation of this parameter with the ratio of the two catalysts depends on three phenomena. First, higher ratios of the LCB/linear catalyst increase the number of branching active sites which favors higher B_n values. Secondly, a decrease in the concentration of the linear catalyst decreases the concentration of macromonomers and hence B_n decreases. Thirdly, in catalyst systems with high $k_{\beta,2}$ values, a decrease in the linear catalyst concentration leads to an increase in average molecular weight (because of less β-hydride elimination). Therefore, by increasing the concentration of the branching catalyst, B_n can also increase.

The presence of chain transfer agent does not change the number of active sites in the reaction mixture, and therefore does not affect the rate of formation of branching points. However, because of the significant decrease in molecular weight and increase in number of polymer molecules B_n decreases, as indicated in Figure 3-4.

Figure 3-5 illustrates the variation of number average molecular weight (M_w) for different process conditions and for different values of the β-hydride elimination rate constant of the linear catalyst. Catalyst systems with higher β-hydride elimination rate constants produce shorter chains (lower molecular weights). The effects of residence time and chain transfer agent are similar to what was explained for Figure 3-2.

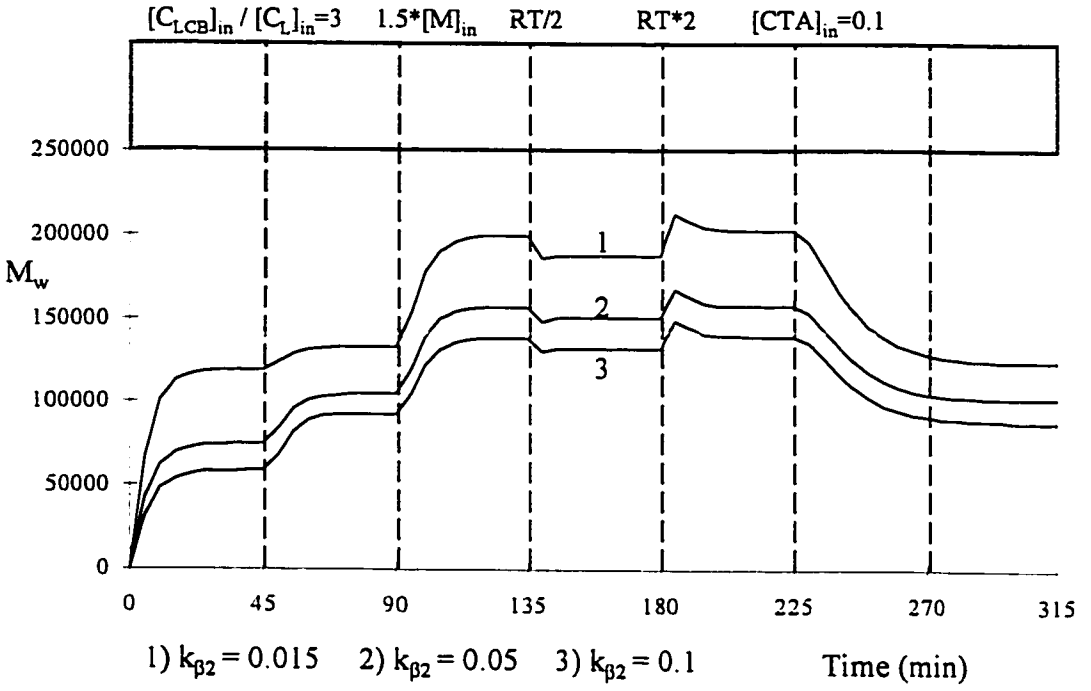

Figure 3-5- Variations in number average molecular weight (M_w) for different process conditions for catalyst systems with different $k_{\beta 2}$ values. The values of $k_{\beta 2}$ are in s^{-1}.

Figure 3-6 shows the variations of polydispersity index for catalyst systems with different $k_{\beta 2}$ values. As shown in this figure, catalyst systems with higher $k_{\beta 2}$ produce more polydisperse polymers. This behavior can be attributed to two phenomena. First, the propagation and the β-hydride elimination reaction rate constants considered initially for both catalysts were equal ($k_{\beta 2}$= $k_{\beta 2}$= 0.015 s^{-1}). This means that the two active sites synthesize approximately equal molecular weight polymers. Therefore, PDI varies around the theoretical value of 2 (case study 1).

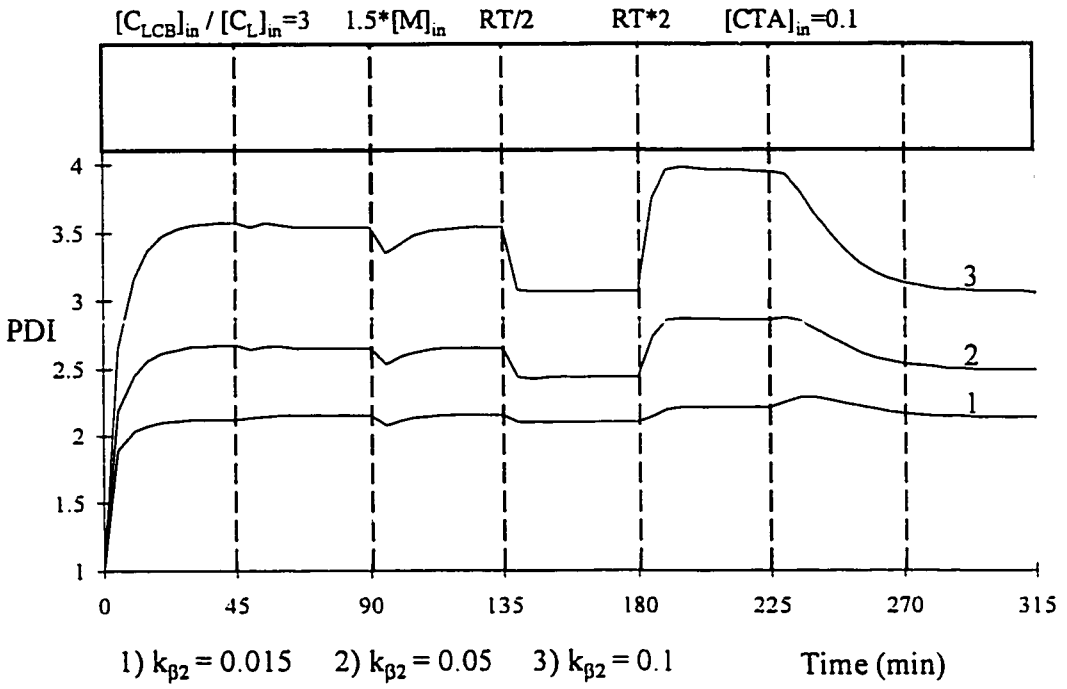

Figure 3-6- Variations in polydispersity index (PDI) for different process conditions for catalyst systems with different $k_{\beta 2}$ values. The values of $k_{\beta 2}$ are in s^{-1}.

As $k_{\beta 2}$ increases, the chains synthesized by the linear catalyst will have lower molecular weights than the ones made with the LCB catalyst (due to higher transfer reaction rate) and, therefore, PDI increases. Secondly, at higher $k_{\beta 2}$ values, the rate of macromonomer production and hence its concentration in the reactor is higher, which translates to higher LCB formation and naturally higher PDI.

Figures 3-7 to 3-11 illustrate the effects of catalyst deactivation at different process conditions for the copolymerization of ethylene with 1-octene using combined catalyst systems. This is an important design aspect for the solution polymerization of ethylene, since the high temperature employed will likely lead to fast catalyst deactivation.

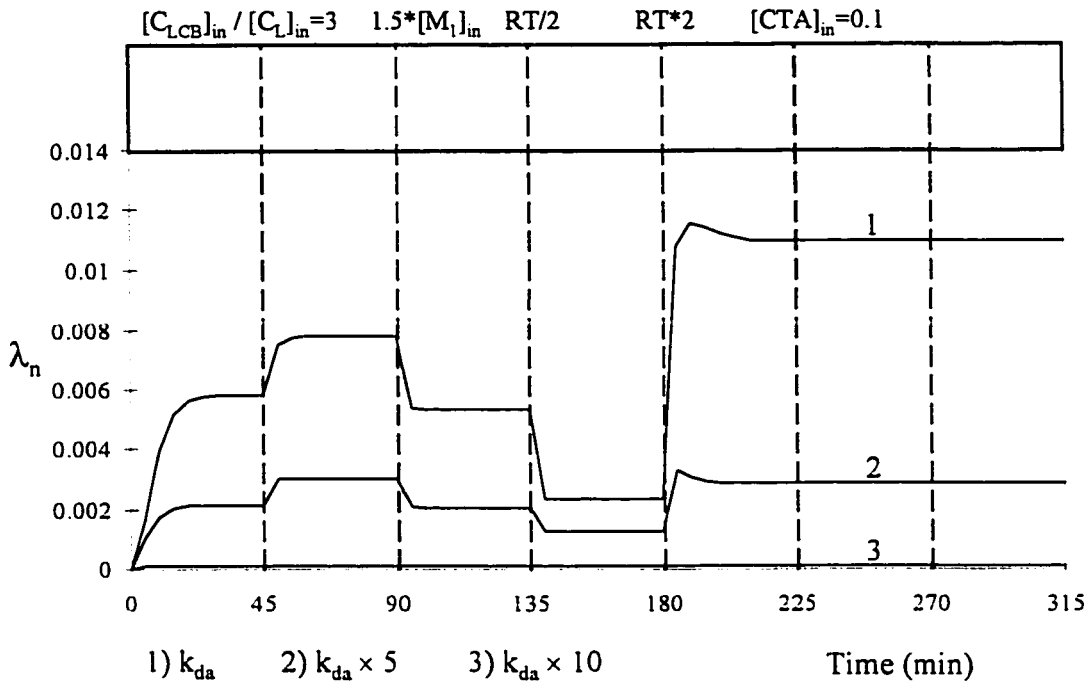

Figure 3-7- Variations in the number of branching points per 1000 carbon atoms (λ_n) for different process conditions for catalyst systems with different k_{da} values of both (LCB and linear) catalysts. k_{da1}=0.007 s^{-1} and k_{da2}=0.003 s^{-1} (Appendix B, Table 2).

Therefore, fewer LCBs are formed in polymerization systems with higher deactivation rates. This effect is demonstrated in Figures 3-7 and 3-8 where λ_n and B_n values change by orders of magnitude as the deactivation reaction rate constants of the catalyst increase. B_n is more sensitive to catalyst deactivation than λ_n, because this reaction not only reduces the number of active sites (less LCB points), but also terminates the chains and leads to the formation of shorter chains, and therefore lower molecular weights will be obtained. By definition, B_n is a function of both number of LCB points and molecular weight. Therefore, the decrease in B_n is more pronounced than in λ_n.

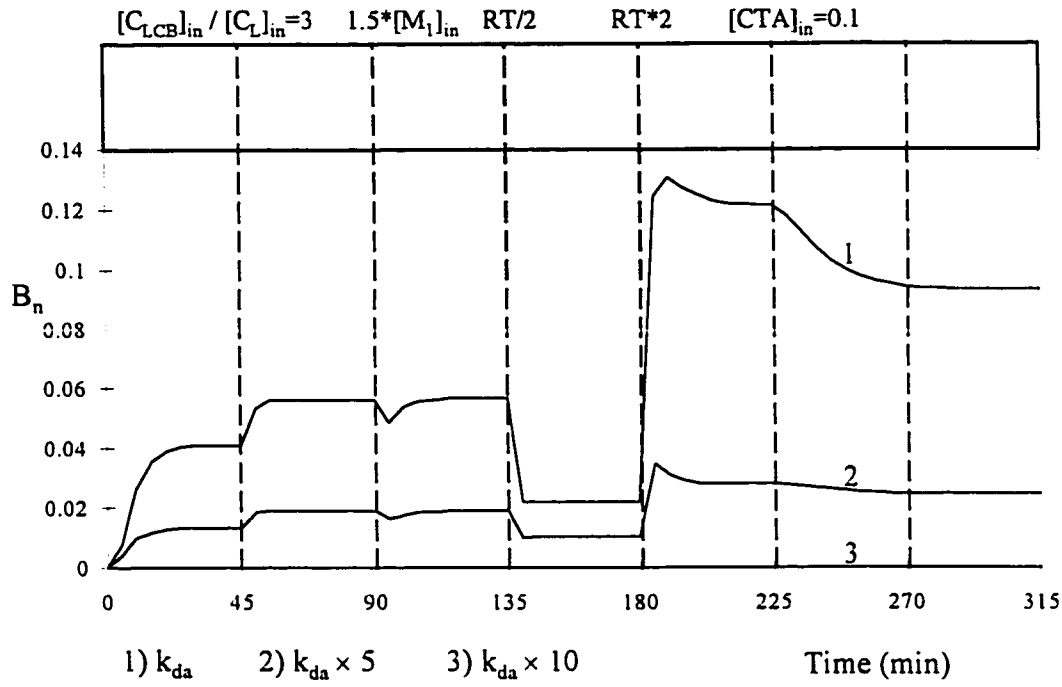

Figure 3-8- Variations in the number of branching points per polymer chain (B_n) for different process conditions for catalyst systems with different k_{da} values of both (LCB and linear) catalysts. k_{da1}=0.007 s^{-1} and k_{da2}=0.003 s^{-1} (Appendix B, Table 2).

Figure 3-9 illustrates the effect of deactivation on weight-average molecular weight for copolymerization of ethylene with 1-octene. As was expected from the reaction mechanism, higher deactivation rate constants lead to the formation of shorter chains.

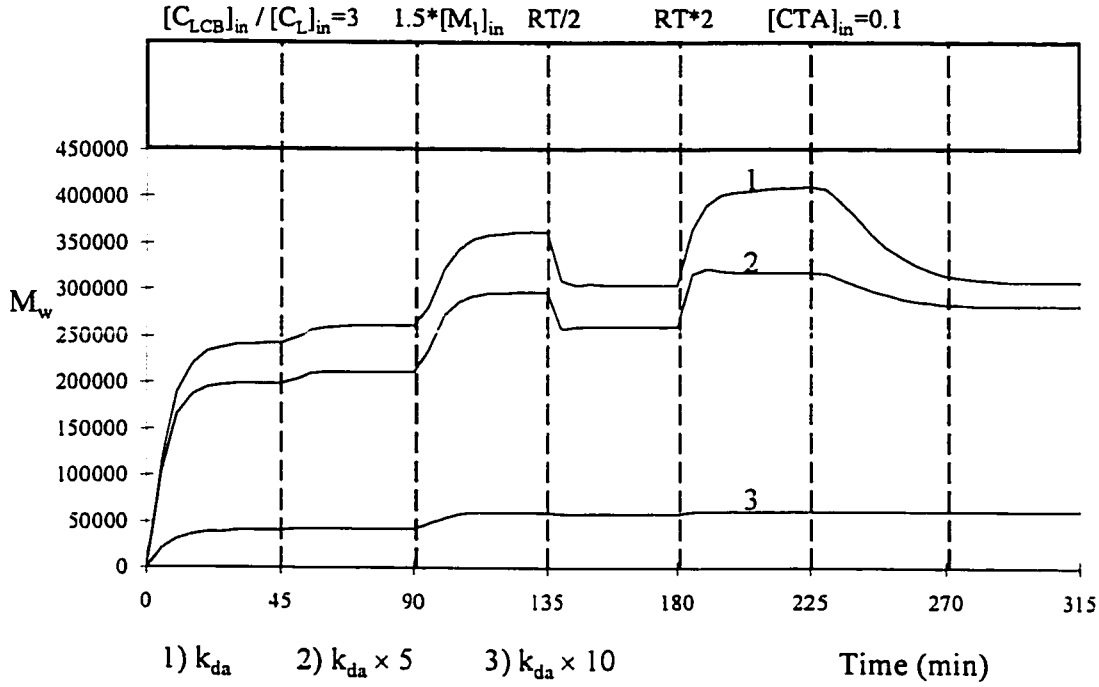

Figure 3-9- Variations in weight average molecular weight (M_w) for different process conditions for catalyst systems with different k_{da} values of both (LCB and linear) catalysts. k_{da1}=0.007 s^{-1} and k_{da2}=0.003 s^{-1} (Appendix B, Table 2).

The effect of catalyst deactivation on the polydispersity index for the copolymerization of ethylene with 1-octene is illustrated in Figure 3-10. In polymerization systems with high catalyst deactivation, growing chains will be terminated by the deactivation reaction and this reaction will be the dominant mechanism in determining the molecular weight. At higher deactivation rates, less LCBs are formed and a greater number of chains will be linear. Therefore, lower polydispersity index values will be obtained.

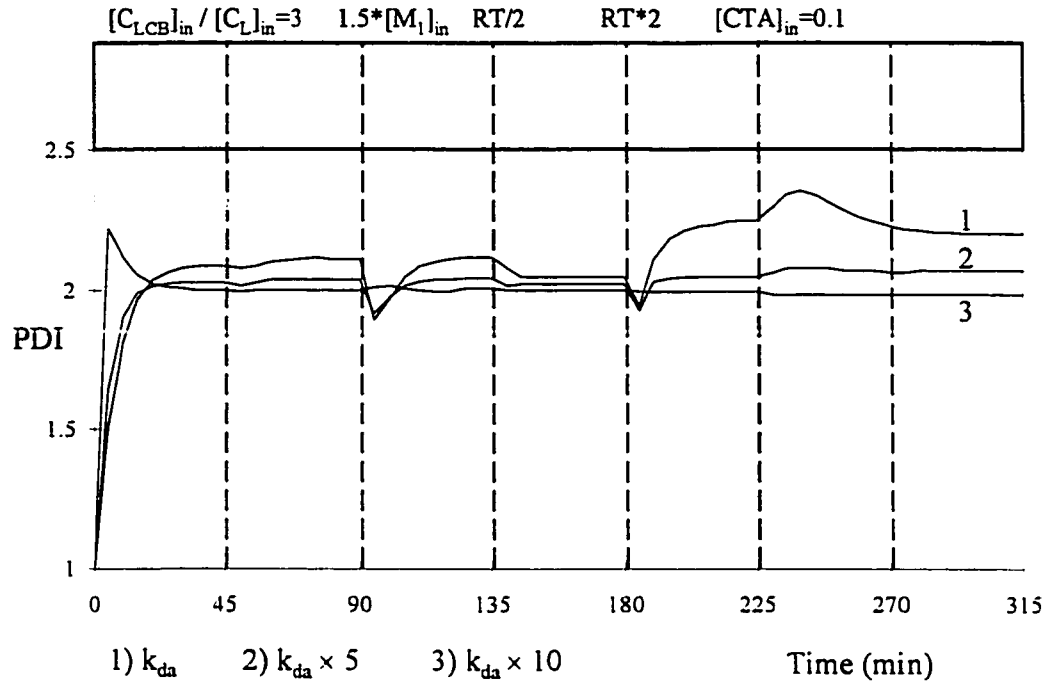

Figure 3-10- Variations in polydispersity index (PDI) for different process conditions for catalyst systems with different k_{da} values of both (LCB and linear) catalysts. k_{da1}=0.007 s^{-1} and k_{da2}=0.003 s^{-1} (Appendix B, Table 2).

Figure 3-11 shows the effect of process conditions on cumulative copolymer composition. Since the LCB catalyst can incorporate more 1-octene than the linear catalyst, employing higher ratios of the LCB/linear catalyst causes higher incorporation of the comonomer and therefore the molar fraction of ethylene in the copolymer (F_1) decreases. Increasing the concentration of ethylene in the feed stream $[M_1]_{in}$, increases F_1 as expected.

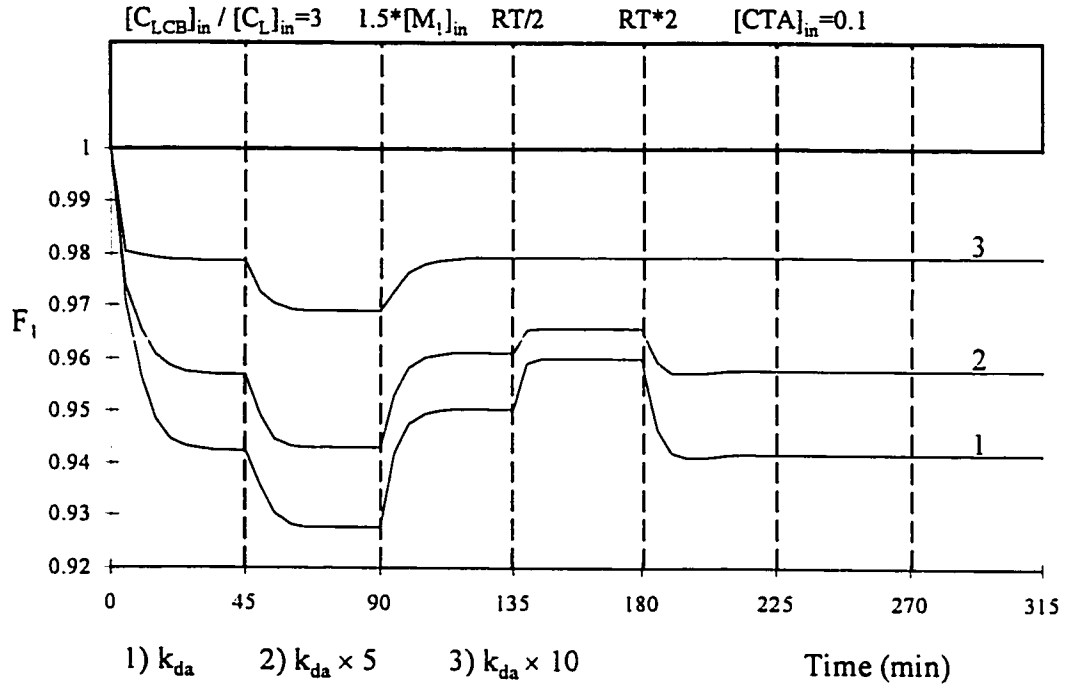

Figure 3-11- Variations in ethylene fraction in copolymer (F_1) for different process conditions for catalyst systems with different k_{da} values of both (LCB and linear) catalysts. k_{da1}=0.007 s^{-1} and k_{da2}=0.003 s^{-1} (Appendix B, Table 2).

1-octene reacts at a much slower rate than ethylene as indicated in Appendix B, Table 2. Therefore, shorter residence times will favor ethylene incorporation in the copolymer. This explains the increase of ethylene in the copolymer with decreasing reactor residence time.

According to the reaction mechanism, the chain transfer reaction does not change the concentration of active sites. As a result, by the introduction of chain transfer agent the propagation rates of comonomers remain constant and there will be no changes in copolymer composition.

3-1-4- Steady-State Simulation Results and Discussion

Although, dynamic simulation results are very useful for process control studies, reactor stability, grade changes etc., a steady state model is more convenient to use for catalyst design and selection. After all a continuous reactor operates at steady state for the most of its useful life and steady state simulation results are very important and useful for a polymerization unit.

For steady state simulation, the 26 differential equations presented in Appendix A were equated to zero and as a result a system of non-linear algebraic equations was obtained. The Newton's method (Gerald, 1994) were used to solve the obtained system of non-linear algebraic equations.

The values of rate constants are similar to the dynamic simulation (unless otherwise stated). These steady-state simulation results are useful to design polymerization recipes for synthesizing polyolefins with predetermined chemical structures (Beigzadeh et al., 1999).

Recipe Design

In order to design a recipe for synthesizing a particular polyolefin, the following steps should be taken: 1) The moment equations (Appendix A) should be equated to zero and solved simultaneously with selected kinetic parameters and polymerization conditions. 2) The effect of process parameters such as reactor residence time, the ratio of the two catalysts, and the effect of the characteristics of the catalyst system on the microstructure of final product should be investigated and plotted. 3) By implementing the preferred characteristics into the obtained plots, the best recipe can be selected.

This procedure will be illustrated in a series of case studies were copolymerizations of ethylene and an α-olefin (such as 1-octene) with a combined metallocene catalyst system are investigated. The catalyst system consists of an LCB catalyst (such as CGC) and a conventional metallocene catalyst (linear catalyst). The behavior of the polymerization system for three different cases using three different hypothetical conventional metallocene catalysts in combination with CGC has been investigated.

According to the proposed kinetic model, the produced macromonomers may have vinyl or vinylidene chain ends (Section 3-1-1). The macromonomers with vinylidene chain ends have much lower polymerization activity than the ones with vinyl unsaturations (because of their bulky chain ends). However, their polymerization rate constant is not zero and they can be polymerized. This has been considered in Appendix B, Table 2 where the values of $k_{LCB,11}$, $k_{LCB,12}$ are much higher than the ones of $k_{LCB,21}$, $k_{LCB,22}$, respectively.

In the following examples three different catalyst systems are used. The same LCB catalyst is considered for all three catalyst systems. All three linear catalysts are considered to have higher β-hydride elimination rate constants than the LCB catalyst. These linear catalysts are distinguished only by the differences in this rate constant, values which are given in Table 3-3.

Table 3-3- β-hydride elimination reaction rate constants of three linear catalysts employed in polymerization simulation.

Catalyst	Kinetic Constant (s^{-1})
Linear Catalyst 1	$k_{\beta,21} = k_{\beta,22} = 0.02$
Linear Catalyst 2	$k_{\beta,21} = k_{\beta,22} = 0.03$
Linear Catalyst 3	$k_{\beta,21} = k_{\beta,22} = 0.04$

According to Table 3-3, the following catalyst systems are used in the examples:

Catalyst system 1: LCB catalyst and linear catalyst 1.

Catalyst system 2: LCB catalyst and linear catalyst 2.

Catalyst system 3: LCB catalyst and linear catalyst 3.

It should be mentioned that operating conditions and catalyst system characteristics (shown in Appendix B Table 2, and Table 3-3) can be altered according to the operating conditions of each particular polymerization system and the recipe design procedure proposed herein will be applicable to any kind of operating conditions and catalyst system.

Considering constant values for total catalyst concentration in feed and constant monomer concentration in reactor (constant pressure), the proper type of linear catalyst, the mole fraction of the LCB catalyst, and the reactor residence time should be determined.

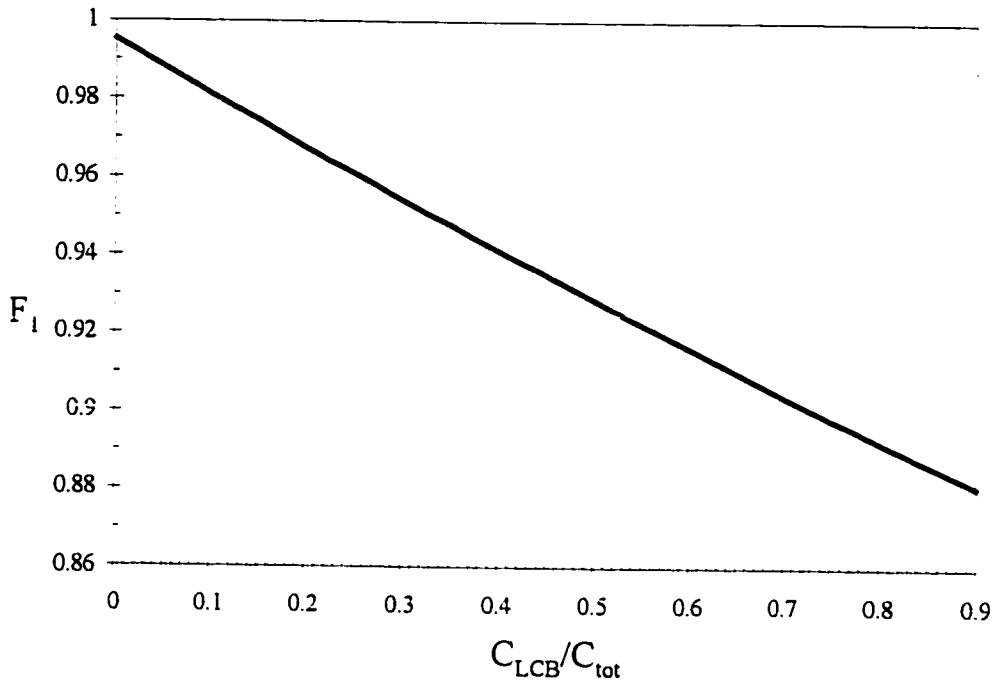

Figure 3-12- Variation in copolymer composition (F_1) versus mole fraction of LCB catalyst (in catalyst feed) for different reactor residence times (F_1 is independent of residence time) of a copolymer made with catalyst system 1 ($k_{\beta,21} = k_{\beta,22} = 0.02\ s^{-1}$).

As stated in Figure 3-12, copolymer composition is not a function of reactor residence time. The content of 1-octene in the copolymer increases with increasing C_{LCB}/C_{tot} ratio, since the comonomer reactivity ratio for the LCB catalyst is higher than that of the linear catalyst (see Appendix B, Table 2).

Figure 3-13 shows the variations of LCB per 1000 carbon atoms as a function of LCB catalyst mole fraction at different reactor residence times for catalyst system 1.

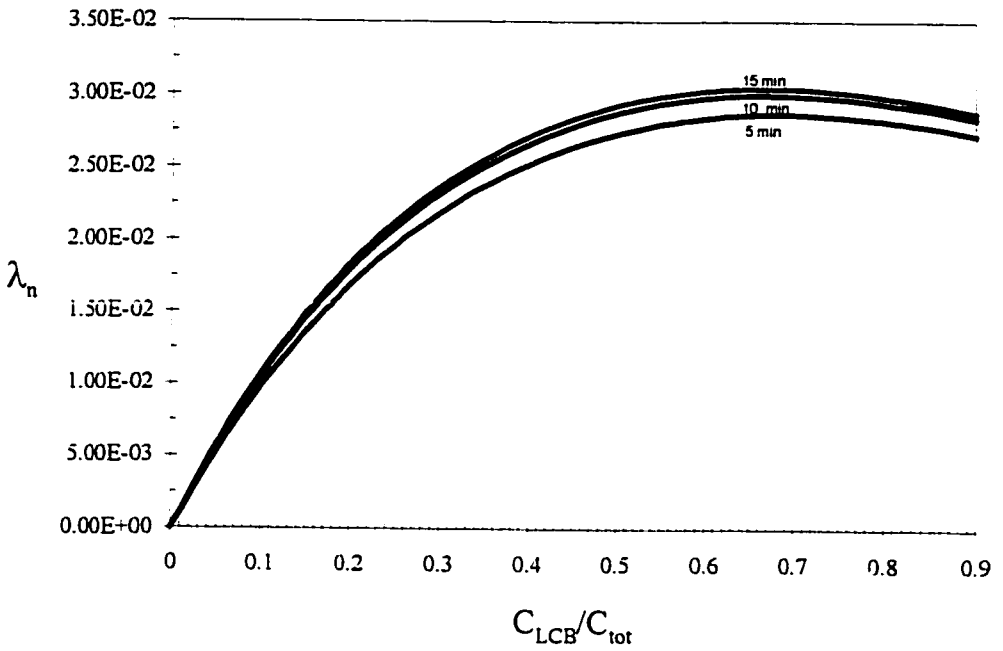

Figure 3-13- Variation in the number of branching points per 1000 carbon atoms (λ_n) versus mole fraction of LCB catalyst (in catalyst feed) for different reactor residence times of a copolymer made with catalyst system 1 ($k_{\beta,21} = k_{\beta,22} = 0.02\ s^{-1}$).

As expected, higher LCB levels are obtained at higher residence times, but by increasing the LCB catalyst mole fraction, λ_n passes through a maximum. This behavior can be related to lower macromonomer concentrations as the mole fraction of linear catalyst decreases. As mentioned, all investigated linear catalysts have higher β-hydride elimination rate constants than the LCB catalyst. Therefore, at higher mole fraction ratios of LCB catalyst, the rate of formation of macromonomers will be lower.

Figure 3-14 shows the effect of LCB catalyst mole fraction ratio for different reactor residence times on weight-average molecular weight.

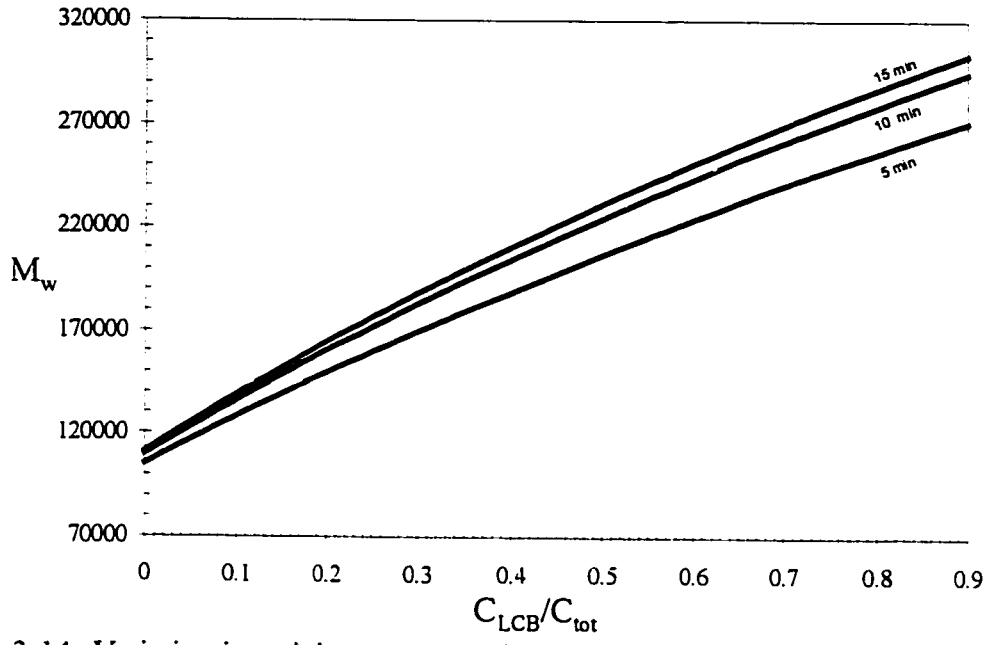

Figure 3-14- Variation in weight average molecular weight (M_w) versus mole fraction of LCB catalyst (in catalyst feed) for different reactor residence times of a copolymer made with catalyst system 1 ($k_{\beta,21} = k_{\beta,22} = 0.02\ s^{-1}$).

LCB takes place in the presence of LCB catalyst. Since higher reactor residence times favor LCB (high polymer concentration) and since LCB formation reaction increases molecular weight, higher M_w values will be obtained at higher residence times. This can explain the diverging behavior of the plots of M_w vs. C_{LCB}/C_{tot} for different reactor residence times.

Figure 3-15 illustrates the effect of LCB catalyst mole fraction for different reactor residence times on polydispersity index (PDI). As shown in this figure, as C_{LCB}/C_{tot} ratio increases, PDI passes through a maximum.

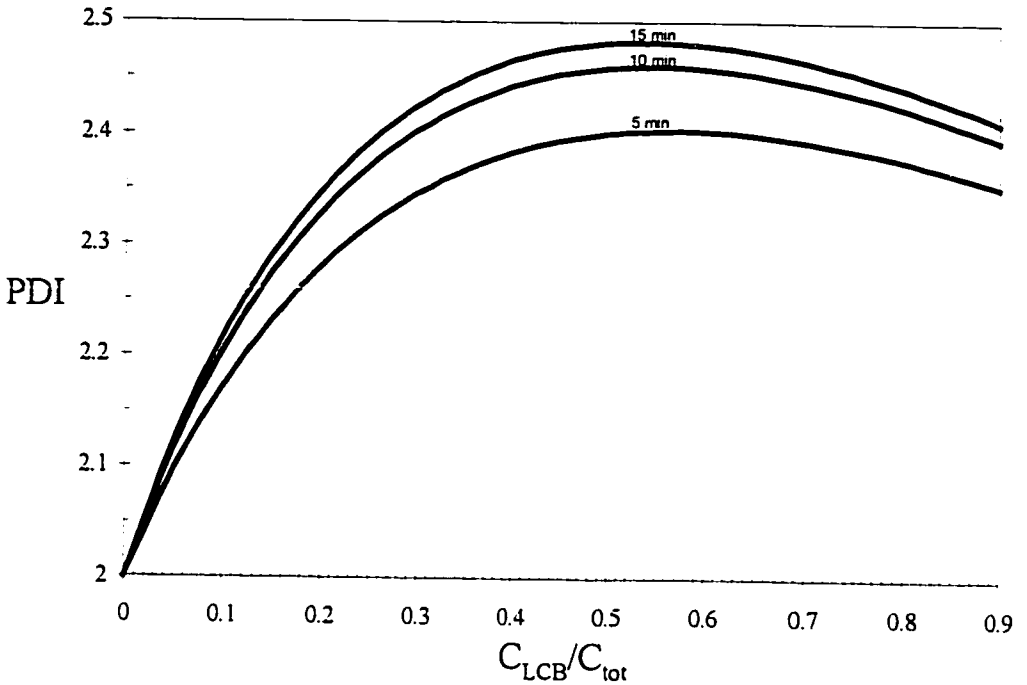

Figure 3-15- Variation in polydispersity index (PDI) versus mole fraction of LCB catalyst (in catalyst feed) for different reactor residence times of a copolymer made with catalyst system 1 ($k_{\beta,21} = k_{\beta,22} = 0.02\ s^{-1}$).

This behavior can be attributed to two phenomena. First, the β-hydride elimination rate constant considered for the linear catalyst is higher than the one of LCB catalyst (while their propagation rate constants are equal, Table 3-3 and Appendix B Table 2). Therefore, the molecular weight of chains made by the linear catalyst will be lower than the ones made with the LCB catalyst. This difference in molecular weights of polymer chains increases PDI as the molar fraction of the LCB catalyst in the catalyst inlet stream increases. By increasing the molar fraction of the LCB catalyst, after a certain C_{LCB}/C_{tot} ratio, this site type will be the major component in the combined catalyst system and as the fraction of the LCB catalyst in the catalyst inlet increases, more uniform chains will

be formed and PDI will start decreasing. Secondly, at different C_{LCB}/C_{tot} ratio values, different LCB degrees will be obtained. By increasing the C_{LCB}/C_{tot} ratio, the concentration of LCB active sites increases but the rate of formation of macromonomers decreases (due to higher β-hydride elimination reaction rate constant of linear catalysts). Therefore, the plot of PDI as a function of C_{LCB}/C_{tot} passes through a maximum value which will be in accordance with the maximum LCB formation rate.

The plots of F_1, M_w, λ_n, and PDI for the other catalyst systems follow the same trends (Figures 3-16 to 3-23) as for catalyst system 1.

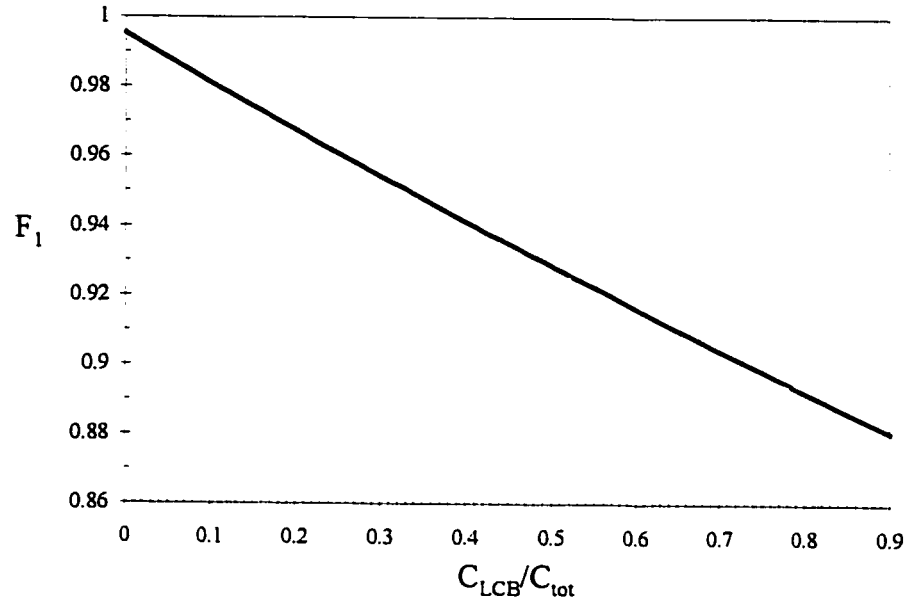

Figure 3-16- Variation in copolymer composition, F_1, versus mole fraction of LCB catalyst (in catalyst feed) for different reactor residence times of a copolymer made with catalyst system 2 ($k_{\beta,21} = k_{\beta,22} = 0.03\ s^{-1}$).

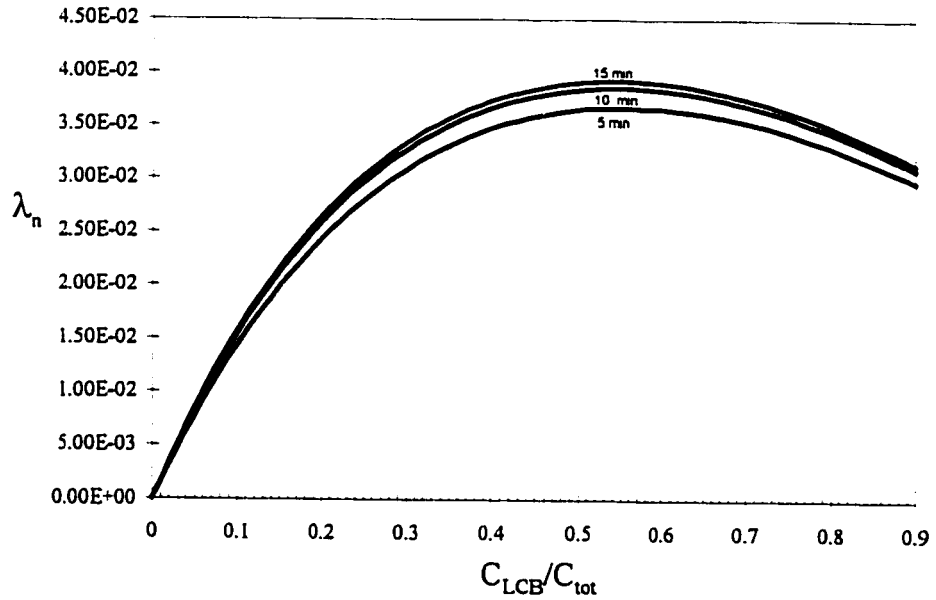

Figure 3-17- Variation in the number of branching points per 1000 carbon atoms (λ_n) versus mole fraction of LCB catalyst (in catalyst feed) for different reactor residence times of a copolymer made with catalyst system 2 ($k_{\beta,21} = k_{\beta,22} = 0.03\ s^{-1}$).

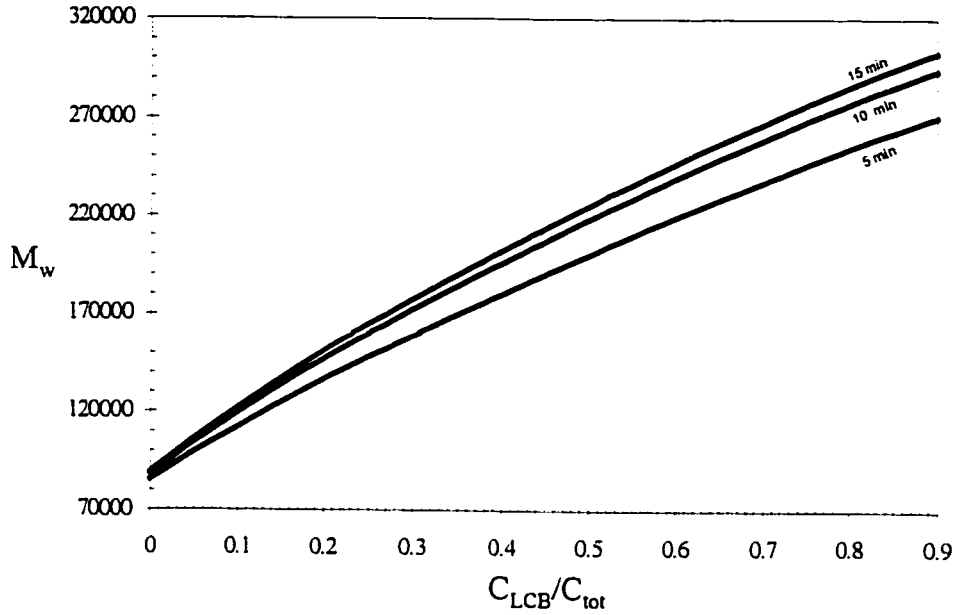

Figure 3-18- Variation in weight average molecular weight (M_w) versus mole fraction of LCB catalyst (in catalyst feed) for different reactor residence times of a copolymer made with catalyst system 2 ($k_{\beta,21} = k_{\beta,22} = 0.03\ s^{-1}$).

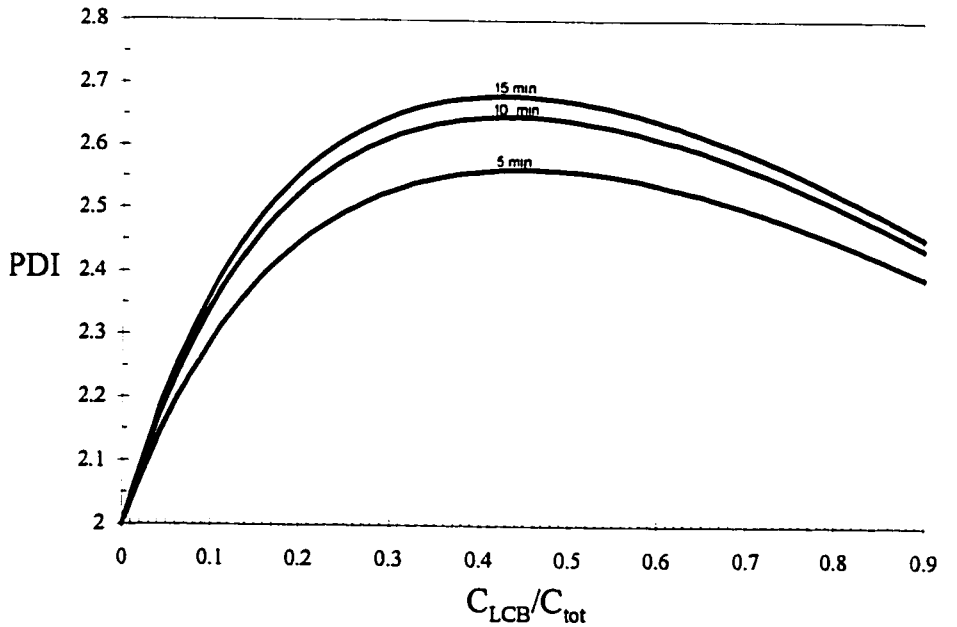

Figure 3-19- Variation in polydispersity index (PDI) versus mole fraction of LCB catalyst (in catalyst feed) for different reactor residence times of a copolymer made with catalyst system 2 ($k_{\beta,21} = k_{\beta,22} = 0.03\ s^{-1}$).

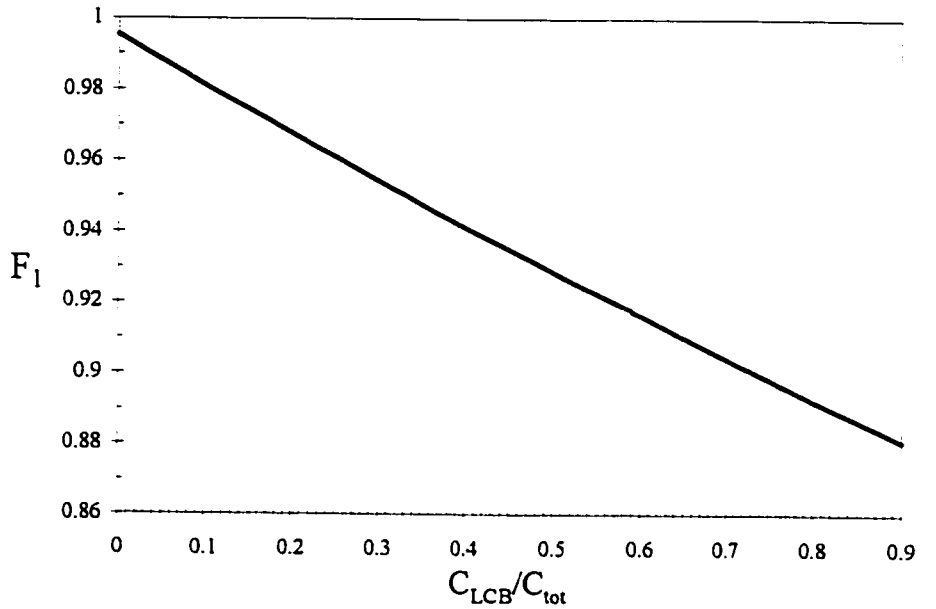

Figure 3-20- Variation in copolymer composition (F_1) versus mole fraction of LCB catalyst (in catalyst) feed for different reactor residence times of a copolymer made with catalyst system 3 ($k_{\beta,21} = k_{\beta,22} = 0.04\ s^{-1}$)

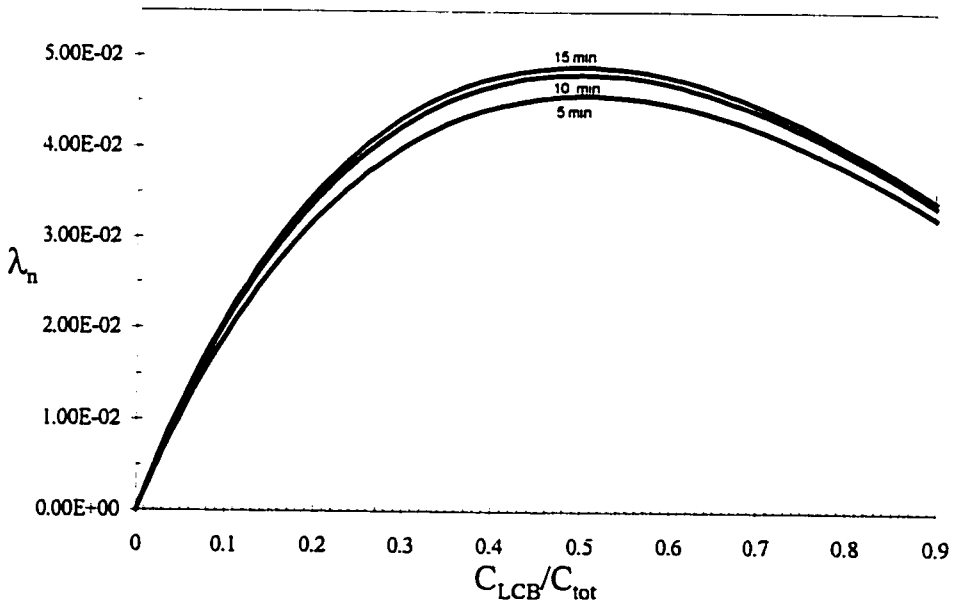

Figure 3-21- Variation in the number of branching points per 1000 carbon atoms (λ_n) versus mole fraction of LCB catalyst (in catalyst feed) for different reactor residence times of a copolymer made with catalyst system 3 ($k_{\beta,21} = k_{\beta,22} = 0.04\ s^{-1}$).

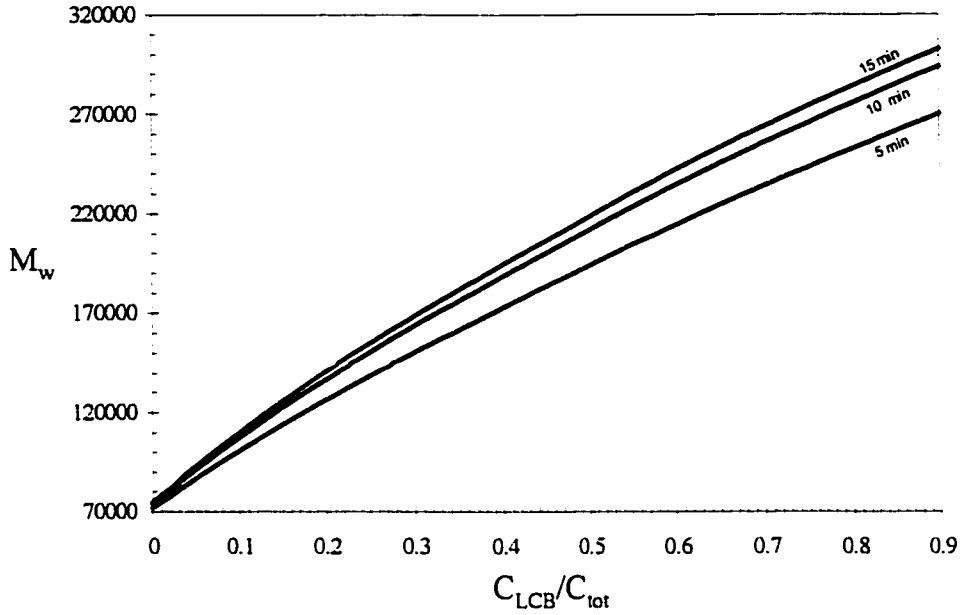

Figure 3-22- Variation in weight average molecular weight (M_w) versus mole fraction of LCB catalyst (in catalyst feed) for different reactor residence times of a copolymer made with catalyst system 3 ($k_{\beta,21} = k_{\beta,22} = 0.04\ s^{-1}$).

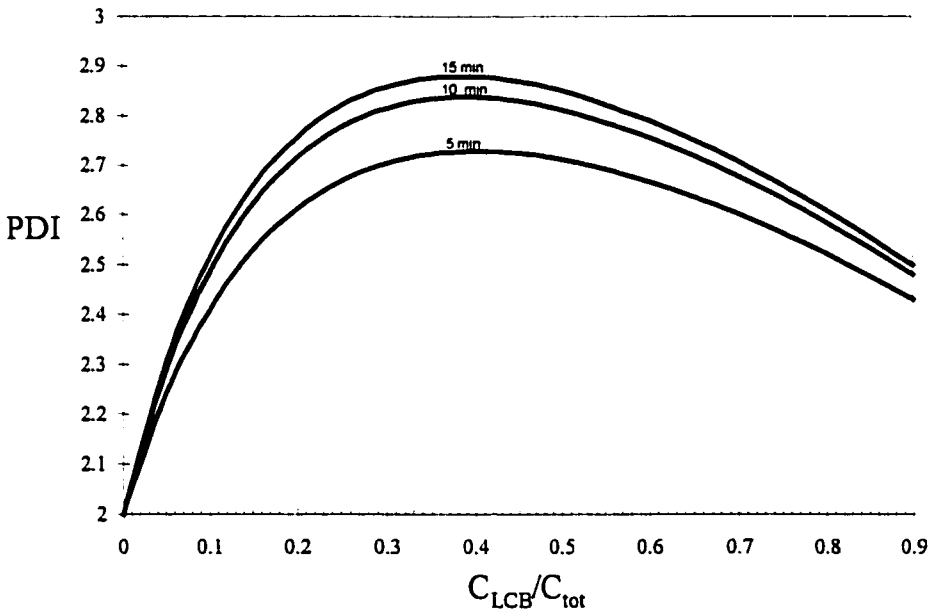

Figure 3-23- Variation in polydispersity index (PDI) versus mole fraction of LCB catalyst (in catalyst feed) for different reactor residence times of a copolymer made with catalyst system 3 ($k_{\beta,21} = k_{\beta,22} = 0.04\ s^{-1}$).

The following case studies show how recipes can be designed using the plots of F_1, λ_n, M_w, and PDI obtained for different catalyst systems. In each of these examples a particular polyolefin with certain chemical structure has been considered as the main target and suitable catalyst systems and operation conditions are determined using Figures 3-12 to 3-23.

Case study 1

An ethylene/1-octene copolymer with the following characteristics is to be synthesized in a CSTR at steady state.

Mole fraction of ethylene in copolymer, F_1: 0.96 - 0.97

Long-chain branches per 1000 carbon atoms, λ_n: >1.5E-2

Weight-average molecular weight, M_w: 150000-160000

Polydispersity Index, PDI: 2.3 - 2.4

Starting with the catalyst system 1, according to Figure 3-12, F_1 values between 0.96-0.97 correspond to C_{LCB}/C_{tot} values between 0.19-0.26, independent of reactor residence times.

According to Figure 3-13 the C_{LCB}/C_{tot} limits satisfying λ_n >1.5E-2 are shown in Table 3-4.

Table 3-4- The C_{LCB}/C_{tot} limits satisfying λ_n >1.5E-2 for catalyst system 1.

Reactor residence time (min.)	C_{LCB}/C_{tot}
5	0.17-0.90
10	0.15-0.90
15	0.14-0.90

Figure 3-14 can be used to determine suitable limits of C_{LCB}/C_{tot} at different reactor residence times for the desired weight-average molecular weight between 150,000 - 160,000. According to this figure different C_{LCB}/C_{tot} limits at different residence times satisfying the required M_w values are tabulated in Table 3-5:

Table 3-5- The C_{LCB}/C_{tot} limits satisfying $150000<M_w<160000$ for catalyst system 1.

Reactor residence time (min.)	C_{LCB}/C_{tot}
5	0.21-0.25
10	0.16-0.20
15	0.15-0.18

Figure 3-15 illustrates the variation of PDI as a function of C_{LCB}/C_{tot} at different reactor residence times. The C_{LCB}/C_{tot} limits satisfying PDI values between 2.3 - 2.4 can be obtained from this plot for different reactor residence times. These limits are summarized in Table 3-6:

Table 3-6- The C_{LCB}/C_{tot} limits satisfying $2.3<PDI<2.4$ for catalyst system 1.

Reactor residence time (min.)	C_{LCB}/C_{tot}
5	0.23-0.90
10	0.17-0.30
15	0.15-0.26

Inspection of the obtained constraints for C_{LCB}/C_{tot}, shows that catalyst system 1 can be used to produce the desired polyolefin. The conditions that satisfies the required chemical structure are:

Catalyst system 1:

RT = 5 min. C_{LCB}/C_{tot} = 0.23-0.25

RT = 10 min. C_{LCB}/C_{tot} = 0.19-0.20

As can be seen there are two conditions satisfying the desired polymer characteristics. Depending on the catalyst cost and/or limitations of the residence time, either of the above conditions can be used.

If the same type of investigation is repeated for catalyst system 2, the C_{LCB}/C_{tot} values at different residence times satisfying the required properties, summarized in Table 3-7, are obtained.

Table 3-7- The C_{LCB}/C_{tot} limits satisfying the desired polymer characteristics of Case study for catalyst system 2.

Characteristic	Reactor residence time (min.)	C_{LCB}/C_{tot}
F_1 = 0.96 - 0.97 (Fig. 3-16)	All	0.19-0.26
λ_n > 1.5E-2 (Fig. 3-17)	5	0.11-0.90
	10	0.10-0.90
	15	0.09-0.90
M_w = 150000 - 160000 (Fig. 3-18)	5	0.26-0.31
	10	0.21-0.25
	15	0.20-0.24
PDI = 2.3 - 2.4 (Fig. 3-19)	5	0.11-0.17
	10	0.09-0.14
	15	0.08-0.12

As can be seen, there is no common operating conditions satisfying all of the required values. For example, F_1 limits require C_{LCB}/C_{tot} values between 0.19-0.26. But, none of the C_{LCB}/C_{tot} limits satisfying PDI = 2.3-2.4 are in the same range.

Repeating this investigation for catalyst system 3, the C_{LCB}/C_{tot} values at different residence times satisfying the required properties can be summarized in Table 3-8.

As for catalyst system 2, there is no common operating conditions satisfying all of required values. For example, F_1 limits requires C_{LCB}/C_{tot} values between 0.19-0.26. But, none of the C_{LCB}/C_{tot} limits satisfying PDI = 2.3-2.4 are in the same range.

Table 3-8- The C_{LCB}/C_{tot} limits satisfying the desired polymer characteristics of Case study 1 for catalyst system 3.

Characteristic	Reactor residence time (min.)	C_{LCB}/C_{tot}
F_1 = 0.96 - 0.97 (Fig. 3-20)	all	0.19-0.26
λ_n > 1.5E-2 (Fig. 3-21)	5	0.08-0.90
	10	0.07-0.90
	15	0.06-0.90
M_w = 150000 - 160000 (Fig. 3-22)	5	0.30-0.35
	10	0.25-0.29
	15	0.24-0.27
PDI = 2.3 - 2.4 (Fig. 3-23)	5	0.07-0.10
	10	0.05-0.08
	15	0.04-0.07

Case study 2:

An ethylene/1-octene copolymer with the following characteristics is to be synthesized in a CSTR at steady state.

Mole fraction of ethylene in copolymer , F_1: 0.89 - 0.90

Long-chain branches per 1000 carbon atoms, λ_n: >3.5E-2

Weight-average molecular weight, M_w: 260000-270000

Polydispersity Index, PDI: 2.5 - 2.6

Starting with the catalyst system 1 and doing the same type of investigation as in Case study 1, the C_{LCB}/C_{tot} values at different residence times satisfying the required properties, are tabulated in Table 3-9:

Table 3-9- The C_{LCB}/C_{tot} limits satisfying the desired polymer characteristics of Case study 2 for catalyst system 1.

Characteristic	Reactor residence time (min.)	C_{LCB}/C_{tot}
F_1 = 0.89 - 0.90 (Fig. 3-12)	all	0.74-0.83
λ_n > 3.5E-2 (Fig. 3-13)	5	not applicable
	10	not applicable
	15	not applicable
M_w = 260000 - 270000 (Fig. 3-14)	5	0.81-0.88
	10	0.69-0.75
	15	0.65-0.70
PDI = 2.2 - 2.3 (Fig. 3-15)	5	not applicable
	10	not applicable
	15	not applicable

As can be seen, there is no common operating conditions satisfying all of the required values. Therefore, catalyst system 1 can not be employed to synthesize the desired polyolefin.

If the same sort of investigation is done for catalyst system 2, the C_{LCB}/C_{tot} values at different residence times satisfying the required properties can be summarized in Table 3-10:

Inspection of the obtained constraints for C_{LCB}/C_{tot} in this table, shows that catalyst system 2 can be employed in the production of the desired polyolefin. The conditions that satisfy the required chemical structure are:

Catalyst system 2:

RT = 10 min. C_{LCB}/C_{tot} = 0.74 - 0.78

Table 3-10- The C_{LCB}/C_{tot} limits satisfying the desired polymer characteristics of Case study 2 for catalyst system 2.

Characteristic	Reactor residence time (min.)	C_{LCB}/C_{tot}
F_l = 0.89 - 0.90 (Fig. 3-16)	all	0.74-0.83
λ_n > 3.5E-2 (Fig. 3-17)	5	0.41-0.72
	10	0.36-0.78
	15	0.34-0.80
M_w = 260000 - 270000 (Fig. 3-18)	5	0.82-0.90
	10	0.73-0.78
	15	0.67-0.72
PDI = 2.5 - 2.6 (Fig. 3-19)	5	0.29-0.70
	10	0.19-0.29
		0.63-0.81
	15	0.17-0.25
		0.68-0.84

Doing the same type of investigation on catalyst system 3, the C_{LCB}/C_{tot} values at different residence times satisfying the required properties are tabulated in Table 3-11:

Table 3-11- The C_{LCB}/C_{tot} limits satisfying the desired polymer characteristics of Case study 2 for catalyst system 3.

Characteristic	Reactor residence time (min.)	C_{LCB}/C_{tot}
F_l = 0.89 - 0.90 (Fig. 3-20)	all	0.74-0.83
λ_n > 3.5E-2 (Fig. 3-21)	5	0.24-0.85
	10	0.22-0.87
	15	0.21-0.88
M_w = 260000 - 270000 (Fig. 3-22)	5	0.83-0.90
	10	0.72-0.79
	15	0.68-0.73
PDI = 2.5 - 2.6 (Fig. 3-23)	5	0.71-0.83
	10	0.78-0.89
	15	0.81-0.90

The obtained C_{LCB}/C_{tot} limits show that catalyst system 3 can be employed in production of the desired polyolefin. The conditions that satisfy the required chemical structure are:

Catalyst system 3:

1) RT = 5 min. $C_{LCB}/C_{tot} = 0.83$

2) RT = 10 min. $C_{LCB}/C_{tot} = 0.78\text{-}0.79$

Catalyst systems 2 and 3 can be used for synthesizing the required polyolefin in Case study 2. Depending on the availability of the catalyst types and economical feasibility, catalyst systems 2 or 3 might be used. For the case of catalyst system 2, there are two process conditions to choose. Depending on the efficiency, prices of the two metallocene catalysts, and other economical and/or operational limitations of the process, either of the conditions can be selected.

3-2- LCB Formation in Ethylene Polymerization.

A Simple Model for Semi-Batch Reactors

In this section a simple model for long-chain branch formation in ethylene homopolymerizatin using combined catalyst systems is presented. The main purpose of developing such a model is to find an analytical expression that describes how LCB frequency varies with catalyst system characteristics. This can become a useful tool to quickly select catalyst combinations that produce polymer with an optimum LCB frequency. However, this simple model does not predict molecular weights.

3-2-1- Polymerization Mechanism and Kinetics

In this model, the following steps for the homopolymerization of ethylene are considered: propagation, transfer to monomer, β-hydride elimination, and long chain branch formation. Based on these steps, the reaction mechanism can be presented as:

Propagation:

$$P_n + M \rightarrow P_{n+1} \qquad k_{p1}$$

$$Q_n + M \rightarrow Q_{n+1} \qquad k_{p2}$$

Chain Transfer Reaction:

$$P_n \rightarrow D_n^{=} + P_0 \qquad k_{\beta 1}$$

$$Q_n \rightarrow D_n^{=} + Q_0 \qquad k_{\beta 2}$$

$$P_n + M \rightarrow D_n^{=} + P_1 \qquad k_{fm1}$$

$$Q_n + M \rightarrow D_n^{=} + Q_1 \qquad k_{fm2}$$

Long-chain branching:

$$P_n + D_m^{=} \rightarrow P_{n+m} \qquad k_{LCB}$$

where:

$D^{=}$ = Macromonomer concentration

M = monomer concentration

C = Total catalyst concentration

P = CGC active sites concentration

Q = linear catalyst active sites concentration

k_{pi} propagation rate constant for site-type i.

$k_{\beta i}$ β-hydride elimination rate constant for site-type i.

k_{fmi} transfer to monomer rate constant for site-type i.

k_{LCB} long-chain branch formation rate constant for.

According to the above polymerization mechanism, the rate of macromonmer formation can be expressed as:

$$\frac{dD^{=}}{dt} = \left(k_{\beta 1} + k_{fm1}M\right)P + \left(k_{\beta 2} + k_{fm2}M\right)Q - k_{LCB}P\,D^{=} \qquad (3\text{-}31)$$

Let r represent the mole fraction of CGC in catalyst mixture, therefore:

$$r = P/C \qquad \Rightarrow \qquad P = r\,.\,C \qquad (3\text{-}32)$$

Substituting Equation (3-32) into (3-31) and with some algebraic manipulation the following expressions can be easily obtained:

$$\frac{dD^{=}}{dt} = \left(k_{\beta 1} + k_{fm1}M\right)P + \left(k_{\beta 2} + k_{fm2}M\right)(C - P) - k_{LCB}P\,D^{=} \tag{3-33}$$

$$\frac{dD^{=}}{dt} = \left[\left(k_{\beta 1} + k_{fm1}M\right) - \left(k_{\beta 2} + k_{fm2}M\right)\right]P + \left(k_{\beta 2} + k_{fm2}M\right)C - k_{LCB}P\,D^{=} \tag{3-34}$$

$$\frac{dD^{=}}{dt} = C\left\{\left[\left(k_{\beta 1} + k_{fm1}M\right) - \left(k_{\beta 2} + \dot{k}_{fm2}M\right)\right]r + k_{\beta 2} + k_{fm2}M - k_{LCB}\,r\,D^{=}\right\} \tag{3-35}$$

Considering the fact that, in semi-batch polymerization of ethylene the monomer pressure and therefore its concentration are considered constant, Equation (3-35) turns into an ordinary differential equation with separable variables, that can be easily integrated using the following initial conditions:

$$D^{=} = 0 \qquad at \qquad t = 0 \tag{3-36}$$

Consequently, the time variation of macromonomer concentration can be expressed as:

$$D^{=} = \frac{\left[\left(k_{\beta 1} + k_{fm1}M\right) - \left(k_{\beta 2} + k_{fm2}M\right)\right]r + k_{\beta 2} + k_{fm2}M}{k_{LCB}\,r}\left[1 - \exp(-k_{LCB}\,C\,r\,t)\right] \tag{3-37}$$

The average number of long-chain branches per 1000 carbon atoms at any time is proportional to the ratio of the total number of LCBs formed to the total number of monomers incorporated, therefore:

$$\overline{\lambda}_n = 500\frac{\int_0^t k_{LCB}PD^{=}dt}{\int_0^t M\left(k_{p1}P + k_{p2}S\right)dt} = 500\frac{\int_0^t k_{LCB}\,r\,D^{=}dt}{\int_0^t M\left[\left(k_{p1} - k_{p2}\right)r + k_{p2}\right]dt} \tag{3-38}$$

Substituting $D^{=}$ form Equation (3-37) into (3-38) results in:

$$\bar{\lambda}_n = 500\frac{\int_0^t \left\{\left[\left(k_{\beta 1}+k_{fm1}M\right)-\left(k_{\beta 2}+k_{fm2}M\right)\right]r+k_{\beta 2}+k_{fm2}M\right\}\left[1-\exp\left(-k_{LCB}\,C\,r\,t\right)\right]dt}{\int_0^t M\left[\left(k_{p1}-k_{p2}\right)r+k_{p2}\right]dt}$$

(3-39)

The number of branches per 1000 carbon atoms can be easily calculated by integrating the numerator and the denominator of Equation (3-39):

$$\bar{\lambda}_n = 500\times\frac{\left[\left(k_{\beta 1}+k_{fm1}M\right)-\left(k_{\beta 2}+k_{fm2}M\right)\right]\ r+k_{\beta 2}+k_{fm2}M}{M\left[\left(k_{p1}-k_{p2}\right)r+k_{p2}\right]\ t}\left[t-\frac{1-\exp\left(-k_{LCB}\,C\,r\,t\right)}{k_{LCB}\,C\,r}\right]$$

(3-40)

Equation (3-40) is an analytical expression for LCB degree as a function of catalyst system characteristics. This equation can be used to investigate how LCB degree varies with the type and composition of the combined catalyst system, at constant reaction conditions (constant temperature and pressure).

3-2-2- Results and Discussions

In this simulation, homopolymerization of ethylene using two site-type metallocene catalysts in a semi-batch reactor were studied. Typical values for ethylene polymerization kinetic parameters, used in computer simulation, are given in Table 3-12.

Five different catalyst systems have been considered. The same branching catalyst (CGC) has been considered for all five catalyst systems. These linear catalysts are distinguished only by the differences in their $k_{\beta 2} + k_{fm2}M$ kinetic parameters, which are given in Table 3-13. All other rate constants are assumed to remain constant.

Table 3-12- Values of kinetic constants and reaction conditions used in simulation.

k_{p1}	4000 *L/mol·s*
k_{p2}	4000 *L/mol·s*
$k_{\beta 1} + k_{fm1}M$	0.1 s^{-1}
k_{LCB}	600 *L/mol·s*
C	4 *μmol/L*
M	0.9 *mol/L*
t (polymerization time)	600 *s*

Table 3-13- Values of $k_{\beta 2} + k_{fm2}M$ for different linear catalysts.

Catalyst System	$k_{\beta 2} + k_{fm2}M$
Linear catalyst 1	0.05 s^{-1}
Linear catalyst 2	0.1 s^{-1}
Linear catalyst 3	0.2 s^{-1}
Linear catalyst 4	0.3 s^{-1}
Linear catalyst 5	0.5 s^{-1}

The values of the kinetic constants and reaction conditions mentioned in Tables 3-12 and 3-13 were substituted in Equation (3-40) and the values of LCB frequency, λ_n, versus the mole fraction of CGC in the catalyst mixture, r, for all five catalyst systems were plotted in Figure 3-24. The numbers appearing on the curves correspond to the catalyst systems used.

The linear catalyst used in catalyst system 1 has a lower $k_\beta + k_{fm}M$ than CGC. This means lower rate of macromonomer formation and therefore lower macromonomer concentration, which translates to lower long-chain branching degree. Curve 1 in Figure 3-24 corresponds to this catalyst system and, as expected, higher amounts of linear catalyst cause lower branching degrees.

Catalyst system 2 uses a linear catalyst with the same $k_\beta + k_{fm}M$ value as CGC which means that the linear catalyst generates macromonomer with the same rate as CGC does. In this system, although varying the catalyst composition does not alter the macromonomer concentration, it certainly changes the concentration of branching catalyst, which results in lower LCB frequencies at higher linear catalyst fractions. This is illustrated in curve 2 where LCB degree obtained at $r = 1$ has the highest value.

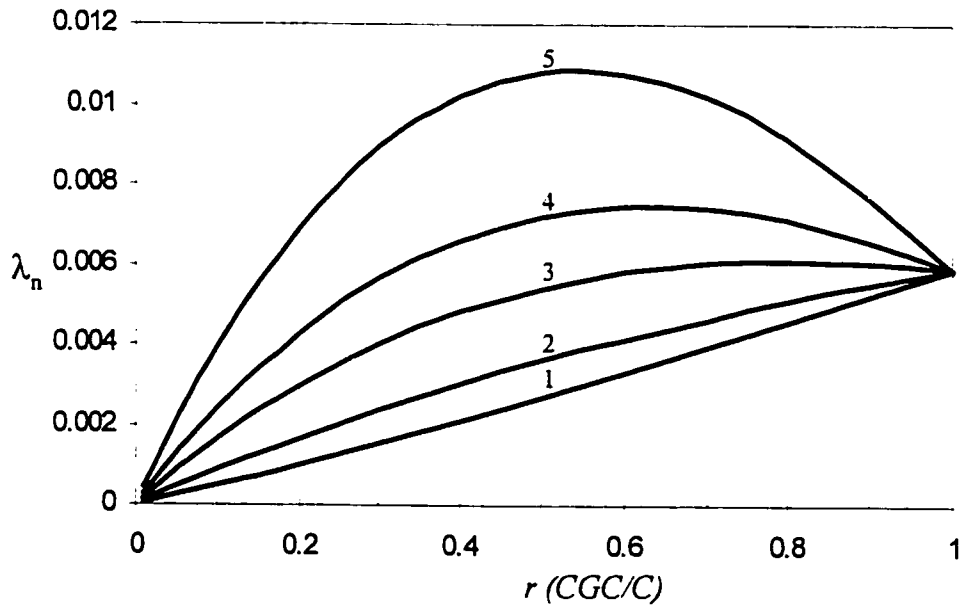

Figure 3-24- Plot of Equation (3-40) for the five tested catalyst systems.

Curves 3, 4, and 5 correspond to the catalyst systems with higher $k_\beta + k_{fm}M$ than CGC. No branching was observed when only linear catalysts were used. As the mole fraction of CGC in the binary catalyst system increases, the LCB frequencies increase up to a maximum point. The decrease in LCB frequency by increasing the mole fraction of CGC is attributed to the lower rate of macromonomer formation as all the linear catalysts in these systems have higher rate of macromonomer formation than CGC. Therefore, at higher mole fractions of CGC, the rate of formation of macromonomers will be lower resulting in lower LCB degrees. The existence of optimum LCB values as a fraction of CGC is in agreement with modeling results obtained in Section 3-1 (Figures 3-13, 3-17, 3-21).

Important insights can be obtained from the application of this simple model: First, in order to increase LCB frequency using combined catalyst systems, the linear catalyst must have a higher rate of macromonomer production than CGC. Second, provided the first condition is met, there is an optimum composition for every combined catalyst system that maximizes the content of long-chain branches.

3-3- Modeling of Branch Structure in CGC Polymerization Systems.

With the development of homogeneous constrained geometry catalyst (CGC) systems, production of ethylene polymers having long-chain branches has become possible. The unique molecular structure of these polymers delivers improved melt viscosity characteristics without sacrificing physical properties (Swogger and Kao 1993). Despite the extensive research performed on the characteristics of CGC polymerization systems and CGC polymers by different research groups, the branching structure in these resins has not been studied extensively.

Generally, two types of branched chains may be assumed to be present in CGC polyethylene resins. 1) Chains with comb-like branches, which only contain main branches directly connected to the main chain backbone, and 2) Dendritic (hyper-branched) chains containing main branches, and branches on branches (connected to the main branches). The schematics of these chains are illustrated in Figure 3-25.

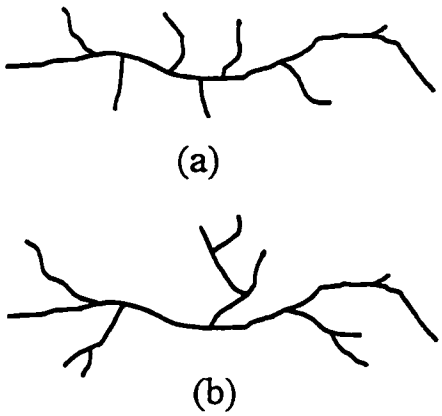

Figure 3-25: Schematic of the possible structure of branched chains synthesized with CGC systems, (a) comb-like branched chain, (b) dendritic (hyper-branched) chain.

Apparently, the presence and amount of either type of these branched chains affect the physical and rheological properties of the polymer (Brant and Canich 1995, Brant et al. 1995). Therefore, in order to find structure-property correlations it is essential to have a good understanding of the branching structure of the polymer. The present section is an attempt to visualize the branching structure in polyethylene resins synthesized by CGC systems (Beigzadeh et al. 1999b). The obtained branching structure is a logical consequence of the currently accepted polymerization mechanism.

The main mechanism for LCB formation in the CGC polymerization systems as proposed by Lai et al. (1993, 1997) and expanded by others (Soares and Hamielec 1996, 1997; Beigzadeh et al. 1997,1999) is the incorporation of macromonomers. These macromonomers are being made in-situ as the polymerization is carried out. Considering the proposed branching mechanism, Monte Carlo simulation can be employed to simulate branched chains. These simulated chains will then be studied further to investigate the branching structure in CGC polyethylene resins.

3-3-1- Model Development

In metallocene polymerizations, the β-hydride elimination reaction is the main mechanism for in-situ macromonomer formation. These macromonomers, which usually contain terminal unsaturations can add to the active sites and form long chain branches, as discussed extensively in previous sections.

Based on the above-mentioned mechanism, a Monte Carlo model was developed to simulate the microstructure of the branched polyethylene resins synthesized with CGC systems. The flow chart of the computer program is shown in Figure 3-26.

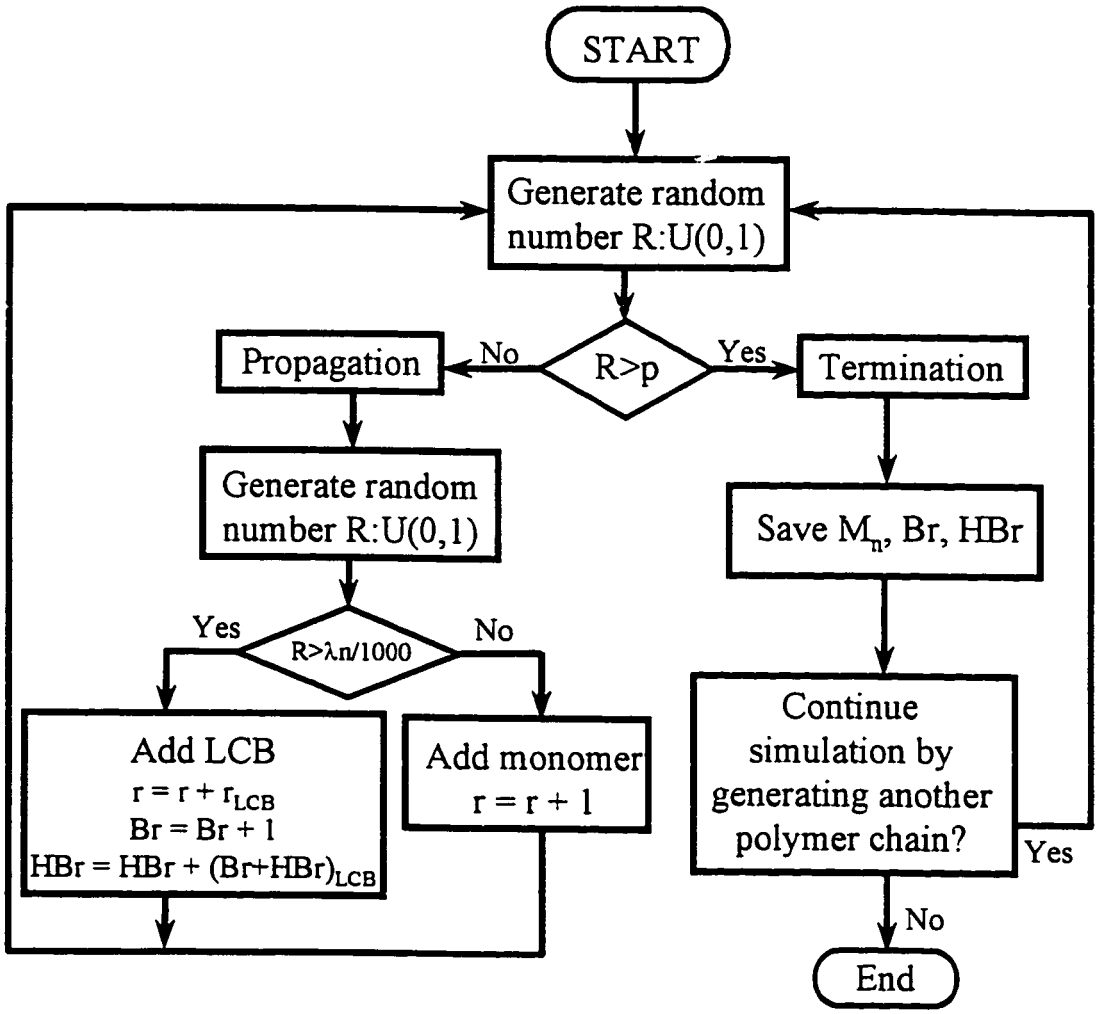

Figure 3-26- Flow chart of the computer program for the Monte Carlo model. M_n: number average molecular weight, r: chain length, LCB: long-chain branch, Br: number of main branches, HBr: number of branches on branches (hyper branches).

The number average chain length, X_n, is related to the propagation probability, p, by the following equation (3-42): (Flory 1953)

$$X_n = \frac{1}{1-p} \tag{3-42}$$

Therefore, the propagation probability can be easily calculated by rearranging Equation (3-42) :

$$p = \frac{X_n - 1}{X_n} \tag{3-43}$$

Three hundred thousand chains with propagation probability of p = 0.9997 and average branching frequency of λ_n = 0.1 (one branch per 10000 carbon atoms) were simulated.

As illustrated in the flow chart, the generated random number, R_1, is compared with the propagation probability, p, determining whether or not the chain propagates. In the case of propagation, another random number is generated to determine whether monomer addition or branching takes place. In the case of branching, one of the previously simulated chains is randomly selected as the macromonomer to be incorporated as a branch. With the incorporation of each macromonomer, the number of the main branches of the chain being simulated is increased by one unit. All main branches, and branches on branches of the incorporated macromonomer are counted as branches on branches for the propagating chain. Therefore, the increase in the number of branches on branches can be easily calculated by adding the number of main branches, and branches on branches of the incorporated macromonomer. At the termination of each chain, the molecular weight (M_n), the number of main branches (Br), and the number of branches on branches (HBr) are recorded.

3-3-2- Results and Discussion

Figure 3-27 compares the weight distribution of a branched polymer with that of a linear polymer (Schultz-Flory distribution) simulated with the same propagation probability. The existence of a tail in the high molecular weight region of the branched polymer distribution is evident. It is clear that terminal branching distorts the molecular weight distribution towards higher molecular weights.

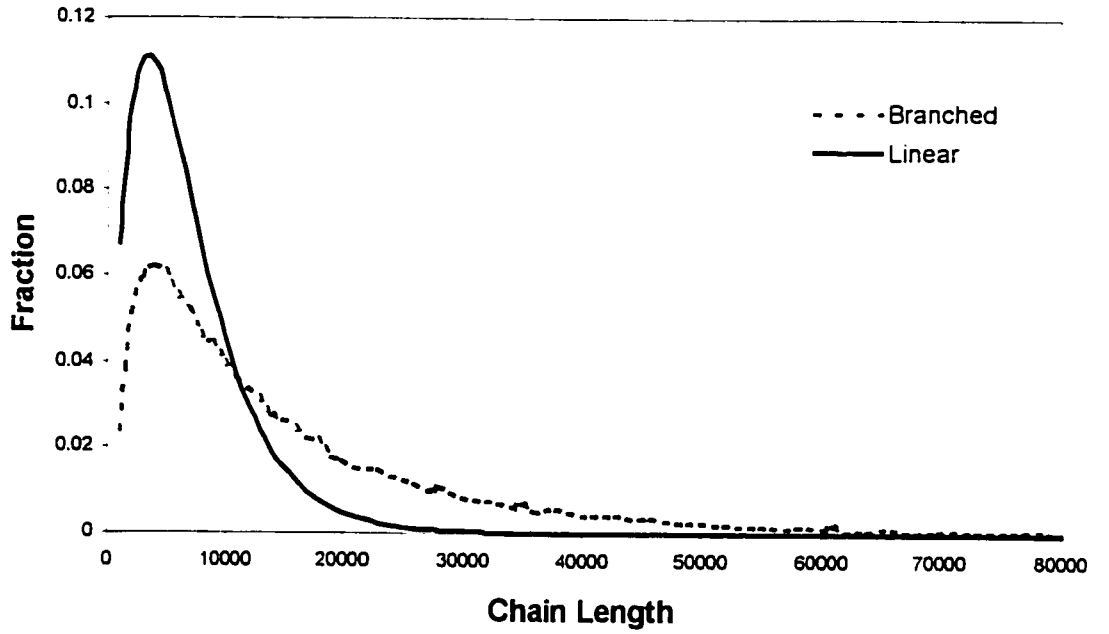

Figure 3-27- Weight distributions of a branched chain and a linear chain simulated with the same propagation probability. $p = 0.9997$, $\lambda_n = 0.1$.

Figure 3-28 compares the weight distribution of all chains, including linear, comb-like, and hyper-branched chains, with the weight distribution of the branched chains (comb-like and hyper-branched) only. Seemingly, from chain lengths of around 23000 and higher, the two distributions are the same. This suggests that almost all of the chains having chain lengths greater than 23000 are branched.

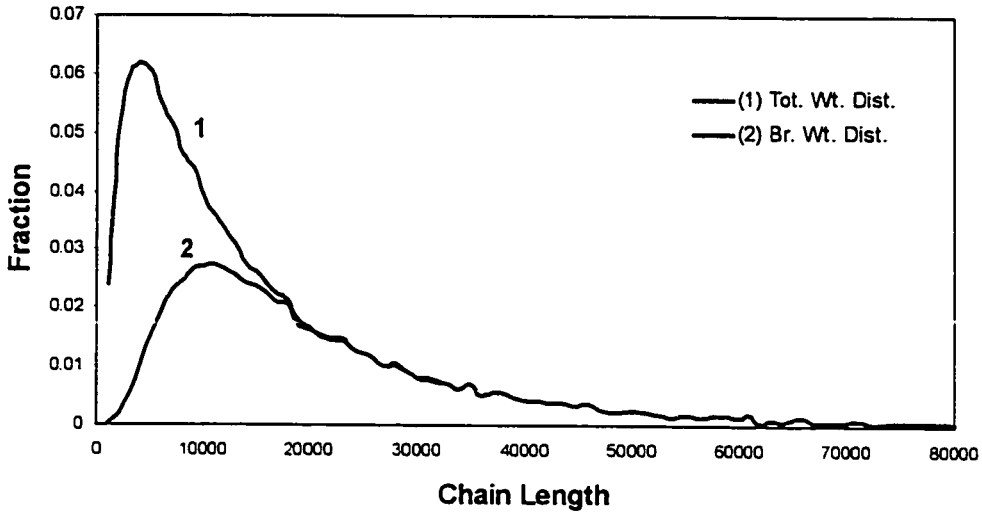

Figure 3-28- The comparison of total weight distribution with the weight distribution of branched chains. $p = 0.9997$, $\lambda_n = 0.1$.

Figure 3-29 adds the weight distribution of dendritic (only hyper branched) chains to the distributions shown in Figure 3-28. Similar to the trends observed in Figure 3-28, from chain lengths of around 30000 and after, the distribution of dendritic chains overlays with the total and branched chains distributions. Apparently, almost all of the chains with chain lengths greater than 30000 are hyper-branched.

Finally, Figure 3-30 illustrates the weight distribution of different branching structures. The concentration of highly dendritic chains with up to eight main branches and 25 branches on branches is non-zero in this figure. Although the amount of these chains is not high, very small amounts of these highly branched chains may significantly affect rheological properties (Kim, 1998; Khadir and Gauthier, 1997a,b).

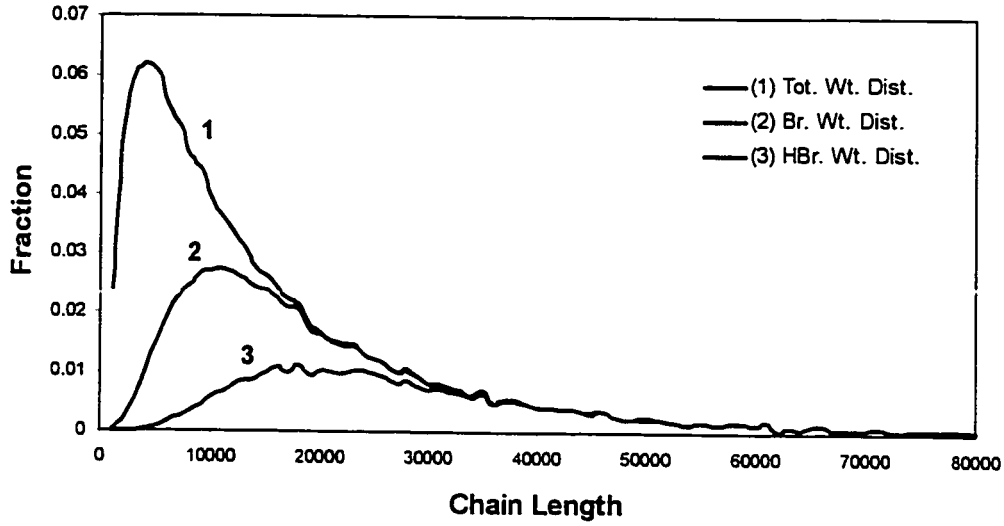

Figure 3-29- The comparison of total weight distribution with the weight distributions of branched and hyper-branched chains. $p = 0.9997$, $\lambda_n = 0.1$.

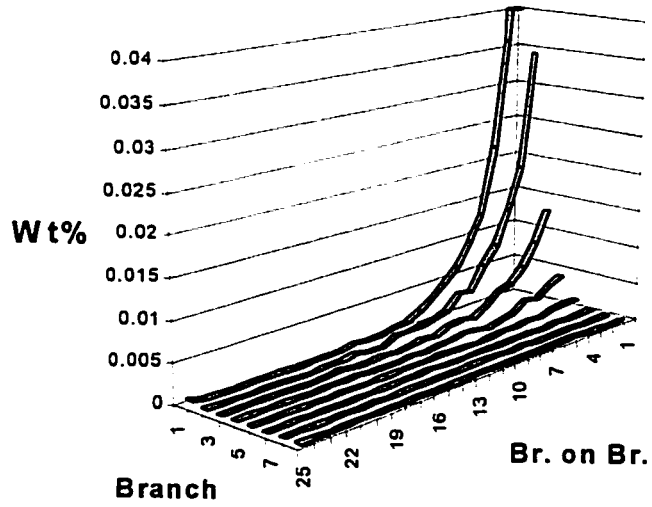

Figure 3-30- Weight distribution of chains having different branching structures. $p = 0.9997$, $\lambda_n = 0.1$.

3-3-3- Concluding Remarks

The branching structure of polyethylene resins synthesized with constrained geometry catalyst systems was studied using a Monte Carlo model (Beigzadeh et al. 1999b). It was found that terminal branching distorted the molecular weight distribution and generated a tail in the high molecular weight region, as compared to the linear polyethylene resins.

It was also shown that comb-like (chains with only main branches) and dendritic (chains with branches on branches) branched chains were formed in CGC polymerization systems and also that the observed tail in the high molecular weight region of the molecular weight distribution could be attributed to the existence of these branched chains. Perhaps the enhanced rheological properties of CGC polyethylene resins could be explained by the presence of these hyper-branched, high molecular weight chains, since in many applications, high molecular weight, highly-branched polymers are used as viscosity modifiers (Kim, 1998; Khadir and Gauthier, 1997a,b).

Chapter 4

Characterization

4-1- Introduction

The degree of long-chain branching, along with molecular weight and chemical composition, is one of the fundamental parameters needed to fully describe polymer structure and melt-processing properties (Van Krevelen 1990). Since the fundamental work of Zimm and Stockmayer (1949), the influence of long-chain branching on polymer properties has been studied extensively (Meira 1991) and over the years its importance has become increasingly apparent.

The purpose of this chapter is to explain the techniques used to analyze the synthesized polymer samples for their microstructure characteristics. Gel permeation chromatography will be first studied. This technique can be used for molecular weight distribution (MWD) measurements. It will also be explained how multi-detector GPC instruments can be used to estimate long chain branching frequency. ^{13}C-NMR

spectroscopy will then be discussed. This technique can be used to measure long chain branching frequencies of polyethylene samples and also comonomer content of ethylene/α-olefin copolymers.

4-2- Gel Permeation Chromatography

Gel permeation chromatography (GPC) is an acronym in wide usage for the chromatographic separation of macromolecules according to their size. The term size exclusion chromatography (SEC) is the general name for this process, emphasizing the mechanism of separation rather than directing attention to a particular class of column-packing materials (gels) or macromolecules. GPC is a liquid column chromatographic technique in which a sample solution is introduced onto a column filled with a rigid porous gel and is carried through the column by a solvent. Ideally, size separation is achieved by differential pore permeation. All molecules experience a solute-to-wall exclusion effect inside the pore. Because of greater steric interference, the larger molecules are kept away from the wall of the pore. The volume of the pore, which is effectively accessible, is thus greater for a small molecule than for a large one. As a result, small molecules stay longer in the column than large molecules, or in other words molecules with different sizes have different retention volumes. Clearly, if V, the retention volume, can be directly related to MW by means of an appropriate calibration, then in principle a chromatogram can be made easily to yield MW averages and distributions. The details of the instrument and different calibration techniques have been discussed elsewhere (Glockner 1986, Mitchell 1987, Cooper 1989, and Kroschwitz 1990).

The key to a successful and useful GPC analysis is the choice of appropriate detectors. There are several types of detectors available for GPC which are used to continuously monitor the column effluent through measurement of some physical property of what is essentially a very dilute polymer solution. Differential refractometry, spectrophotometry, light scattering photometry, and viscometry are the most commonly used detectors (Cooper 1989).

The advantages of GPC over other techniques of MW determination are the simplicity of the operation and the ability to yield MWDs as well as MW averages. A great disadvantage, however, is that unless a molecular weight detector is coupled to the instrument, GPC cannot be used as an absolute method. Rather, a calibration procedure must be used, which in practice can present considerable difficulties.

The simplest type of calibration is the peak-position calibration. The calibration curve is established experimentally by relating the peak-retention volume to molecular weight for a series of known narrow standards. The details of the calibration procedure are explained elsewhere (Cooper 1989). Although this is a very simple method, such calibrations are valid only for the same polymer-solvent-temperature combination.

Universal calibration, which is the most commonly used calibration method, is a rigorous method to transform the polymer standard peak-position calibration curve to a suitable curve characterizing different polymer types (Grubisic et al. 1967). This method utilizes the hydrodynamic volume of polymeric molecules and can be expressed in terms of the product of the molecular weight, MW, and the intrinsic viscosity, $[\eta]$. In general, GPC universal calibration curves for different types of polymers merge into a single plot

when the calibration data are plotted as log[η]MW versus retention volume (Grubisic et al. 1967). The details of the calibration procedure can be found elsewhere (Cooper 1989).

4-2-1 Determination of LCB Degree Using Multi-Detector GPC

Long-chain branching can be determined experimentally by multi-detector gel-permeation chromatography. The basis for all GPC-related methods is the universal retention volume-hydrodynamic volume relation (universal calibration) proposed by Grubisic et al. (1967). However, branched molecules have a smaller hydrodynamic volume than linear molecules and thus will elute in GPC with lower molecular weight linear molecules. Therefore the true molecular weight distribution (MWD) of branched chains is different from that obtained with a calibration curve for linear molecules (Ram and Miltz 1971). Specifically, the GPC-viscometry method which has been most widely used has the problem of establishing the intrinsic viscosity-molecular weight relationship suitable for a particular branched resin.

The most prevailing relationship between the intrinsic viscosity and the molecular weight is the simple Mark-Houwink equation, which presents the intrinsic viscosity as a power-law function of molecular weight. However, intrinsic viscosity behavior departs seriously from the Mark-Houwink equation at both low and very high molecular weights (Van Krevelen 1990). Also, the behavior of branched polymers does not always follow this relation. One approach to solve this problem is the Ram-Miltz (1971) procedure, which is based on the assumption that the relationship between the intrinsic viscosity and molecular weight for a branched polymer can be described by a polynomial expression when the molecular weight is above a certain threshold value, M_0. However, the

shortcoming for the Ram-Miltz method may stem from the fact that the threshold value M_0, beyond which the branching occurs, is not an intrinsic property of the polymer and can be markedly different for the same polymer prepared by different synthetic methods. Based on the polynomial expression proposed by Ram and Miltz (1971), Jin and Guo (1990) developed a procedure by which LCB and M_0 for a particular resin could be simultaneously evaluated. However, their procedure required a tedious combination of trial and error and graphical analysis.

Mirabella and Wild (1990) employed a multi-detector high-temperature GPC equipped with concentration and viscometer detectors to determine the long-chain branching distribution (LCBD) of a number of commercial polyethylene samples. They showed that the GPC-viscometry technique is suitable for the determination of LCB and LCB distribution (LCBD) of the polyethylene resins. They reported that this technique could be reliably applied only when the molecular weight was above 3×10^4. They also reported that the LCB of a large number of typical commercial LDPE resins was constant across the majority of the MWD and did not increase at high MW.

Seo and Kim (1994) presented a procedure, based on the Mark-Houwink equation and Zimm-Stockmayer relationships, that could describe the behavior of polymer solutions, and from that, the long-chain branching number could be more easily and accurately determined. Their simple general procedure can depict the behavior of intrinsic viscosity for both linear and branched polymers over a very wide range of molecular weight.

4-2-2 Theoretical Considerations and Procedure

The viscosity of dilute polymer solutions depends on the nature of the polymer and the solvent, the concentration of the polymer, its average molecular weight and molecular weight distribution, the temperature and the rate of deformation (Van Krevelen 1990). The most important characteristic quantity in a very dilute solution under low deformation rate is the intrinsic viscosity, [η] defined as:

$$[\eta] = \lim_{c \to 0} \frac{\eta_2 - \eta_1}{\eta_1 c} \tag{4-1}$$

where η_1 and η_2 are the viscosities of the pure solvent and the solution, respectively, and c is the concentration of solute in solution. The intrinsic viscosity is related to the dimension of isolated polymer molecules and can be presented as a function of molecular weight by the Mark-Houwink relation, which can be derived theoretically:

$$[\eta] = KM^{\alpha} \tag{4-2}$$

where M is the molecular weight of the polymer, and K and α are constants that depend on temperature, solvent, and polymer type (Van Krevelen 1990). However, a plot of log[η] versus log$M$ for many polymer solutions shows deviation from the linear relationship at both low and very high molecular weights. The failure of the Mark-Houwink relationship at low molecular weights is attributed to the non-Gaussian character of short flexible chains, and at very high molecular weights is due to hydrodynamic interaction (Lovell 1989). Therefore, when the Mark-Houwink relation is applied to the data, attention must be given to the nature of the calibration and also to the fact that the dilute solution properties of branched polymers differ from those of linear polymers of the same composition. A branched molecule has higher segmental density

and, therefore, occupies less volume and has lower intrinsic viscosity than a similar linear molecule of the same molecular weight. Figure 4-1 shows a typical plot of log[η] versus log$M$ of long-chain branched low-density polyethylene samples.

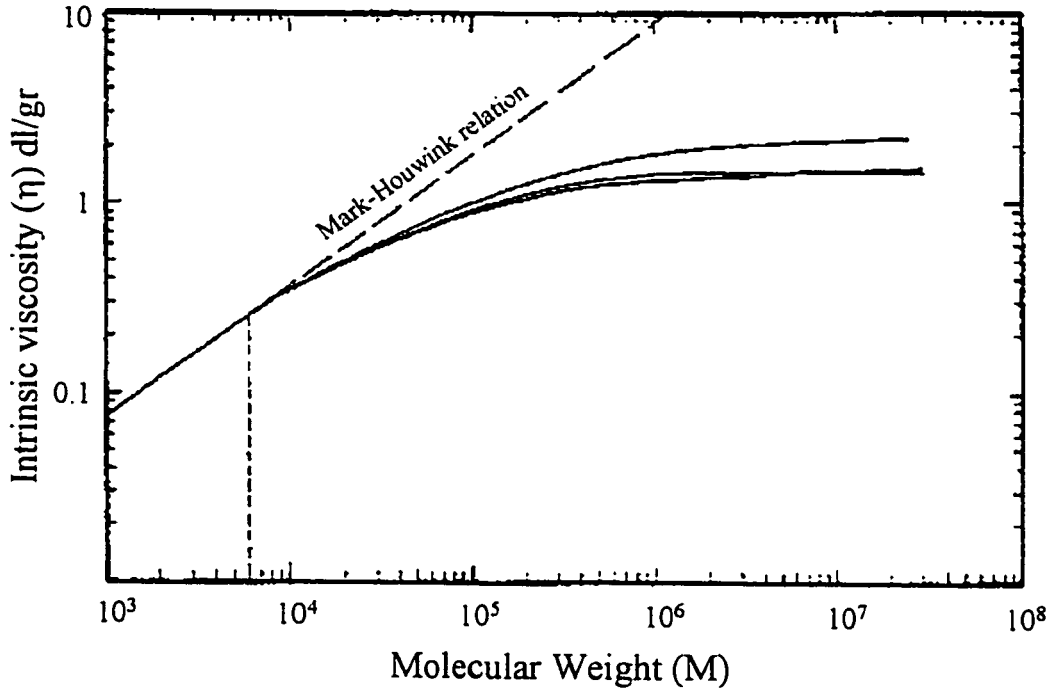

Figure 4-1- Intrinsic viscosity versus molecular weight for three LDPE samples in TCB, 130°C. (Ram and Miltz 1971)

In this figure, the deviation from Mark-Houwink equation at higher molecular weight and the lower viscosity of branched molecules with respect to linear ones are demonstrated.

The starting point in LCB determination using the GPC-viscometry is the result of the theoretical work of Zimm and Stockmayer (1949). They defined the structure parameter g' as:

$$g' = \frac{[\eta]_{Br}}{[\eta]_L} < 1 \tag{4-3}$$

where $[\eta]_{Br}$ is the intrinsic viscosity of the branched species and $[\eta]_L$ is that of the linear species with the same molecular weight. On the other hand, the branching parameter g is expressed in terms of the dimensions of branched and linear polymer of the same molecular weight:

$$g = \frac{\left\langle R_G^2 \right\rangle_{Br}}{\left\langle R_G^2 \right\rangle_L} \tag{4-4}$$

where $\left\langle R_G^2 \right\rangle$ is the squared radius of gyration of the macromolecule.

Zimm and Kilb (1959) showed that the two branching parameters g and g' are interrelated by:

$$g' = g^e \tag{4-5}$$

where the exponent e depends on the type of branches and is in the range of 0.5-1.5 (Zimm and Stockmayer 1949, Zimm and Kilb 1959, Small 1975)

Finally, the number of branches per macromolecule, n, is obtained using Equations (4-6) and (4-7) for monodisperse and polydisperse polymers, respectively. (Zimm-Stockmayer 1949)

$$g = \left[\left(1 + \frac{n}{7} \right)^{1/2} + \frac{4n}{9\pi} \right]^{-1/2} \tag{4-6}$$

$$g = \frac{6}{n} \left\{ \frac{1}{2} \left(\frac{2+n}{n} \right)^{1/2} \ln \left[\frac{(2+n)^{1/2} + n^{1/2}}{(2+n)^{1/2} - n^{1/2}} \right] - 1 \right\} \tag{4-7}$$

When n is greater than 5, the following empirical equation proposed by Lecacheux et al., (1982) is also accurate within 3% error (Seo and Kim 1994).

$$g = \frac{3}{2}\left(\frac{\pi}{n}\right)^{1/2} - \frac{5}{2n} \tag{4-8}$$

Considering the above-mentioned methodology for LCB determination using GPC-viscometry technique, the following step-by-step procedure should be utilized in order to calculate the LCB frequency averages λ_n (the number LCB per 1000 carbon atoms) and B_n (the number of LCB per molecule).

1. From the obtained log[η] versus log$M$ data (Figure 4-1) calculate the structure parameter g' at each molecular weight using Equation (4-3).
2. The branching parameter g can be then calculated at each molecular weight using Equation (4-5).
3. Equations (4-6) and/or (4-7) can be used to calculate the number of LCB per molecule at each molecular weight.
4. The average LCB frequencies are calculated from Equations (4-9) and (4-10).

$$\overline{B_n} = M_n \sum_i \frac{w_i}{M_i} n_i \tag{4-9}$$

$$\lambda_n = \frac{14000}{M_n} \times B_n \quad \text{(only for polyethylene)} \tag{4-10}$$

where w_i is the weight fraction of the chains having chain length i, n_i is the number of LCB per molecule of the chains having chain length i, M_i is the molecular weight of chains having chain length i, and M_n is the number-average molecular weight of the polymer sample.

4-3- ^{13}C Nuclear Magnetic Resonance Spectroscopy

Nuclear magnetic resonance spectroscopy (NMR) is the most valuable spectroscopic technique available to organic chemists. It is the method of structure determination that organic chemists first turn to for information. Mass spectroscopy provides information about the molecular weight and formula of a molecule and infrared spectroscopy provides information about a molecule's functional groups. Nuclear magnetic resonance spectroscopy does not replace or duplicate either of these techniques; it rather complements them by providing a map of the carbon-hydrogen framework of an organic molecule.

Many kinds of nuclei behave as if they were spinning about an axis. Since they are positively charged, these spinning nuclei act like tiny magnets and therefore interact with an externally applied magnetic field. Not all nuclei act this way, fortunately both the proton ^{1}H and the ^{13}C nucleus do have spins. In the absence of a strong external magnetic field, the nuclear spins of magnetic nuclei are oriented randomly. When a sample containing these nuclei is placed between the poles of a strong magnet, however, the nuclei adopt specific orientations. A spinning ^{1}H or ^{13}C nucleus can orient so that its own tiny magnetic field is aligned either with (parallel to) or against (antiparallel to) the external field (McMurry 1992). The orientations do not have the same energy and therefore are not present in equal amounts. The parallel orientation is slightly lower in energy, making this spin state slightly favored over the antiparallel orientation. If the oriented nuclei are now irradiated with electromagnetic radiation of the proper frequency, energy absorption occurs, and the lower energy state "spin-flips" to the higher energy state. When this spin-flip occurs, the nuclei are said to be in resonance with the applied

radiation, hence the name, *nuclear magnetic resonance* (Kroschwitz 1990). The exact amount of radio frequency (rf) energy necessary for resonance depends both on the strength of the external magnetic field and on the identity of the nuclei being irradiated.

All nuclei in molecules are surrounded by the electron clouds. When a uniform external magnetic field is applied to a sample molecule, the circulating electron clouds set up tiny local magnetic fields of their own. These local magnetic fields act in opposition to the applied field so that the effective field actually felt by the nucleus is a bit smaller than the applied field.

$$H_{effective} = H_{applied} - H_{local} \qquad (4\text{-}11)$$

In describing this effect, it is said that nuclei are shielded from the applied field by the circulating electron clouds that surround them. Since each kind of nucleus in a molecule is in a slightly different electronic environment, each nucleus is shielded to a slightly different extent, and the effective magnetic field actually felt is not the same for each nucleus. If the NMR instrument is sensitive enough, the tiny differences in the effective magnetic fields experienced by different nuclei can be observed, and one can see different NMR signals for each different kind of nucleus. Compared with a naked nucleus, a shielded nucleus might require higher or lower applied field strength to provide the particular effective field strength at which absorption occurs. Shielding thus shifts the absorption upfield or downfield. Such shifts in the position of NMR absorptions, arising from shielding by electrons, are called chemical shifts (Morrison 1983).

The unit in which a chemical shift is most conveniently expressed is parts per million (ppm) of the total applied magnetic field. The reference point from which chemical shifts are measured is, for practical reasons, the signal of an actual compound (usually tetramethylsilane $(CH_3)_4Si$). Because of the low electronegativity of silicon, the shielding of protons in the silane is greater than in most other organic molecules; as a result, most NMR signals appear in the same direction from the tetramethylsilane signal (downfield). The most commonly used scale is the δ (delta) scale. The position of tetramethylsilane signal is taken as 0.0 ppm. Most chemical shifts have δ values between 0 to 10 in ^{1}H-NMR, and 0 to 250 in ^{13}C-NMR.

In some ways, it is surprising that carbon NMR is even possible. After all, ^{12}C, the most abundant carbon isotope, has no nuclear spin and is not observable by NMR. ^{13}C is the only naturally occurring carbon isotope with a spin, but its natural abundance is only about 1.1%. Thus, only about 1 of every 100 carbons in organic molecules is observable by NMR. ^{13}C-NMR makes it possible to count the different kinds of carbon in a molecule of unknown structure. In addition, we can get information about the chemical (magnetic) environment of each kind of carbon by observing its chemical shift.

Most ^{13}C resonances are between 0 and 220 ppm downfield from the TMS reference line, with the exact chemical shift of each ^{13}C resonance dependent on that carbon's environment within the molecule (Silverstein et al. 1991).

The use of ^{13}C nuclear magnetic resonance (NMR) spectroscopy in the molecular characterization of molecules has advanced our knowledge into structural areas that have been nearly impossible to measure by other spectroscopic techniques. Innovative applications have led to determinations of polymer configurational distributions,

comonomer sequence distributions, average sequence length, structure and distribution of short branches, LCB determination, and analyses of non-reactive end groups (Randall 1977, 1989). The key to the success of ^{13}C-NMR studies is a structural sensitivity. A sensitivity to polymer repeat unit sequences of length from two to five, seven, and even nine adjacent repeat units has been observed (Randall 1989). In addition to this excellent structural sensitivity, the quantitative sensitivity of ^{13}C-NMR has been improved in recent years. Long-chain branching in polyethylene can be detected at a level of even less than one per thousand atoms (Randall 1989).

4-3-1- Nomenclature of Carbons in Polyolefins

In contrast to step-growth polymers where functional groups of hetero atoms allow the individual repeat units to be identified, the monomer identity is lost in chain-growth polymers such as poly(α-olefin) or an ethylene/α-olefin copolymer. For example, a polyethylene is actually a long chain of methylene sequences, and in polypropylene head-to-tail versus tail-to-head repeat unit sequences can not be distinguished when there are no repeat unit inversions. In ethylene/α-olefin copolymers where α-olefin inversion can occur, the sequence descriptions may not be unique. For example in ethylene-propylene copolymers, a PP sequence can not be distinguished from a PEP sequence (Figure 4-2).

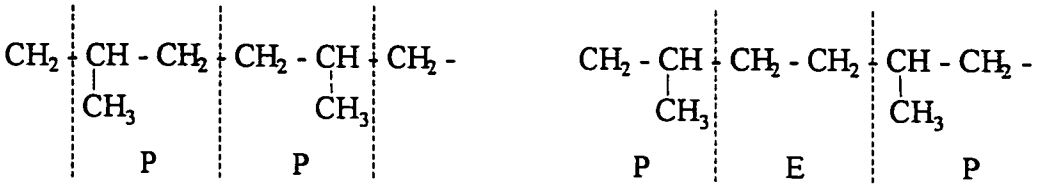

Figure 4-2- Analogous monomer sequences in ethylene/propylene copolymers.

Since the above molecular structures are the same and it is only the sequence descriptions that differ, it must be pointed out that ^{13}C-NMR resonances from polymers arise from carbon atoms in specific structural environments, and it is up to the polymer chemist to translate a carbon resonance identification to an identification of the precise sequence in which it resides. Therefore, in addition to a sequence identification (for copolymers) a carbon atom nomenclature is needed. An efficient nomenclature system was proposed and nicely expanded by Carman (1971) and Randall (1973). Methylene carbons located along the backbone of an ethylene/α-olefin copolymer chain are identified by a pair of Greek letters, indicating the location of the nearest methine carbons in either direction. The Greek letter α indicates that a methine carbon is bonded to a methylene carbon of interest. Two Greek letters, αα, indicate that the identified methylene carbon is sandwiched between two methine carbons. A β indicates that a methine carbon is two carbons away from the carbon of interest, and so forth. Since neighboring carbon contributions to chemical shifts seldom exceed four carbons away, a methine carbon four or more carbons from the methylene carbon of interest is indicated by δ^+. This nomenclature method is schematically illustrated in the following ethylene-α-olefin copolymer (Figure 4-3)

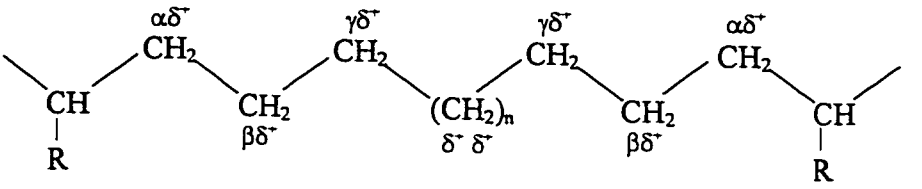

Figure 4-3- Carbon nomenclature in polyolefins.

Carbon nomenclature and peak assignments in ^{13}C-NMR analysis of polyolefins have been studied by many researchers (Lindeman et al. 1971, Randall 1973, 1977, 1989, Hansen et al. 1977, Kimura et al. 1984, De Pooter et al. 1991, Liu et al. 1999). A typical ^{13}C-NMR spectrum of a polyethylene sample, along with peak assignments and chemical shifts, is given in Appendix D.

4-3-2- Long-Chain Branching Determination

The presence of long-chain branching (LCB) has been clearly evident in low-density polyethylenes prepared by free radical polymerization in high pressure reactors. The identification of long-chain branches in high density polyethylenes has been more elusive because of relatively low LCB degrees in these polymers. Recently, with the advent of constrained geometry metallocene catalysts, synthesis of polyethylenes with only long-chain branches is possible (Lai et al 1993, 1997). Melt index decreases upon either processing or during conversion of reactor-produced granules to pellets have often been associated with shear-induced long-chain branching. The structure of long-chain branches in polyethylene is called a "Y" type, which gives rise to methine, $\alpha\delta^+$, $\beta\delta^+$, and

$\gamma\delta^+$ carbons corresponding to those observed in ethylene/1-octene copolymers (Figure 4-4a,b).

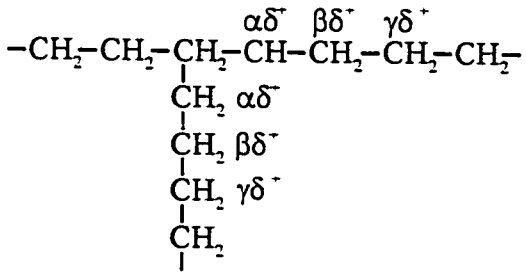

(a)

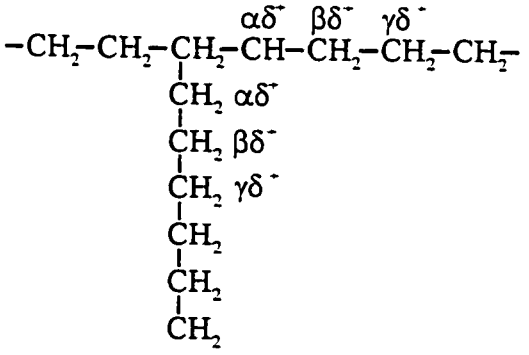

(b)

Figure 4-4- a) "Y" long-chain branch in PE, b) ethylene/1-Octene structural sequence

Since NMR cannot distinguish among branches longer then C6, therefore, ethylene/1-octene copolymers serve as good reference polymers for identifying resonances in high-density polyethylenes associated with long-chain branches. Detection of these resonances in high-density polyethylene where no α-olefin was added during polymerization should be strongly indicative of the presence of long-chain branching.

It should be mentioned that in order to detect LCB degrees in a range of 1 per 10000 carbon atoms or less, sufficient instrumental sensitivity should be available. A distinct requirement for branching measurements in this range is the availability of sufficient dynamic range during data acquisition. Nuclear magnetic resonance spectrometers, which have computers operating either with double precision arithmetic or utilizing floating point arithmetic during data acquisition, are absolutely required. Otherwise the information leading to branching identification is truncated after only a few data acquisitions (Randall 1989).

Generally, for polyethylene samples, two types of end groups dominate over other types that possibly could be present. They are:

saturated end group

$$\underset{}{-CH_2-}\underset{3s}{CH_2}-\underset{2s}{CH_2}-\underset{1s}{CH_3}$$

1-olefin end group

$$-CH_2-\underset{a}{CH_2}-CH=CH_2$$

A ratio of the end group intensities to the total intensity of the remaining spectral resonances leads to a direct determination of the average carbon number of the polyethylene molecule and, subsequently, to a number-average molecular weight. However, number average molecular weight determination using the ^{13}C-NMR spectrum is not accurate for high molecular weights.

The number-average molecular weight is given by:

$$M_n = \frac{\text{total carbon intensity}}{\text{number of polymer chains}} \times 14 \qquad (4\text{-}12)$$

In terms of peak intensities, the number-average molecular weight is given by:

$$M_n = \frac{(1s + 2s + 3s + \delta^+\delta^+ + 3a) \times 14}{(1/2)(s + a)} \tag{4-13}$$

where s is the average intensity for $1s$, $2s$, and $3s$ and the polymer molecule is assumed to be linear.

The following definitions are needed for quantitative analysis:

B_n = average number of long-chain branches per molecule.

s = average intensity for saturated end-group carbon. (Appendix D)

a = the 33.88 ppm allylic carbon atom intensity. (Appendix D)

α = the average intensity of a carbon from a branch. (For instance $\alpha\delta^+$ carbon)

T_{tot} = the total carbon intensity.

Using the above definitions and intensities of different peaks in the ^{13}C-NMR spectra, the average number of long-chain branches per polymer molecule, B_n, can be calculated.

As defined before, α is the average intensity of a carbon atom in a branch (for instance $\alpha\delta^+$ carbon atoms). Suppose α is the intensity of a carbon in the following schematic of a branch (Figure 4-5):

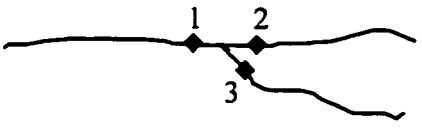

Figure 4-5- Schematic of a branched polyethylene

Since the situations of carbon atoms in locations 1, 2, and 3 are the same, ^{13}C-NMR gives the same intensity for all three of them. Knowing the fact that only one of them is in the long-chain branch and the other two reside in the main chain, the average intensity of branches would be equal to $\alpha/3$.

The number of moles of polymer chains is equal to half of the number of main chain ends (excluding the chain ends of branches). Referring to the above definitions, the total number of chain ends is equal to the summation of intensities of allylic and saturated end group carbons.

Total number of chain ends = $s + a$ (4-14)

Therefore, the number of main chain ends (excluding the chain ends of long-chain branches) is equal to:

$$\text{number of main chain ends} = (s+a) - \frac{\alpha}{3} \tag{4-15}$$

Using the above expression, the number of moles of polymer chains can be easily calculated:

$$\text{number of moles of polymer chains} = \frac{1}{2}\left[(s+a) - \frac{\alpha}{3}\right] \tag{4-16}$$

Knowing the average number of branches and number of polymer chains, the average number of branches per polymer molecule, B_n, can be easily calculated:

$$B_n = \frac{\text{The average number of branches}}{\text{number of polymer chains}} \tag{4-17}$$

$$B_n = \frac{\frac{\alpha}{3}}{\frac{1}{2}\left[(s+a) - \frac{\alpha}{3}\right]} \tag{4-18}$$

$$\Rightarrow \quad B_n = \frac{2\alpha}{3(s+a)-\alpha} \tag{4-19}$$

Frequently, long-chain branching is expressed as the number of branches per 1000 or 10000 carbon atoms as opposed to the number of branches per molecule. This parameter can be also determined by ^{13}C-NMR. As discussed before, the average number of long-chain branches is $\alpha/3$. Therefore the number of branches per 1000 carbon atoms, λ_n, can be easily calculated:

$$\lambda_n = \frac{\text{average number of long-chain branches}}{\text{total number of carbon atoms}} \tag{4-20}$$

$$\Rightarrow \quad \lambda_n = \frac{\alpha/3}{T_{tot}} \times 1000 \tag{4-21}$$

For the cases where only long-chain branches are present (like in polyethylenes made by CGC technology) the above methodology can be directly used to find the LCB frequencies, B_n and λ_n.

Chapter 5

Experimental

5-1- Materials

5-1-1- Reagents

All the reagents used in the experiments (except catalysts) are listed in Table 5-1. All air-sensitive compounds were handled and stored in a dry box (Nexus, Vacuum/Atmospheres Co.) under ultra-high purity nitrogen atmosphere.

Solvents and liquid comonomers were purified by contacting them with molecular sieves under nitrogen bubbling for at least 12 hours in order to remove moisture and oxygen. Approximately 600 grams of activated type 4A molecular sieves were added to 4L of solvent capped with a rubber septum. Ultra-high purity nitrogen was bubbled through a thin transfer needle in the solvent and purged through another needle connected to an oil bubbler The molecular sieves were baked in furnace at 400 °C for 8 hours and were cooled down to room temperature in a dry atmosphere prior to use.

Table 5-1- Specification of the reagents used in experiments

Name	Chemical Formula	Grade	Supplier
1,2,4- Trichlorobenzene (TCB)	$C_6H_3Cl_3$	Distilled	EM Science
Ethanol	C_2H_5OH	Denatured	BDH
Hexane	C_6H_{14}	HPLC	EM Science
Hydrochloric Acid	HCl	ACS	BDH
Irganox 1010	$C_{73}H_{108}O_{12}$	N/A	CIBA-GEIGY
Isopar E *	C_8H_{18}	Distilled	Exxon Chemical Co.
Methylaluminoxane (MAO)	$(CH_3)_2Al(OAlCH_3)_nAl(CH_3)$	30% in Toluene	Albermarle
n- Decene	$C_{10}H_{20}$	94%	Aldrich
n- Eicosene	$C_{20}H_{40}$	90%	Aldrich
n- Hexadecene	$C_{16}H_{32}$	92%	Aldrich
n- Hexene	C_6H_{12}	97%	Aldrich
n- Octene	C_8H_{16}	98%	Aldrich
Toluene	$C_6H_5CH_3$	ACS	BDH
Trimethylealuminum (TMA)	$(CH_3)_3Al$	1 M in Hexane	Aldrich
Tris(pentafluorophenyl) borane (TPFB)	$C_{18}F_{15}B$	3.58% solution in Isopar E	Dow Chemical Co.

* 2, 2, 3 tri-methyl pentane.

5-1-2- Gases

Nitrogen, ethylene, and hydrogen were the only gases used in the experiments. Nitrogen was employed for purging the solvent, comonomers, pipe lines, polymerization reactor, and providing an inert atmosphere in the dry box. Ethylene and nitrogen were purified prior to use by passing them through molecular sieves (type 4A for nitrogen and 5A calcium alumino-silicate for ethylene), and copper(II) oxide supported on alumina to remove moisture and oxygen, respectively. Hydrogen was used as transfer agent and used without further purification. Table 5-2 shows the specification of these gases.

Table 5-2- Specification of the gases used in experiments

Name	Formula	Grade	Supplier
Ethylene	C_2H_4	CP	PRAXAIR
Nitrogen	N_2	UHP	PRAXAIR
Hydrogen	H_2	UHP	PRAXAIR

5-1-3- Catalysts

Four different catalysts were used for the polymerization experiments. Titanium (N-1, 1-dimethylethyl) dimethyl (1-(1,2,3,4,5-η)-2,3,4,5-tetramethyl-2,4-cyclopentadiene-1-yl) silanaminato))(2-)N)-dimethyl (1% solution in Isopar E), from now on called CGC-Ti, donated by The Dow Chemical Co. The other three were purchased from Aldrich. The chemical specifications of these catalysts are given in Table 5-3.

Table 5-3- Polymerization Catalysts

Name	Formula	Supplier
Bis(cyclopentadienyl)zirconium dichloride	Cp_2ZrCl_2	Aldrich
Bis(cyclopentadienyl)hafnium dichloride	Cp_2HfCl_2	Aldrich
Dichloro[*rac*-ethylene bis(indenyl)] zirconium(IV)	$Et[Ind]_2ZrCl_2$	Aldrich
Constrained Geometry Catalyst (CGC-Ti)	See Figure 5-1	Dow Chemical

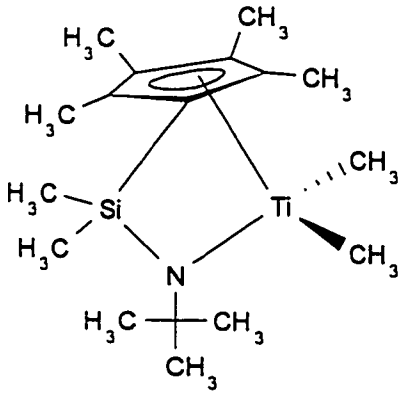

Figure 5-1- The chemical structure of CGC-Ti.

5-2- Polymerization Procedure and Apparatus

Although the highest branching degree for a given average residence time is achieved in a CSTR, polymerization kinetic studies are better performed in semi batch systems. Therefore, a semi batch reactor system was designed and installed for polymerization kinetics studies. The schematic of this reactor system is shown in Figure 5-2. Polymerization experiments were carried out in this 600 ml Autoclave Engineers Zipperclave equipped with a magnetic-driven stirrer operating up to 2000 rpm, an

electrical heater, and a cooling coil which can operate with water or oil. The reactor is rated for pressures of up to 17.24 MPa (2500 psi).

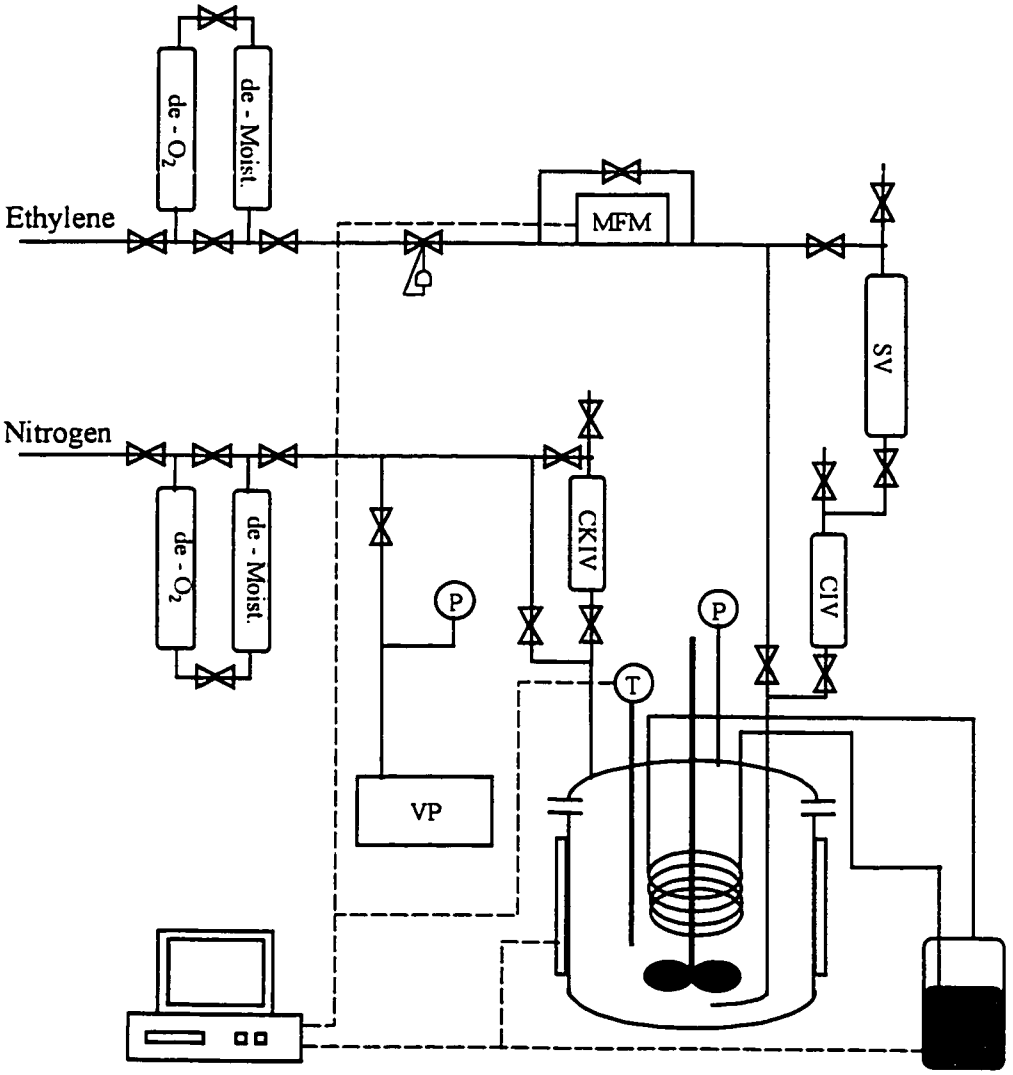

Figure 5-2. Schematic of the semibatch polymerization reactor system.

CIV: Catalyst injection vessel; CKIV: Catalyst killer injection vessel; De-Moist.: de-moisturizing column; De-O_2: de-oxygenating column; MFM: Mass flow meter; Oil bath: cooling oil bath; P: Pressure gauge; T: Thermocouple; VP: Vacuum pump

The reactor pressure (ethylene pressure) is adjusted by an in-line pressure regulator, installed in the ethylene feed line. The reactor temperature is controlled by two

(heating and cooling) control loops. The control is performed by a personal computer through analog to digital (A/D) and digital to analog (D/A) boards. Two independent proportional-integral (PI) control loops are used to control the heat-exchanger oil flow in the cooling coil and the power delivered to the electrical heater. Excellent temperature control was achieved using this control technique, as the reactor temperature was maintained within ±0.7 °C of the set point for all reported polymerizations. The mass flow rate of ethylene is monitored with an in-line mass flow meter (MFM) installed in the ethylene feed line.

Before polymerization, vacuum was applied to the reactor for about 15 minutes. The reactor was then pressurized with ethylene to 50 psi. This cycle was repeated three times to remove oxygen and moisture. Then 400 ml of purified Isopar E was transferred to the reactor by a transfer needle through a septum inlet under nitrogen pressure. 0.5 grams of a 1 molar tri(methyl)aluminum (TMA) solution in hexane was added to the reactor to scavenge all impurities traces. Next, measured amounts of co-catalysts (MAO and TPFB) and then comonomer (in the case of copolymerization) were added. Hydrogen (if needed) was then added to the reactor by injecting a measured volume of this gas using a syringe through the septum inlet. The reactor was then heated up to the reaction temperature and pressurized with ethylene until the solvent was saturated. Measured amounts of catalysts were transferred to the catalyst injection vessel through the septum inlet and the vessel was pressurized with ethylene. Polymerization started by injecting the catalysts into the reactor. All of the polymerization runs were conducted at 140°C and 1792 kPa (260 psi) for 10 minutes. To terminate the reaction, the monomer feed line was closed and acidic ethanol was injected into the reactor using the catalyst killer injection

vessel. The reactor was then depressurized and cooled down to 40 °C. The reactor content was poured into a beaker containing enough ethanol to precipitate and wash the polymer. The precipitated polymer was adequately washed with excess ethanol, filtered, and dried in vacuum at 60°C for 10 hours.

5-3- Characterization

5-3-1- Gel Permeation Chromatography

Gel permeation chromatography (GPC) was used to determine molecular weight, molecular weight distribution, and long-chain branching degree of polymer samples. GPC analysis were performed on a high temperature Waters 150CV Plus™ instrument equipped with three Waters Styragel HT6E columns, using a differential refractive index and a Viscotek viscometer (four capillaries) detector. About 4 mg of polymer sample was dissolved in 1,2,4-trichlorobenzene (TCB) as solvent. All GPC runs were carried out at 140 °C and at a flow rate of 1.0 ml/min. A universal calibration method (Grubisic et. al. 1967) with narrow polystyrene standards was used. To prevent polymer degradation, 1.5 grams of anti-oxidant (Irganox 1010) was added to 4 liters of TCB.

Long-chain branching frequency was determined using the methodology proposed by Ram and Miltz (1971) and was explained in detail in Section 4-2-2. Figure 5-3 illustrates the viscosity plot of one of the analyzed samples. It is clearly evident that the plot of $\log[\eta]$ versus $\log M$ deviates from the straight line predicted by the Mark-Houwink relation. The intrinsic viscosity versus molecular weight data, collected from the analysis of each sample, were exported to a spreadsheet. The Mark-Houwink parameters were estimated by determining the slope and the intercept of the line generated from the

continuation of the linear part of the viscosity plot curve (Figure 5-3). Equations (4-3) to (4-5) and Equations (4-7), (4-9), and (4-10) were used to estimate the long-chain branching frequencies. It should be mentioned that only the deviations from the straight line observed in the high MW range were used in LCB calculation. The deviations observed in the low MW range are attributed to non-Gaussian character of short flexible chains (Seo and Kim 1994). As discussed in Section 4-2-2 the value of the parameter *e* appeared in Equation 4-5 is in the range of 0.5-1.5. Mirabella and Wild (1990) showed

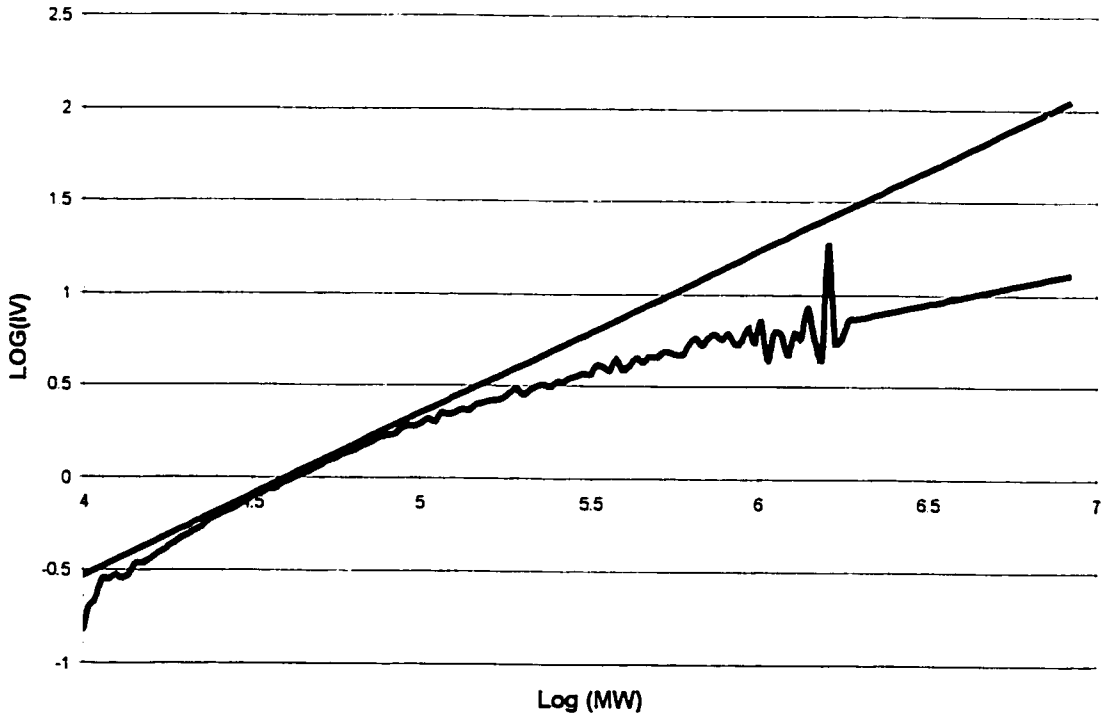

that the value is closer to 0.5 for polyethylene. They calculated an average value of e = 0.65. As suggested by Viscotek (ref. private communication) the value of e = 0.70 was used in Equation 4-5.

Figure 5-3- Typical log[η] versus log$M$ obtained from GPC analysis.

5-3-2- ^{13}C-NMR Spectroscopy

^{13}C NMR was used to measure the long-chain branching and comonomer content of the samples. The samples were dissolved in TCB in a 10 mm diameter tube (approximately 35wt% of polymer in solution). The polymer was dissolved at 150 °C for 30 minutes before being analyzed at 125 °C on a Bruker AC-300 NMR spectrometer. The inverse gate decoupling method was used to decouple protons from carbon nuclei. The number of scans performed for each spectrum was around 10000. Peak assignments and long chain branch frequency calculations were done according to the methodology proposed by Randall (1973, 1977, 1989) and explained in detail in Section 3-3-2. Figure 5-4 illustrates a typical spectrum of a long-chain branched polyethylene sample synthesized with a single-site type catalyst.

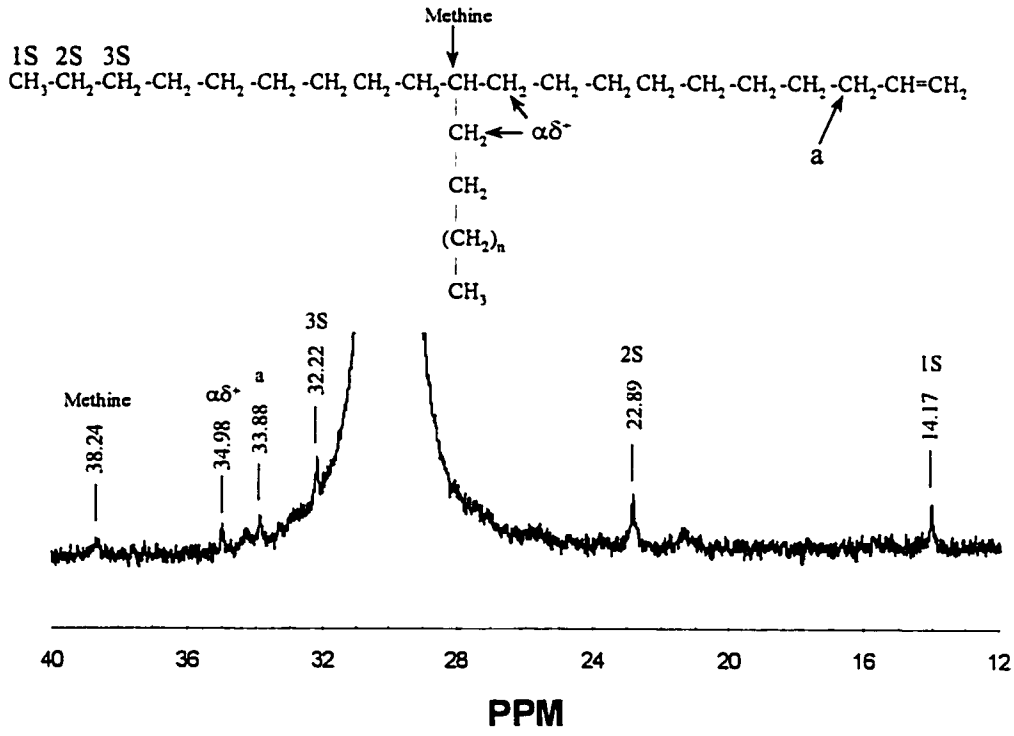

Figure 5-4- Typical ^{13}C-NMR spectrum of a long-chain branched polyethylene sample

Copolymer samples were characterizaed by ^{13}C-NMR for their comonomer content. A typical spectrum of an analyzed copolymer is shown in Figure 5-5. The comonomer content of the samples were calculated using the procedures proposed by DePooter et al., (1991).

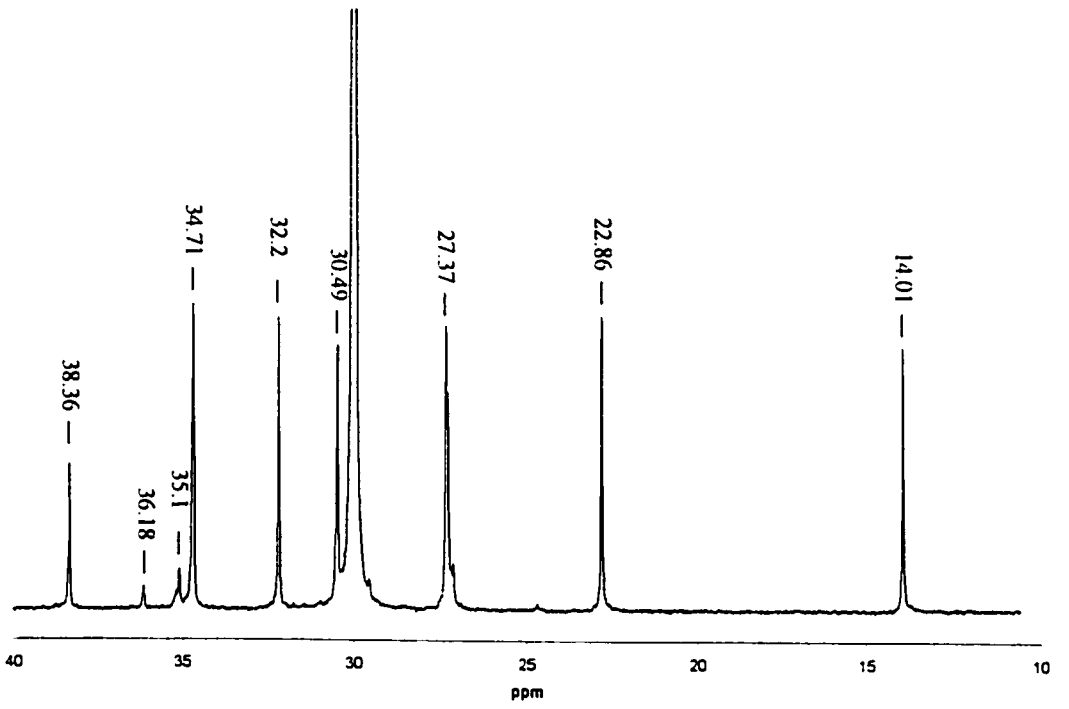

Figure 5-5- ^{13}C-NMR spectrum of an ethylene/1-octene copolymer.

5-4- Polymerization with Combined Metallocene Catalysts

The main purpose of the polymerization experiments described in this section is to evaluate the model proposed in Sections 3-2-3 to 3-2-5. Simulation results suggested that the use of combined catalyst systems was an efficient technique to control long-chain

branching degree in ethylene polymerization (Beigzadeh et al. 1997, 1999a,b). Additionally, the presence of the second metallocene can be used to broaden the molecular weight distribution of the produced polymer, for applications where broad uni- and multi-modal distributions are required.

According to the results obtained, in order to accelerate long-chain branch formation, the linear metallocene catalyst used in the combined system must be able to generate more macromonomers (dead chains with terminal double bonds) than CGC-Ti. Therefore, the first step is to find a suitable catalyst to be used in combination with CGC-Ti. For this purpose, three different catalysts with different geometries (Table 5-3) were selected and polymerization experiments were carried out with each individual catalyst. Table 5-4 shows the polymerization conditions for the four polymerization runs performed with the three linear catalysts and CGC-Ti.

Table 5-4- Reaction conditions used in the polymerization experiments.

Temperature	140 °C
Pressure	260 psi
Catalyst concentration	4 (μm/l)
MAO/CGC-Ti	500
TPFB/ CGC-Ti	100
Solvent	Isopar E

The synthesized polyethylene samples were characterized with ^{13}C-NMR for their terminal double bond contents. The ratio of the concentration of terminal double bonds (area under the peak at 33.88 ppm) to the concentration of all other carbon structures

(Equation (4-12) and (4-13)) was used as the selection criterion. The results of this analysis are given in Table 5-5.

Table 5-5- Summary of ^{13}C-NMR analysis results.

Catalyst	^{13}C-NMR data (area under the peak)			$(a / T_{tot})\times 10^4$
	Allylic carbon (a)	Saturated chain ends. (Average of 1S, 2S, and 3S)	Total carbon intensity (T_{tot})	
$Et[Ind]_2ZrCl_2$	9.65	9.84	9899	9.75
Cp_2HfCl_2	0.89	3.7	9589	0.93
Cp_2ZrCl_2	1.43	4.9	9795	1.46
CGC-Ti	2.23	5.31	9724	2.29

From the results given in Table 5-5, it is evident that: 1) Among the three linear catalysts tested, $Et[Ind]_2ZrCl_2$ is the only one that generates more terminal double bonds than CGC-Ti. 2) Comparing the number of allylic carbons with saturated chain ends, it seems that β-hydride elimination and/or transfer to monomer are the dominant transfer mechanisms in $Et[Ind]_2ZrCl_2$ polymerization systems.

Based on the above-mentioned conclusions, $Et[Ind]_2ZrCl_2$ was used as the CGC-Ti partner in the combined catalyst.

In order to evaluate the kinetic model proposed in Sections 3-2-3 to 3-2-5, five polymerization experiments with combined CGC-Ti/$Et[Ind]_2ZrCl_2$ were carried out. In these experiments, the overall amount of catalyst in the reactor was kept constant at 1.6 μmol for all runs, but the ratio CGC-Ti/(CGC-Ti+$Et[Ind]_2ZrCl_2$) was varied from 0 to 1.0. All other polymerization conditions were as presented in Table 5-4.

The synthesized samples were analyzed by ^{13}C-NMR and GPC for their long-chain branching degree and molecular weight distribution. Table 5-6 shows the summary of the ^{13}C-NMR analysis of these samples.

Table 5-6- Summary of ^{13}C NMR results and calculated LCB degrees for polyethylene samples synthesized by combined and individual CGC-Ti/Et[Ind]$_2$ZrCl$_2$.

No.	CGC-Ti Mol%	NMR Data (area under the peak)			Unsaturated / saturated chain ends	Total Carbon intensity	Br. Per 10000 C[a]
		$\alpha\delta^+$ carbon	Average of 1S, 2S, and 3S	Allylic Carbon (a)			
1	0	0	9.84	9.65	0.98	9899	0
2	20	4.42	8.16	7.34	0.90	9833	1.50
3	35	6.33	7.8	6.32	0.81	9716	2.17
4	50	12.41	7.02	5.33	0.76	9815	4.21
5	65	5.24	7.08	4.67	0.66	9757	1.79
6	80	6.81	5.75	3.1	0.54	9736	2.33
7	100	2.92	5.31	2.23	0.42	9724	1.00

[a]Branch per 10000 C = $(1/3)\alpha\delta^+$/Total carbon intensity × 10^4

Figure 5-6 illustrates how the number of long-chain branches per 10000 carbon atoms depends on the fraction of CGC-Ti in the binary mixture. These branching degrees were calculated using the ^{13}C-NMR analysis data.

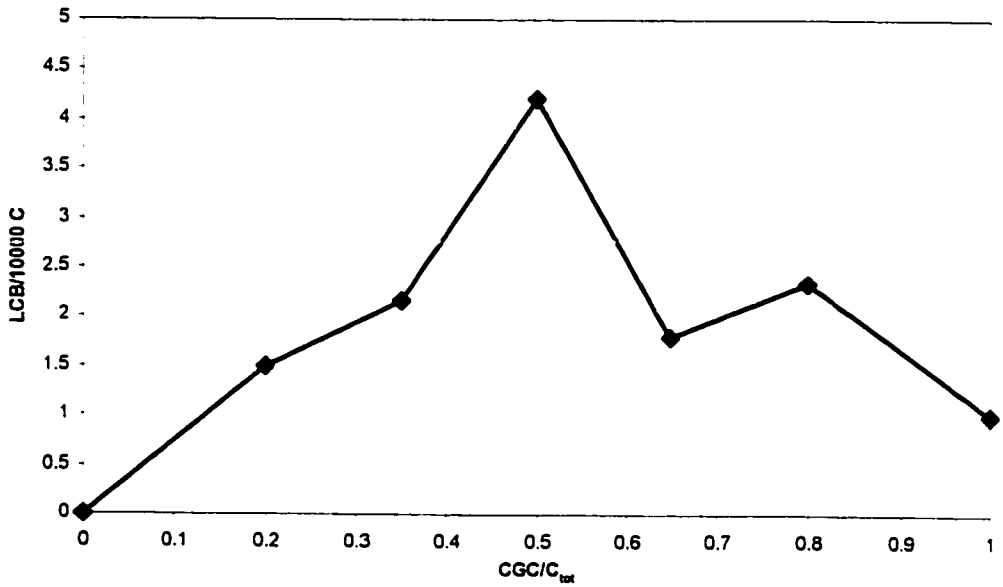

Figure 5-6- Effect of of CGC-Ti mole fraction (^{13}C-NMR data) on total LCB degree.

As shown in this Figure 5-6, the plot of branching degree versus CGC-Ti mole fraction passes through a maximum. No branching was observed when only $Et[Ind]_2ZrCl_2$ was used. As more CGC-Ti was employed in the binary catalyst system (CGC-Ti%=0.2, 0.35, and 0.5) the measured LCB frequencies increased up to a maximum corresponding to CGC-Ti%=0.5. By increasing the mole fraction of CGC-Ti to more than 50%, the branching content started decreasing (CGC-Ti%=0.65 and 0.8) to the LCB content obtained when only CGC-Ti was used. As suggested by the proposed reaction mechanism in Chapter 3 (Beigzadeh et al. 1997, 1999a), this behavior can be attributed to a lower macromonomer concentration as the mole fraction of $Et[Ind]_2ZrCl_2$ decreases.

The same samples were analyzed with the multi-detector GPC described in Section 5-3-1 for their LCB degree and the obtained results are plotted in the same

fashion as Figure 5-6 along with the branching data obtained from ^{13}C-NMR. Figure 5-7 illustrates how well GPC and NMR results agree.

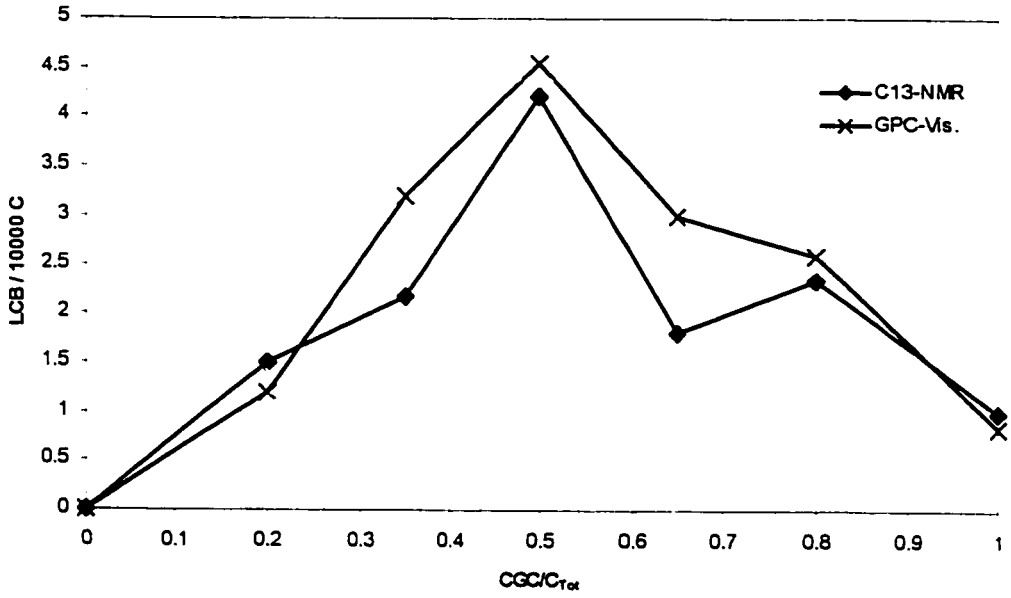

Figure 5-7- Variation of LCB degree with CGC-Ti mole fraction (^{13}C-NMR and GPC-viscometer data).

The molecular weight distribution (MWD) of polymers produced with combined catalysts is the superposition of the MWDs of polymer chains produced at each metallocene. Figure 5-8 shows the MWD of a polyethylene sample synthesized with the CGC-Ti/Et[Ind]$_2$ZrCl$_2$ (CGC-Ti/C$_{Tot}$ = 0.5) and the MWDs of the polyethylene samples made with individual CGC-Ti and Et[Ind]$_2$ZrCl$_2$. It is evident that the catalysts in the combined catalysts system behave independently and, as a result, a bimodal MWD is obtained.

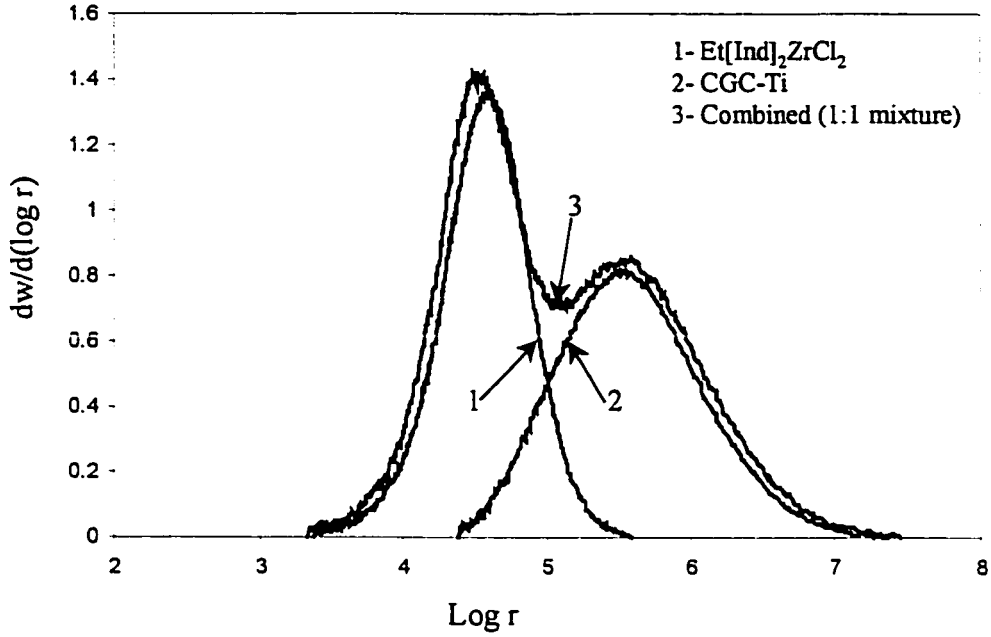

Figure 5-8- MWD of the samples synthesized with combined and individual CGC-Ti and $Et[Ind]_2ZrCl_2$.

Figure 5-9 illustrates the MWD of the five samples synthesized with the combined catalyst system. Increasing the fraction of CGC-Ti in the catalyst mixture increases the high molecular weight peak of the bimodal MWD, suggesting that the chains synthesized with CGC-Ti have higher molecular weight averages than the chains made with $Et[Ind]_2ZrCl_2$. This shows how easily different bimodal MWD polyethylene resins can be synthesized with combined catalyst systems.

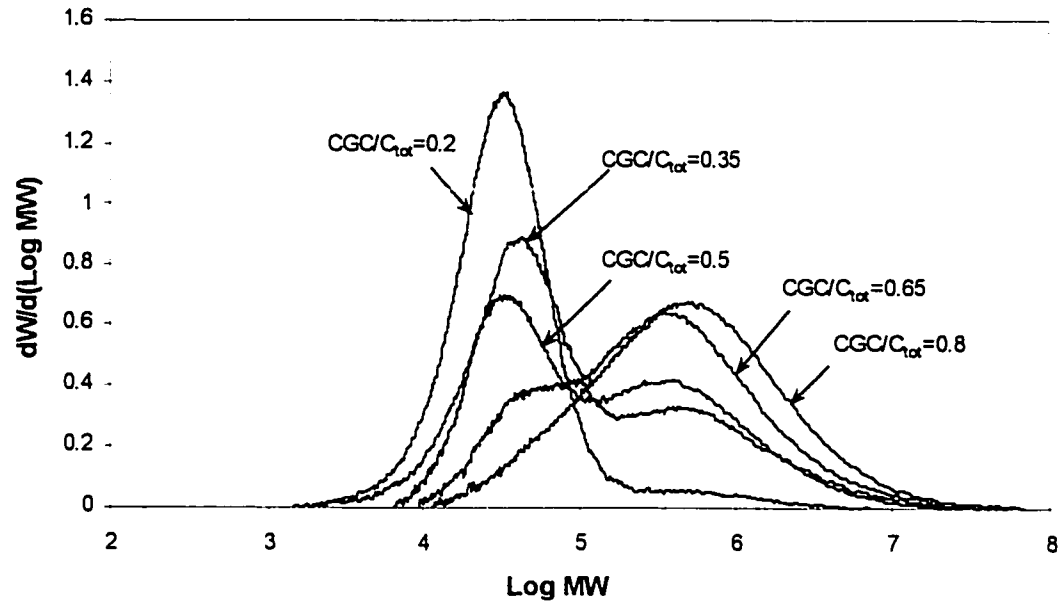

Figure 5-9- Molecular weight distribution of polyethylene samples synthesized with combined CGC-Ti/Et[Ind]$_2$ZrCl$_2$

According to the simulation results obtained in Chapter 3, the presence of chain transfer agent (CTA) does not alter the rate of LCB formation. Therefore, adding hydrogen (CTA) to this polymerization system, should not change the number of LCB per 1000 carbon atoms, λ_n. In order to verify this hypothesis, the same series of experiments were performed at two different hydrogen levels (10 and 20 ml of hydrogen) with replicate runs at H_2 = 10 ml. The synthesized samples were analyzed by ^{13}C-NMR, and GPC for their long-chain branching degree and molecular weight distribution. Figure 5-10 illustrates the number of LCB per 10000 carbon atoms versus the mole fraction of CGC-Ti in the combined catalyst mixture for samples synthesized in the absence of hydrogen, in the presence of 10 ml of hydrogen (two replicates), and in the presence of

20 ml of hydrogen. As can be seen, the presence of hydrogen does not affect the observed optimum value for CGC-Ti mole fraction. The slight decrease observed in LCB degrees by addition of hydrogen could be attributed to two reasons: 1) lower activity of the transferred active sites (active sites attached to a hydrogen atom) results in lower rate of polymer production which translates into lower concentration of macromonomers. 2) Although UHP hydrogen was used in polymerization experiments, it was not completely free of impurities. This results in deactivation of some of the active sites and therefore, less polymer chains (and hence macromonomers) are formed and according to Equation 3-30, less LCB are formed at lower macromonomers concentration

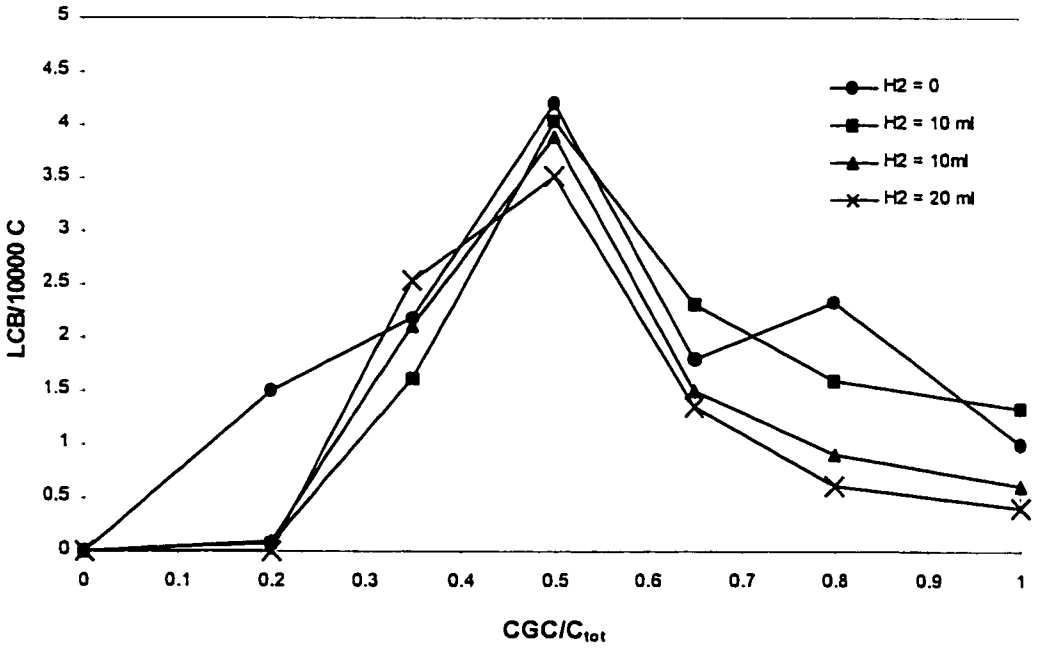

Figure 5-10- Hydrogen effect on the variation of LCB degree with CGC-Ti mole fraction (^{13}C-NMR data).

The same samples were analyzed with the multi-detector GPC for their LCB degrees. The obtained results are plotted in Figures 5-11 and 5-12. Although some deviations between the LCB degrees obtained from GPC and ^{13}C-NMR are observed, the same general LCB frequency dependency on CGC-Ti fraction is identified, including the CGC-Ti mole fraction that produces polyethylene with a maximum degree of LCB. The agreement between the two characterization methods and mathematical modeling predictions for LCB formation is a remarkable observation made for the first time in this investigation.

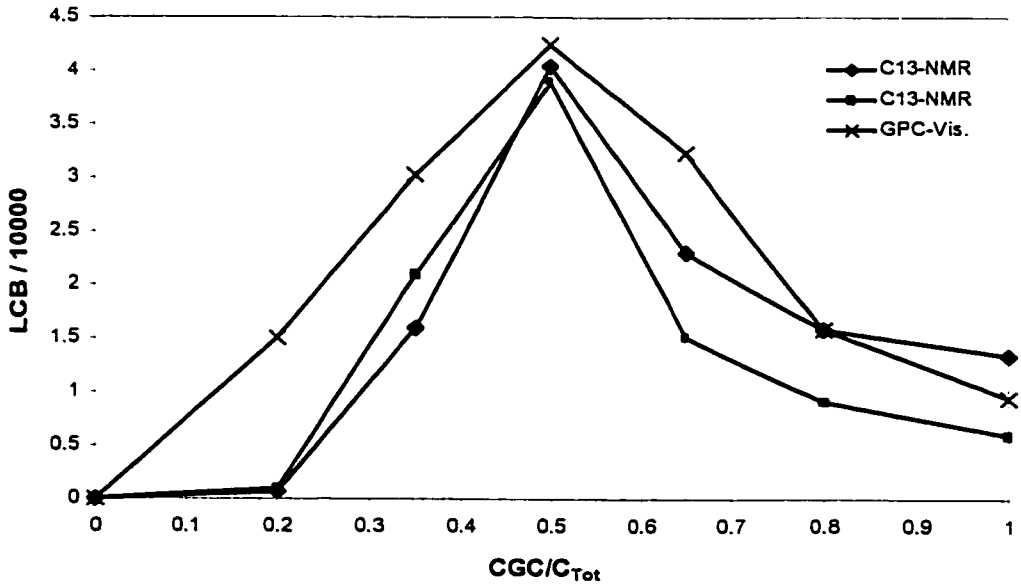

Figure 5-11- Effect of the variation of LCB degree with CGC-Ti mole fraction obtained from ^{13}C-NMR and GPC-viscometer analyses (H_2 = 10 ml).

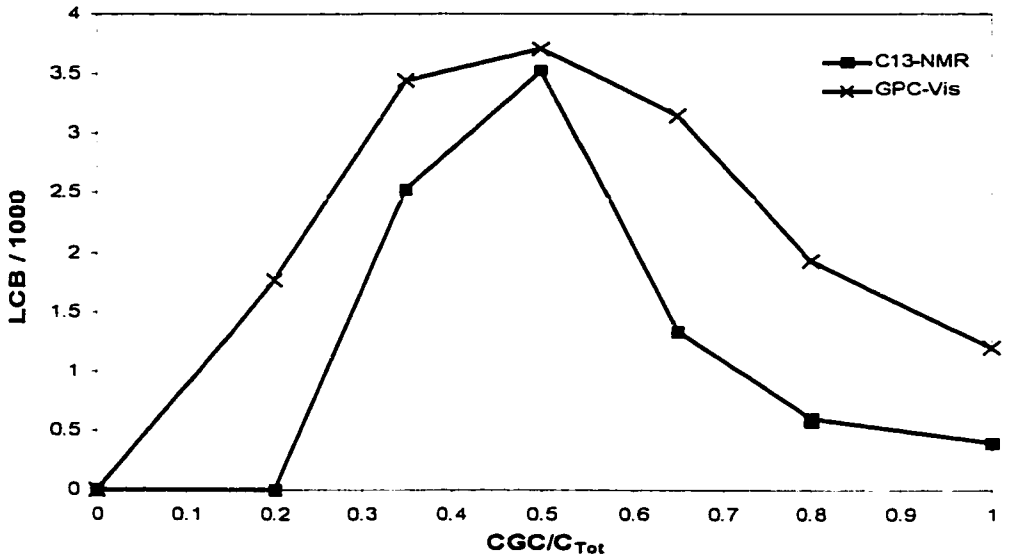

Figure 5-12- Effect of the variation of LCB degree with CGC-Ti mole fraction obtained from ^{13}C-NMR and GPC-viscometer analyses (H_2 = 20 ml).

The effect of hydrogen on MWD is illustrated in Figures 5-13 and 5-14. By adding hydrogen, the peak corresponding to the chains synthesized with CGC-Ti moves towards lower molecular weights, while the peak corresponding to the Et[Ind]$_2$ZrCl$_2$-made polymer chains does not shift as much.

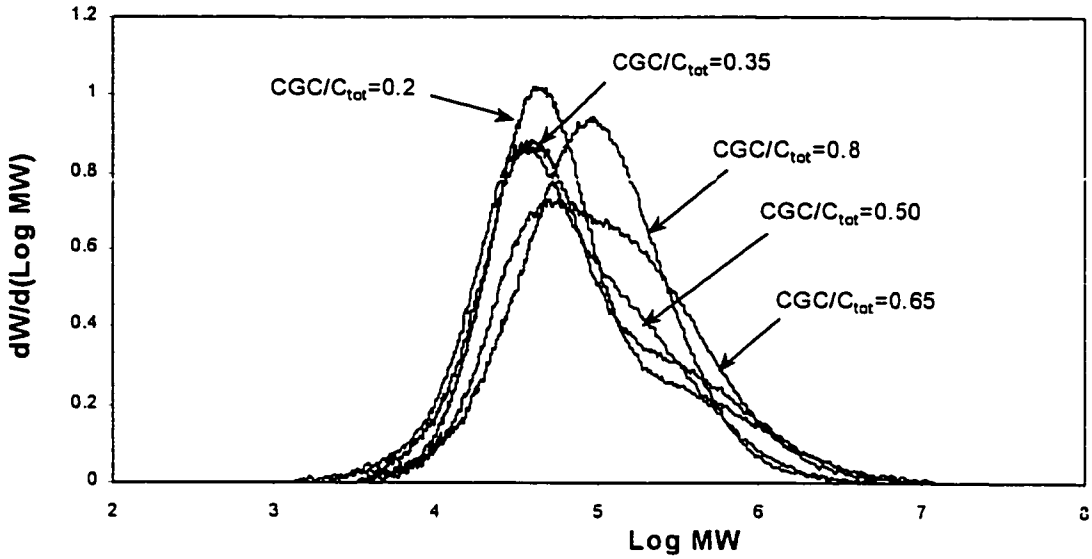

Figure 5-13- Molecular weight distribution of polyethylene samples synthesized with combined CGC-Ti/Et[Ind]$_2$ZrCl$_2$. H_2 = 10 ml.

As shown in Figure 5-8, the MWD of polymer produced by the combined catalysts represents the superposition of the MWDs of the polymers produced on each metallocene. Therefore, one can conclude that, the MWD of the polymer produced by Et[Ind]$_2$ZrCl$_2$ does not change significantly with hydrogen concentration but the MWD of polyethylene produced by CGC-Ti decreases significantly with the addition of hydrogen. This is in agreement with the results of the NMR analysis presented in Table 5-5, as β-hydride elimination and/or transfer to monomr were found to be the dominant molecular weight determining steps for polyethylene samples made with Et[Ind]$_2$ZrCl$_2$.

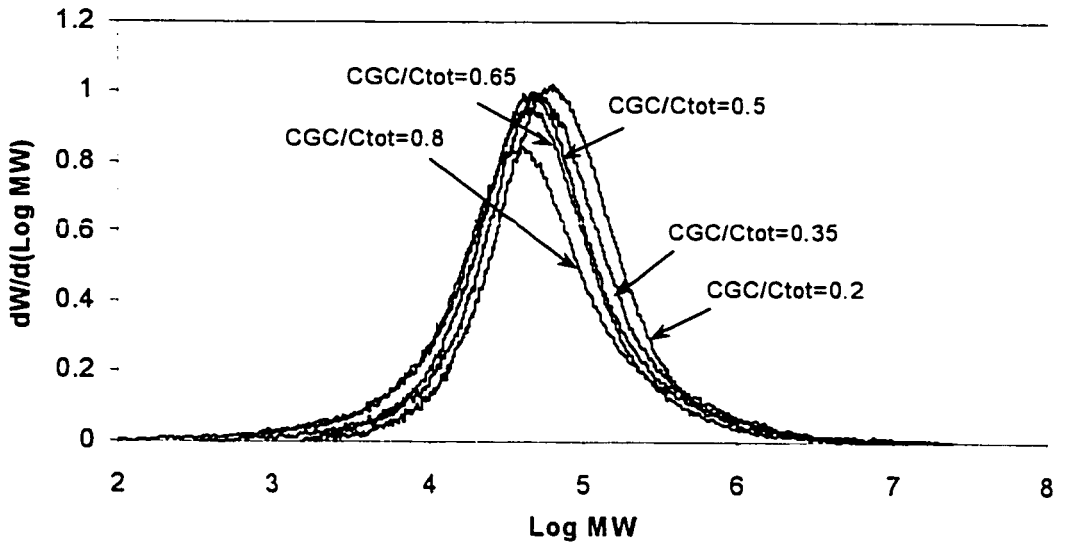

Figure 5-14- Molecular weight distribution of polyethylene samples synthesized with combined CGC-Ti/Et[Ind]$_2$ZrCl$_2$. H_2 = 20 ml.

This demonstrates how easily the breadth of the overall MWD of polyethylene made with the combined catalyst can be manipulated by simply varying hydrogen concentration. Similar observations were made by Kim et al. (1998, 1999) for slurry polymerization of ethylene with Et[Ind]$_2$ZrCl$_2$.

5-5- Model Predictions and Parameter Estimation

As observed in the previous sections, the modeling results obtained in Chapter 3 could adequately predict the general trends observed in LCB variation with mole fraction of CGC in the combined catalyst polymerizations. In this section, the simple model developed in Section 3-2 for semi-batch operation will be further examined. This model describes how LCB degree varies with catalyst type and polymerization conditions, according to Equation (3-40):

$$\bar{\lambda}_n = 500 \times \frac{\left[\left(k_{\beta 1} + k_{fm1}M\right) - \left(k_{\beta 2} + k_{fm2}M\right)\right] r + k_{\beta 2} + k_{fm2}M}{M\left[\left(k_{p1} - k_{p2}\right) r + k_{p2}\right] t} \left[t - \frac{1 - \exp\left(-k_{LCB} C r t\right)}{k_{LCB} C r} \right] \tag{3-40}$$

Inspection of this equation and Tables 3-12 and 3-13 show that in order to make any LCB predictions, 5 kinetic parameters must be known. These parameters are listed in Table 5-7.

Table 5-7- List of the kinetic parameters required in Equation (3-40).

Required kinetic parameter
k_{p1} ($k_{p,\,CGC}$, propagation rate constant for CGC-Ti)
$k_{\beta 1} + k_{fm1}M$ ($(k_{\beta,\,CGC} + k_{fm,\,CGC}M)$, macromonomer formation kinetic parameter for CGC-Ti)
k_{LCB} (long-chain branching rate constant, only for CGC-Ti)
k_{p2} ($k_{p,\,Ind}$, propagation rate constant for $Et[Ind]_2ZrCl_2$)
$k_{\beta 2} + k_{fm2}M$ ($(k_{\beta,\,Ind} + k_{fm,\,Ind}M)$, macromonomer formation kinetic parameter for $Et[Ind]_2ZrCl_2$)

As observed in previous sections and discussed in Chapter 3, metallocene active sites in combined catalyst systems, act independently of each other, i.e. the existence of one site does not affect the polymerization kinetics of the other active site. This means that the kinetic data obtained from single catalyst experiments are applicable to polymerization systems with combined catalysts. The following explains the procedures used to estimate each kinetic parameter, stated in Table 5-7, individually.

It should be mentioned here that the methods presented in the following sections are simple procedures to find a rough estimation of required kinetic parameters. Precise estimation of parameters requires a detailed statistical analysis of the uncertainties associated with the estimation of each parameter and is beyond the scope of this chapter.

5-5-1- Estimation of the Propagation Rate Constant

As explained in Section 5-2, the ethylene feed line of the polymerization reactor was equipped with an in-line mass flow meter. In all of the polymerization experiments, ethylene was supplied through the feed line on demand to keep the reactor pressure constant. Therefore, measuring ethylene feed flow rate through the in-line mass flow meter is equivalent to monitoring the monomer consumption rate or in other words the polymerization rate.

According to the polymerization mechanism presented in Section 3-2, the rate of monomer consumption can be expressed as:

$$-\frac{dM}{dt} = k_p M_t C \qquad (5\text{-}1)$$

where:

$-dM/dt$ is the rate of monomer consumption (obtained from the in-line mass flow meter data)

M_l is the ethylene concentration in liquid phase, which is considered constant (due to the constant ethylene pressure)

C is the catalyst or active site concentration

k_p is the propagation rate constant.

To estimate k_p, two different cases may be considered:

Catalyst deactivation is negligible

In this case the concentration of active sites is considered constant ($C=C_0$) throughout the polymerization. Therefore, dM/dt has to be constant. To estimate k_p, an average value for dM/dt is estimated using the flow rate data. C_0 and M_l are known, therefore the propagation rate constant can be calculated using Equation (5-2):

$$k_p = \frac{-dM/dt}{M_l C_0} \tag{5-2}$$

Catalyst deactivation is significant

In this case a first order reaction (Section 3-1-1) for the catalyst deactivation is considered:

$$\frac{dC}{dt} = -k_d C \tag{5-3}$$

Equation (5-3) can be easily integrated using the following initial condition:

$C = C_0 \qquad at \qquad t = 0$

$$\therefore C = C_0 \exp(-k_d t) \tag{5-4}$$

Substituting Equation (5-4) into Equation (5-1) results in:

$$\frac{-dM}{dt} = k_p M_l C_0 \exp(-k_d t) \tag{5-5}$$

Rearranging Equation (5-5):

$$\ln\left(-\frac{dM}{dt}\right) = \ln\left(k_p M_l C_0\right) - k_d t \tag{5-6}$$

Equation (5-6) states that the plot of $\ln(-dM/dt)$ vs. t is a straight line with:

$$slope = -k_d \tag{5-7}$$

$$intercept = \ln (k_p M_l C_0) \tag{5-8}$$

The intercept and slope are calculated by fitting a straight line to $\ln(-dM/dt)$ versus time data. As shown in Equation (5-7), the catalyst deactivation rate constant is directly estimated by the calculation of slope. The propagation rate constant, k_p, is estimated by rearranging Equation (5-8). All other parameters (M_l and C_0) are constant and known.

$$k_p = \frac{\exp(intercept)}{M_l C_0} \tag{5-9}$$

Figure 5-15 is the plot of ethylene flow rate versus time obtained from the in-line mass flow meter signal for the polymerizations of ethylene using CGC-Ti. The downward trend of ethylene flow rate with time is the indication of a consistent drop in polymerization rate. This shows that catalyst deactivation does happen and therefore should be considered in estimating k_p.

The periodic fluctuations observed in Figure 5-15 is due to the temperature fluctuation as shown in Figure 5-16.

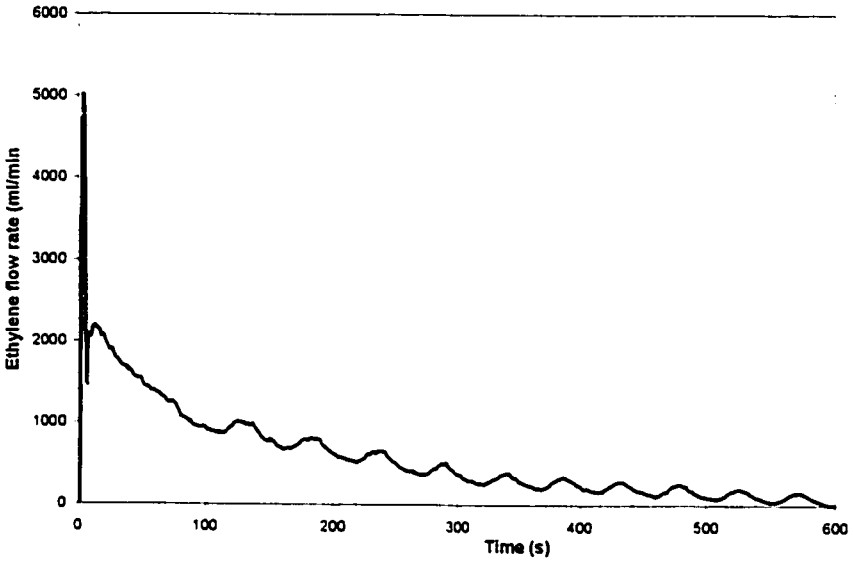

Figure 5-15- Ethylene flow rate versus time for CGC-Ti polymerization system.

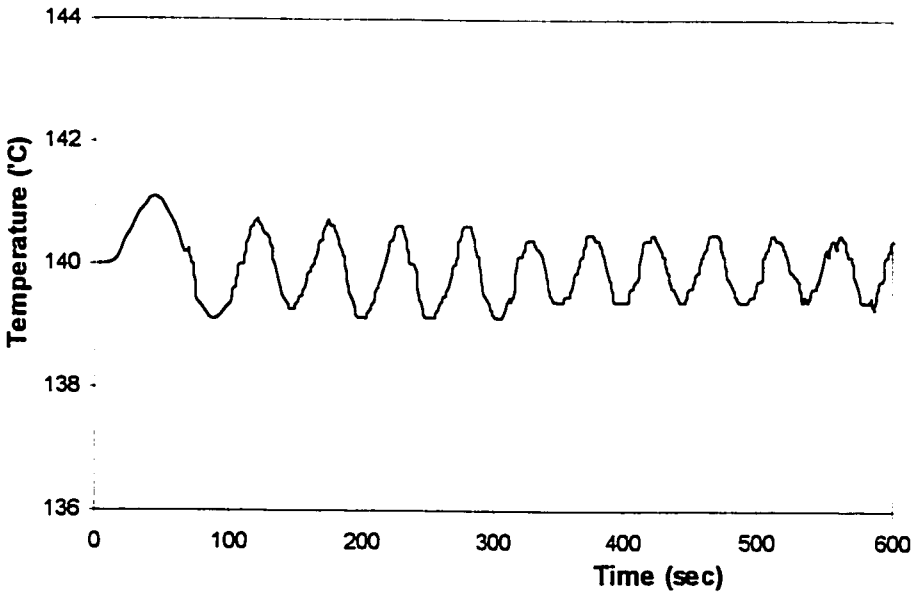

Figure 5-16- Temperature versus time for CGC-Ti polymerization system.

Figures 5-17 shows the plot of ln(*-dM/dt*) versus time, as stated in Equation (5-6), along with the fitted line and its equation. This plot is made using the data employed in Figure 5-15.

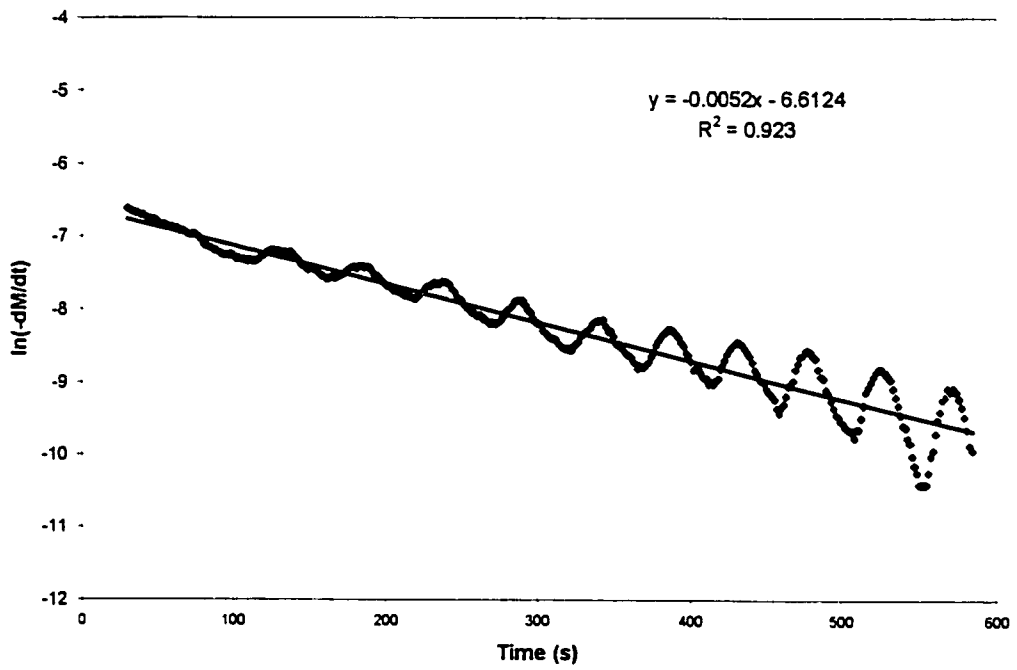

Figure 5-17- Plot of Equation (5-6) for the polymerization of ethylene with CGC-Ti.

Because of the initial fluctuations in flow rate, due to the injection of catalyst (Figure 5-15) and hence pressure disturbance, the data points collected during the first 30 seconds of the polymerization were not used in calculation (Figure 5-17).

As shown in Figure 5-17, the slope and the intercept of the fitted line are:

slope = -0.0052

intercept = -6.6124

As stated in Table 5-4, the initial catalyst concentration, C_0, for all polymerization experiments was $C_0 = 4\times10^{-6}$ mol/l. A computer program, based on Chao-Seader

(Appendix E) correlation (Smith and Van Ness 1975) using the reaction conditions stated in Table 5-4, was employed to calculate the monomer concentration in the liquid phase. This concentration was estimated to be $M_l = 0.9$ mol/l.

Substituting the calculated values into Equations (5-7) and (5-9), the estimated k_d, and k_p are:

$k_{p,\,CGC} = 373.22\ L/(mol{\cdot}s)$

$k_{d,\,CGC} = 0.0052\ s^{-1}$

Similar analysis on mass flow rate data collected from the polymerization of ethylene with $Et[Ind]_2ZrCl_2$, yields to the following values for k_p and k_d.

$k_{p,\,Ind} = 735.59\ L/(mol{\cdot}s)$

$k_{d,\,Ind} = 0.0056\ s^{-1}$

5-5-2- Estimation of Macromonomer Formation Kinetic Parameter

According to the polymerization mechanism proposed in Section 3-2, the rate of macromonomer formation for a single-site catalyst, can be expressed as:

$$\frac{dD^{=}}{dt} = \left(k_{\beta} + k_{fm} M_l\right) C \qquad (5\text{-}10)$$

where:

$dD^{=}/dt$ is the rate of macromonomer formation

M_l is the ethylene concentration in liquid phase, which is considered constant (due to the constant ethylene pressure)

C is the catalyst or active-site concentration

k_β is the β-hydride elimination rate constant.

k_{fm} is the transfer to monomer rate constant

Substituting Equation (5-4) in (5-10) and integrating the obtained equation using the following initial condition

$$D^= = 0 \qquad at \qquad t = 0$$

results in:

$$D^= = \frac{(k_\beta + k_{fm} M_l) C_0}{k_d} [1 - \exp(-k_d t)] \tag{5-11}$$

Rearranging Equation (5-11):

$$(k_\beta + k_{fm} M_l) = \frac{k_d D^=}{C_0 [1 - \exp(-k_d t)]} \tag{5-12}$$

To estimate ($k_\beta + k_{fm}[M_l]$) the concentration of macromonomers, $D^=$, should be estimated. The number of moles of polymer chains can be estimated from the GPC molecular weight data and the weight of polymer produced:

$$moles\ of\ polymer\ chains = \frac{weight\ of\ produced\ polymer}{M_n} \tag{5-13}$$

where, M_n is the number-average molecular weight obtained from GPC analysis.

As shown in Section 5-4, ^{13}C-NMR analysis data can be used to estimate the ratio of saturated/unstaturated chain ends. $D^=$ can be easily estimated from the chain-end type ratio, and the number of moles of polymer chains. Substituting the value for $D^=$, k_d, C_0, and t in Equation (5-12), ($k_\beta + k_{fm} M_l$) can easily be estimated. The following calculations shows how this parameter was estimated for the polymerization system of ethylene with $Et[Ind]_2ZrCl_2$.

In the polymerization experiment carried out using $Et[Ind]_2ZrCl_2$ as catalyst, 11.5 g polyethylene with M_n = 21326 was synthesized. Therefore, according to Equation (5-13):

$$moles\,of\ polymer\ chains = \frac{weight\ of\ produced\ polymer}{M_n} = \frac{11.5}{21326} = 5.3925 \times 10^{-4}$$

^{13}C-NMR data (Table 5-6) shows that the ratio of saturated/unsaturated chain ends is equal to 0.98. Therefore, the number of moles of terminal double bonds is:

$$moles\,of\ terminal\ bonds = \frac{2 \times 5.3925 \times 10^{-4} \times 0.98}{1.98} = 5.338 \times 10^{-4} \quad mol$$

$$D^{=} = \frac{moles\,of\ terminal\ double\ bonds}{Reaction\ volume} = \frac{5.338 \times 10^{-4}}{0.4(l)} = 1.3345 \times 10^{-3} \quad mol/l$$

substituting in Equation (5-12) yields to:

$$\left(k_{\beta,Ind} + k_{fm,Ind} M_l\right) = 1.9355\ s^{-1}$$

Similar calculations for the polymerization of ethylene with CGC-Ti yields to the following value for the macromonomer formation kinetic parameter:

$$\left(k_{\beta,CGC} + k_{fm,CGC} M_l\right) = 0.0824\ s^{-1}$$

5-5-3- Estimation of the LCB Formation Rate Constant

As the polymerization mechanism proposed in Chapter 3 implies, long-chain branching takes place as a result of the reaction between an active site and a chain with terminal double bond (macromonomer). The rate constant of such reaction, k_{LCB}, is considered to be independent of the length of the macromonomer. In reality, this is a good assumption only if the macromonomer's chain-length is greater than a certain

number. Figure 5-18 illustrates how reactivity ratio varies with the chain length of α-olefins in a typical Ziegler-Natta ethylene polymerization system (Knight and Lai 1993).

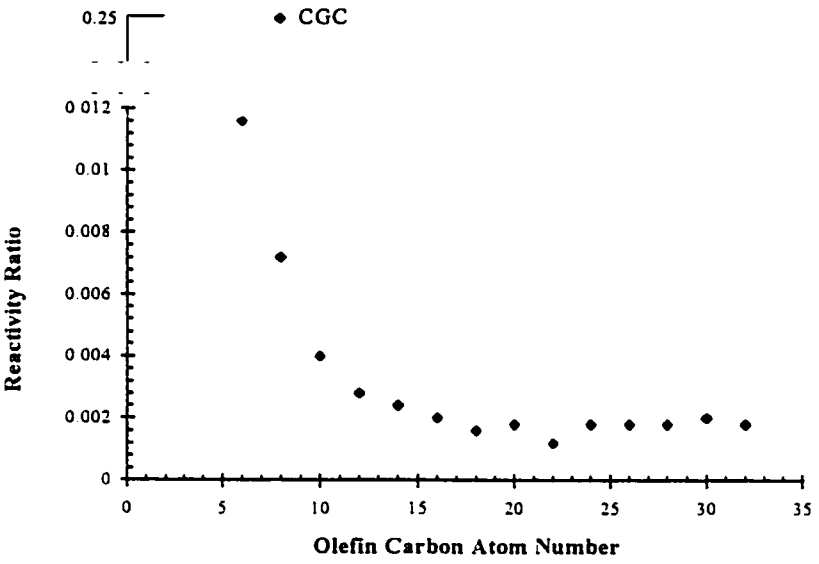

Figure 5-18- Typical values of reactivity ratios for Ziegler-Natta and CGC catalyst (Knight and Lai 1993).

As shown in this figure, although the reactivity ratio varies dramatically for short α-olefins, it levels off for chain lengths of 16 and higher. The same type of behavior is expected to exist for CGC polymerization systems. This means that, if rate constants for the incorporation of α-olefins with different chain lengths in ethylene/α-olefin copolymerization with CGC are plotted, the value that the plot levels off at could be used as the long-chain branching rate constant, k_{LCB}.

Therefore, a series of copolymerization experiments using five different α-olefins were performed. The α-olefins used in these experiments are listed in Table 5-8.

Table 5-8- Comonomers used in copolymerization experiments.

α-olefin	Chemical formula
n-Hexane	C_6H_{12}
n-octene	C_8H_{16}
n-decene	$C_{10}H_{20}$
n-hexadecene	$C_{16}H_{32}$
Eicosene	$C_{20}H_{40}$

All copolymerization experiments were carried out at the same conditions as explained in Section 5-2, except that in each experiment 40 ml of solvent was replaced with the used macromonmer.

The synthesized samples were then analyzed with ^{13}C-NMR and GPC for their comonomer content and molecular weight distribution. Comonomer contents were calculated using the procedures proposed by DePooter et al. (1991).

If the comonomer molecules are considered as dead polymer chains with terminal double bonds (macromonomers), then according to the polymerization mechanism proposed in Chapter 3 the comonomer contents, F_2, can be calculated as:

$$F_2 = \frac{k_{Br} D^=}{k_p M_l + k_{Br} D^=} \tag{5-14}$$

where:

k_{Br} comonomer propagation (branching) rate constant.

k_p ethylene propagation rate constant

M_l ethylene concentration in liquid phase

$D^=$ comonomer concentration

Rearranging Equation (5-14) to calculate the ratio of the rate constants:

$$\frac{k_{Br}}{k_p} = \frac{F_2}{1-F_2} \times \frac{M_1}{D^=} \qquad (5\text{-}15)$$

Equation (5-15) along with the ^{13}C-NMR analysis data was used to calculate the rate constant ratios. The summary of the calculation, and the plot of the variation of k_{Br}/k_p versus comonomer length are given in Table 5-9 and Figure 5-19, respectively.

Table 5-9- Summary of calculations.

Comonomer	Initial concentration (*mol/l*)	Comonomer content, F_2, calculated from ^{13}C-NMR data	$\frac{k_{Br}}{k_p}$
n-hexene	0.7776	0.08053	0.10137
n-octene	0.6265	0.05091	0.07706
n-decene	0.4967	0.03038	0.05677
n-hexadecene	0.3220	0.01125	0.03180
Eicocene	0.02056	0.000567	0.02483

The same decreasing pattern shown in Figure 5-18 is observed in Figure 5-19. Although apparently the k_{Br}/k_p plot has not reached its asymptotic value, even for a comonomer with 20 carbon atoms, its slope is decreasing very quickly as the comonomer becomes longer. This indicates that the value of k_{LCB} / k_p for this catalyst system must be lower than the k_{Br}/k_p calculated for eicocene, i.e.:

$$\frac{k_{LCB}}{k_{p,CGC}} < 0.0248$$

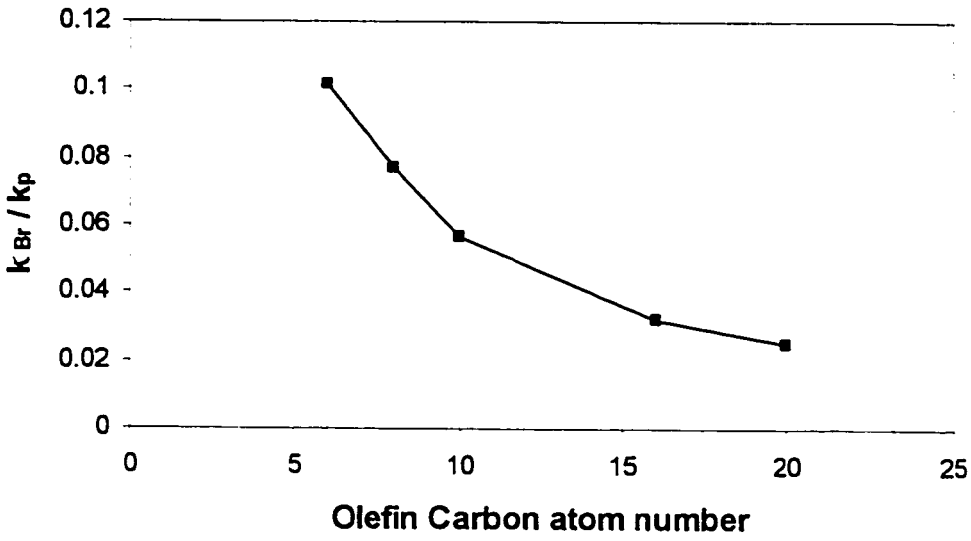

Figure 5-19- Variations of k_{Br}/k_p with α-olefin chain length for the copolymerization of ethylene/α-olefin with CGC-Ti.

The values of kinetic parameters, estimated in Sections 5-5-1 to 5-5-3, are summarized in Table 5-10.

Table 5-10- Summary of polymerization kinetic parameters.

Kinetic parameter	CGC-Ti	$Et[Ind]_2ZrCl_2$
k_p	373.22 *L/(mol.s)*	735.59 *L/(mol.s)*
$k_\beta + k_{fm} M$	0.0824 s^{-1}	1.9355 s^{-1}
k_{LCB} / k_p	< 0.0248	N/A

Substituting the rate constant values given in Table 5-10 in Equation (3-40), the number of branches per 1000 carbon atoms, λ_n, versus the mole fraction of CGC-Ti, *r*,

can be plotted. This plot, along with the obtained experimental data (Figure 5-6), is illustrated in Figure 5-20. It should be mentioned that the value of $k_{LCB} / k_p = 0.024$ was used in Equation (3-40) for this plot.

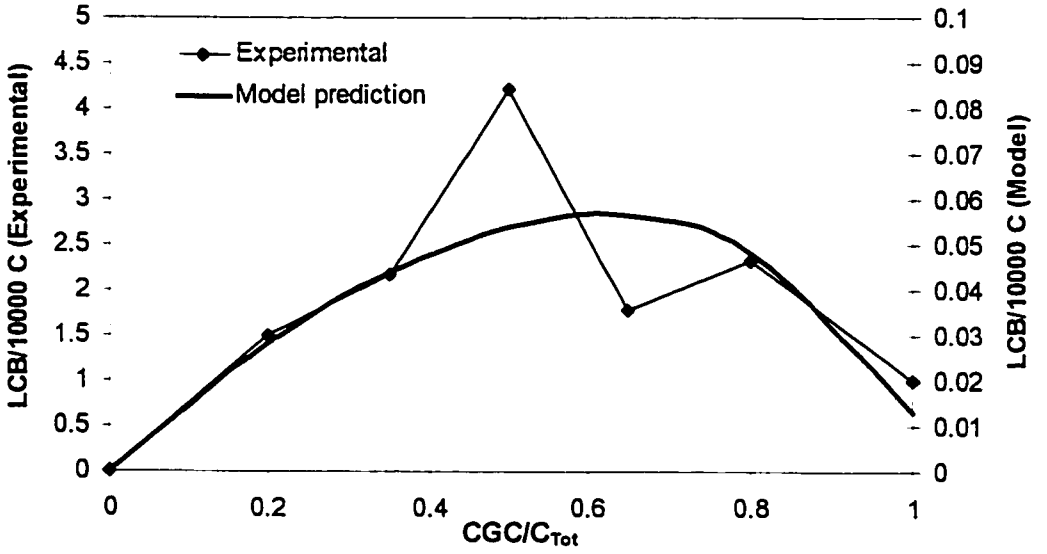

Figure 5-20- Variation of LCB degree with CGC-Ti mole fraction. Model prediction and experimental data (^{13}C-NMR data).

As shown in Figure 5-20, model predictions follow the same trend as the experimental data and the optimum CGC-Ti mole fraction is predicted by the model. However, the model underestimates the branching degrees. This could be related to many unconsidered factors in the model such as: simplifications made in model development in order to obtain an analytical expression for LCB degree variations, and decrease in monomer concentration due to the high polymerization rate during the first minutes of each experiment.

The fact that the model predicts the general trend and, more importantly, the optimum CGC-Ti mole fraction to maximize LCB degree, clearly illustrates the value of this simple model for quickly screening several metallocene combinations for the production of polyethylene with optimum LCB degrees.

5-6- Effect of Cocatalysts

The catalyst systems employed in the polymerization experiments, utilized two compounds as cocatalysts, MAO and TPFB. It has been shown by different research groups (Reddy and Sivaram 1995, Michiels and Escalona 1995, Soga and Kaminaka 1994, Forlini and Fan 1997) that the type and amount of cocatalyst have significant effects on chain microstructure.

Preliminary studies with CGC-Ti on the type of cocatalyst showed that MAO was an essential compound in catalyst system. Several polymerization experiments using different common cocatalysts (TMA, tri(isobutyl)aluminum TIBA) alone or accompanied with tris(pentafluorophenyl)borane (TPFB) were performed but no catalyst activity was observed in the absence of MAO. Since TPFB was suggested as the most effective long-chain branching cocatalyst for CGC-Ti (Lai et al. 1993,1997), in all polymerization experiments the combination of MAO and TPFB was used as cocatalyst.

This section is devoted to the study of the effects of these cocatalysts on molecular weight and LCB degree. The focus of the study is mainly on the effects of the amount of each cocatalyst. Experiment conditions (cocatalysts amounts) were selected based on 2×2 factorial design of experiments (Box et al. 1978). All other reaction conditions (temperature, pressure, solvent, and catalyst concentration) were the same as those discussed in Section 5-3, except that 15 ml of hydrogen (as chain transfer agent) was used in these polymerization experiments.

5-6-1- Design of Experiments

A 2×2 factorial design with three replicates at the center point (Figure 5-21) was used to assign the reaction conditions. The molar ratios of MAO and TPFB to catalyst are considered as factors and number-average molecular weight, M_n, and long-chain branching degree, λ_n, are the responses.

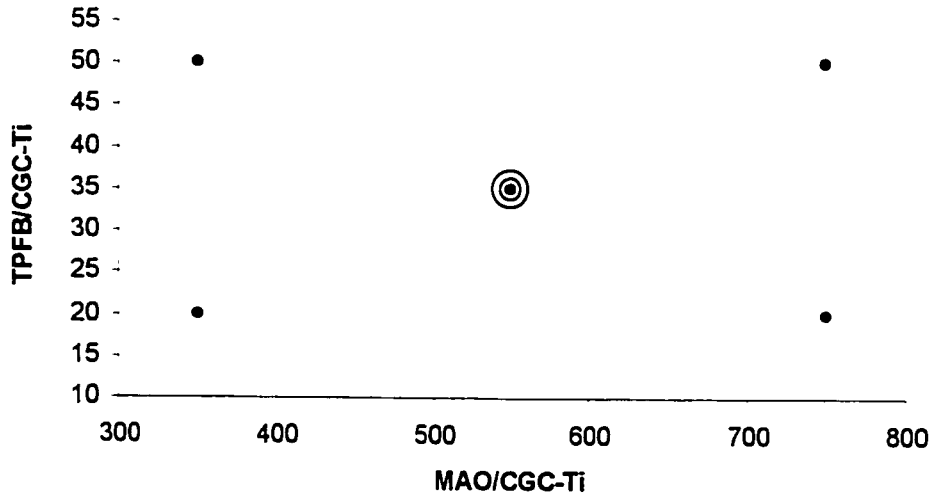

Figure 5-21- Graphical demonstration of the employed factorial design.

The synthesized samples were analyzed with GPC and ^{13}C-NMR for their molecular weight distribution and branching degrees. Table 5-11 shows the design and responses obtained from these analysis.

Table 5-11- Values of the factors and the responses.

FACTORS		RESPONSES	
MAO/CGC-Ti	TPFB/CGC-Ti	M_n	λ_n
750	50	38516	0.142
750	20	21456	0.255
350	50	64325	0.128
350	20	29456	0.173
550	35	31598	0.149
550	35	35261	0.161
550	35	30956	0.171

5-6-2- Effects of Cocatalyst Type on Molecular Weight

Table 5-12 shows the analysis of variance (ANOVA) (Box et al. 1978) for the number-average molecular weight results obtained from GPC measuements.

Table 5-12- ANOVA table for the molecular weight results.

Source		Effect	SS	df	MS	F_{obs}	$F_{0.05,1,2}$
MAO/CGC-Ti		-16904.5	285762120.3	1	285762120	52.97980	18.51
TPFB/CGC-Ti		25964.5	674155260.3	1	674155260	124.9872	18.51
MAO×TPFB (interaction)		-8904.5	79290120.25	1	79290120.3	14.70025	18.51
Error	Lack of fit		58331666.7	1	58331666.7	10.8146	18.51
	Pure error		10787586.0	2	5393793		

Where:

Effect is the average effect of each factor and is equal to:

Effect = Average of response at high level - Average of response at low level

SS is the sum of squares of the variability around the mean and is calculated by:

$SS = 2^{n-2}(\text{effect})^2$, where n = number of factors (n = 2 for this case)

df shows the degrees of freedom available for each factor.

MS is the mean-squared of the variability around the mean (variance) associated with each factor and is calculated by:

MS = SS / df

$\mathbf{F_{obs}}$ (observed F-value) is equal to the ratio of the MS (variance) of each factor to the MS of error. This ratio will be compared to an F-distribution to see if the variances are different.

$\mathbf{F_{0.05,1,2}}$ is the F-value with degrees freedom of 1 and 2 (for numerator and denominator, respectively) having 0.95 of the area under the F-distribution curve. The comparison of F_{obs} with this F-value will result in making conclusions with 95% confidence.

Inspection of Table 5-12 shows that the two-factor interaction is not significant and that there is no lack of fit problem. However, if the confidence level is reduced to 90%, the interaction effect and lack of fit will become significant ($F_{0.1,1,2}$ = 8.53). This makes it difficult to decide: 1) whether or not to include the interaction term in the model and 2) if there is a lack of fit problem. The M_n data presented in Table 5-11 was examined using the Box-Cox transformation analysis (Box et al. 1978). Results of this analysis suggest that if the reciprocal of the number average molecular weight, $1/M_n$, is

used, the residual sum of squares (RSS) becomes minimum, the two-factor interaction is insignificant, and there is no indication of lack of fit.

Table 5-13 shows the ANOVA table for the transformed response, $1/M_n$. The comparison of F_{obs} with $F_{0.05,1,2}$ for the effect of the MAO/catalyst ratio on $1/M_n$, shows that this factor has a significant effect on number-average molecular weight. The positive sign for the MAO effect means that catalyst systems with higher MAO to catalyst ratios synthesize polymers with higher $1/M_n$ values (lower molecular weights).

Table 5-13- ANOVA table for the reciprocal of the molecular weight results.

Source		Effect	SS	Df	MS	F_{obs}	$F_{0.05,1,2}$
MAO/CGC-Ti		1.1536E-5	1.3308E-10	1	1.3308E-10	29.8421	18.51
TPFB/CGC-Ti		-1.9536E-5	3.8166E-10	1	3.8166E-10	85.5921	18.51
MAO×TPFB (interaction)		-1.1215E-6	1.2578E-12	1	1.2578E-12	0.2821	18.51
Error	Lack of fit		1.1E-13	1	1.1e-13	0.0247	18.51
	Pure error		8.9181E-12	2	4.4591e-12		

This effect is better demonstrated in Figure 5-22. The error bars used in this figure indicate the 95% confidence intervals associated with the effect.

Transfer to cocatalyst (in this case to aluminum of MAO) is one of the common transfer reactions in polymerization of olefins with metallocene catalysts. Therefore, the formation of lower molecular weight polymer chains at higher ratios of MAO/CGC-Ti can be attributed to higher rates of transfer to aluminum in this polymerization system.

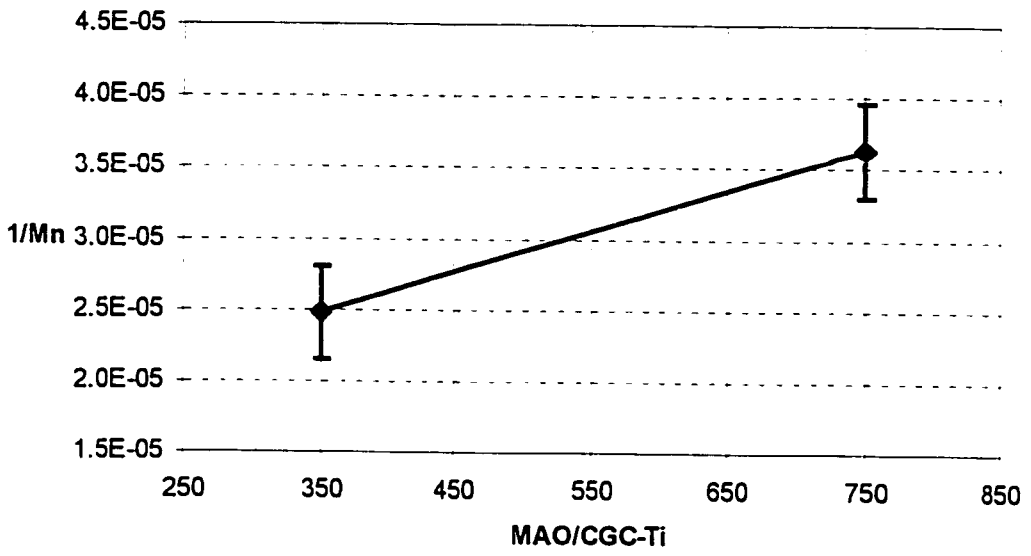

Figure 5-22- Effect of MAO/CGC-Ti ratio on the reciprocal of the number-average molecular weight.

As stated in the ANOVA table, the effect of TPFB/CGC-Ti is quite signficant as well. The negative sign of the effect of this factor, shows that $1/M_n$ decreases (molecular weight increases) as higher ratios of TPFB/CGC-Ti are used. Since this observation had not been previously reported in literature, to the best of our knowledge, two more polymerization experiments at higher levels of this factor (TPFB/CGC-Ti = 100, and 150) were performed to investigate whether or not the same trend was observed. Figure 5-23 illustrates the molecular weight distribution of all four polyethylene samples synthesized at different TPFB/CGC-Ti levels, obtained from GPC analysis.

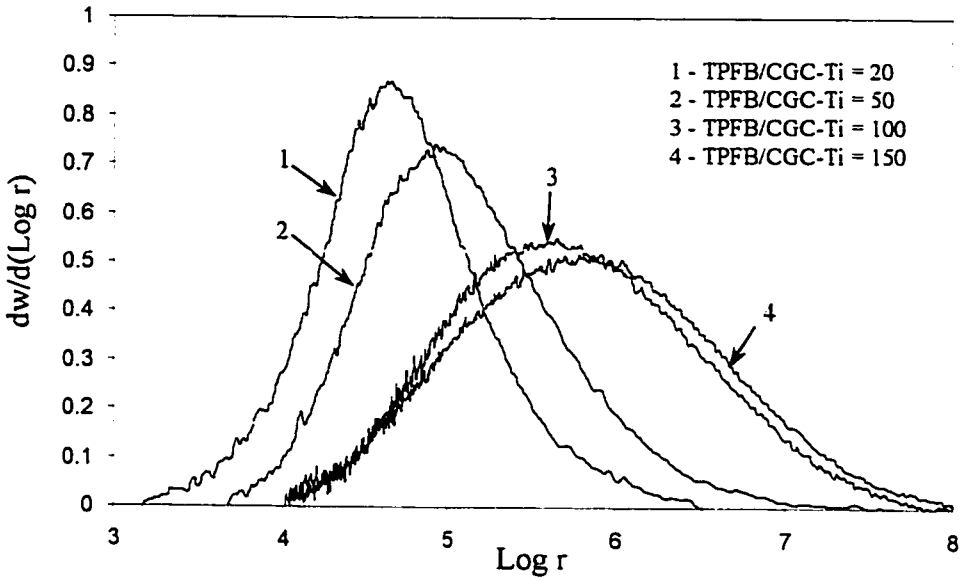

Figure 5-23- MWD of the polyethylene samples synthesized with different TPFB/CGC-Ti ratios. (MAO/CGC-Ti = 350).

As clearly evident in this figure, higher TPFB to catalyst ratio results in the formation of longer polymer chains with broader molecular weight distribution. The molecular weight of the samples rises to values of around 900000 grams/mol and polydispersity indexes escalate to up to PDI = 10 as TPFB/CGC-Ti ratio increases. No simple explanation for this behavior was found, but it is clear that increasing TPFB/CGC-Ti ratio leads to the formation of active sites with increasing ratio of propagation to transfer. This might be an attractive way of producing polyethylene with broad MWD and high MW averages with CGC-Ti.

The two factor interaction effect, as stated in the ANOVA table, was not found to be significant, which means that the effect of one factor does not depend on the value of the other.

5-6-3- Effects of Cocatalyst type on LCB Degree

Table 5-14 shows the analysis of variance for the effects of cocatalyst to catalyst ratios on number of long-chain branches per 1000 carbon atoms, obtained from ^{13}C-NMR analysis.

Table 5-14- ANOVA table for the LCB results.

Source		Effect	SS	df	MS	F_{obs}	$F_{0.05,1,2}$
MAO/CGC-Ti		0.048	0.002304	1	0.002304	18.9890632	18.51276
TPFB/CGC-Ti		-0.079	0.006241	1	0.006241	51.4369545	18.51276
MAO×TPFB		-0.034	0.001156	1	0.001156	9.5274987	18.51276
Error	Lack of fit		0.000344	1	0.000344	2.83556	18.51276
	Pure error		0.000243	2	0.000122		

Inspection of the ANOVA table shows that both main effects are significant with 95% confidence as the observed F-values are greater than the critical F-value and that the 2-factor interaction effect is not significant. However, if the confidence level is reduced to 90%, the interaction effect will become significant ($F_{0.1,1,2}$ = 8.53). This makes it difficult to decide whether or not to include the interaction term in the model. The Box-Cox transformation analysis (Box et al. 1978) of LCB data suggests that if the reciprocal of LCB degree, $1/\lambda_n$, is used, the residual sum of squares (RSS) becomes minimum and the two-factor interaction is insignificant. Table 5-15 shows the ANOVA table for the transformed response, $1/\lambda_n$.

Table 5-15- ANOVA table for the reciprocal of LCB degree results.

Source		Effect	SS	df	MS	F_{obs}	$F_{0.05,1,2}$
MAO/CGC-Ti		-1.31451	1.727943	1	1.727943	9.19347	18.51276
TPFB/CGC-Ti		2.57642	6.637935	1	6.637935	35.31694	18.51276
MAO×TPFB		0.54427	0.296225	1	0.296225	1.57606	18.51276
Error	Lack of fit		0.023741	1	0.023741	0.12631	18.51276
	Pure error		0.375907	2	0.187953		

The MAO/catalyst ratio effect on long-chain branching degree is significant if the confidence level is reduced to 90%. The negative sign means that: higher values of this factor, result in the formation of more long-chain branches. This can be attributed to the lower deactivation of active sites at higher concentrations of MAO, as higher catalyst activity and lower catalyst deactivation have been reported in the literature (Reddy and Sivaram 1995, Huang and Rempel 1995, Olabisi et al. 1997). Figure 3-7 in Chapter 3 shows the effect of catalyst deactivation on LCB degree. The observed result for the effect of MAO is in complete agreement with the modeling results presented in Figure 3-7.

The ANOVA table also shows that TPFB/catalyst ratio has a positive effect on the reciprocal of LCB degree. This means that higher LCB degrees are obtained for lower values of this factor. According to the polymerization mechanism proposed in Chapter 3, the rate of LCB formation is proportional to:

$$\frac{d\lambda_n}{dt} \propto k_{LCB} \times D^{=} \qquad (5\text{-}16)$$

Therefore, the positive effect of this factor on LCB degree may be attributed to two factors: 1) lower macromonomer concentration 2) lower reaction rate constant, k_{LCB}.

As observed in the previous section, any increase in TPFB/CGC-Ti ratio resulted in the production of higher molecular weight polymer, which means lower number of chains and hence lower number of chain ends and therefore lower macromonomer concentration.

In order to see whether or not the LCB formation rate constant alters with the amount of TPFB, a series of ethylene/1-octene copolymerization experiments at different TPFB levels were performed. The idea was to keep the concentration of terminal double bonds (1-octene) constant and by changing the TPFB concentration, investigate if the branch formation (comonomer content of the copolymer) is affected. The synthesized copolymers were analyzed with ^{13}C-NMR for their comonomer contents. Figure 5-24 shows the variations of the comonomer content, F_2, with TPFB/CGC-Ti ratio. As shown in this figure, no significant variation is observed. This means that k_{C8} is not affected by TPFB level. It is reasonable to speculate that the same would be true for larger α-olefins and macromonomers. Therefore, one can assume the k_{LCB} is not affected by TPFB level and that lower macromonomer concentration (due to higher molecular weight) is the main cause of lower LCB formation at a higher TPFB/CGC-Ti ratio.

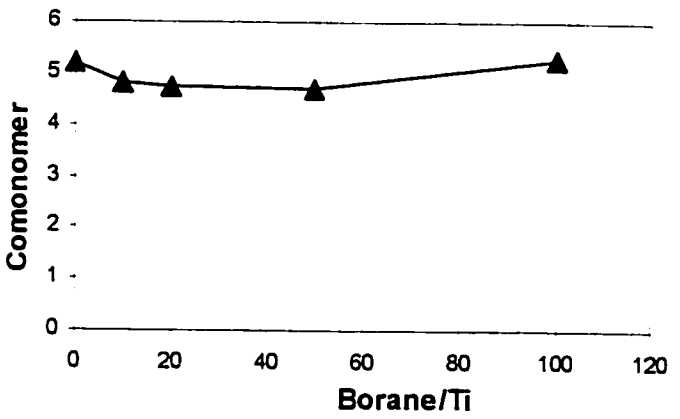

Figure 5-24- Variations of comonomer content with TPFB/CGC-Ti ratio.

Chapter 6

Modeling of Fractionation in CRYSTAF

6-1-Introduction

Physical properties of polymers cannot be uniquely determined by the average values of their molecule properties. For example, the knowledge of molecular weight averages of a polymer sample determined by light scattering or osmometry is usually not sufficient to unequivocally define its mechanical and rheological properties. Polymers with the same average molecular weights may have completely different physical properties due to the difference in their molecular weight distributions. For the case of olefin copolymers, the whole distribution of composition, in addition to the molecular weight, is required to accurately define their physical properties and average copolymer composition or the average branching degrees determined by FT-IR or ^{13}C-NMR

spectroscopy will not be sufficient. Temperature rising elution fractionation (TREF) has been used for determining the chemical composition distribution of semi-crystalline polymers and in particular ethylene/α-olefin copolymers. The operation procedure of TREF has been reported extensively elsewhere (Mirabella 1987; Soares and Hamielec 1995,1999; Elicabe et al. 1996 a,b). In summary, TREF can be divided into two sequential stages, precipitation and elution. In the precipitation step the polymer is dissolved in a good solvent (usually at a temperature higher than its melting point) in contact with an inert support. The precipitation is carried out by slowly decreasing the temperature under well-controlled conditions forming layers of polymer on the support (Mirabella 1987). In the second step, these polymer layers are eluted from the support in the reverse order they were precipitated. By continuous monitoring of the concentration of polymer in the eluted solvent a TREF curve is obtained.

Crystallization analysis fractionation (CRYSTAF), which was first introduced by Monrabal (1994, 1996), is a good alternative to TREF (temperature rising elution fractionation) analysis. While TREF requires two fractionation steps, i.e., crystallization and elution, CRYSTAF is done in a single crystallization step that reduces the analysis time considerably. In both techniques chains of semi-crystalline polymers are fractionated according to their solubility-temperature relationship (molecular structure) (Soares and Hamielec 1995). Although CRYSTAF (or TREF) results are used to estimate the copolymer composition distribution (CCD) in polyolefins via a calibration curve, the true relationship between the CRYSTAF (or TREF) results and CCD is still to be found. Apparently, precise knowledge of the precipitation mechanism in these methods is required to relate the analysis results to the copolymer composition distribution.

6-2- Experimental Apparatus

A schematic of a CRYSTAF apparatus is illustrated in Figure 6-1. A very dilute solution (0.1-0.2 wt%) of a polymer sample at temperatures higher than its melting point is cooled down very slowly (6-12 °C/hr) and the solution concentration is recorded at certain temperature intervals.

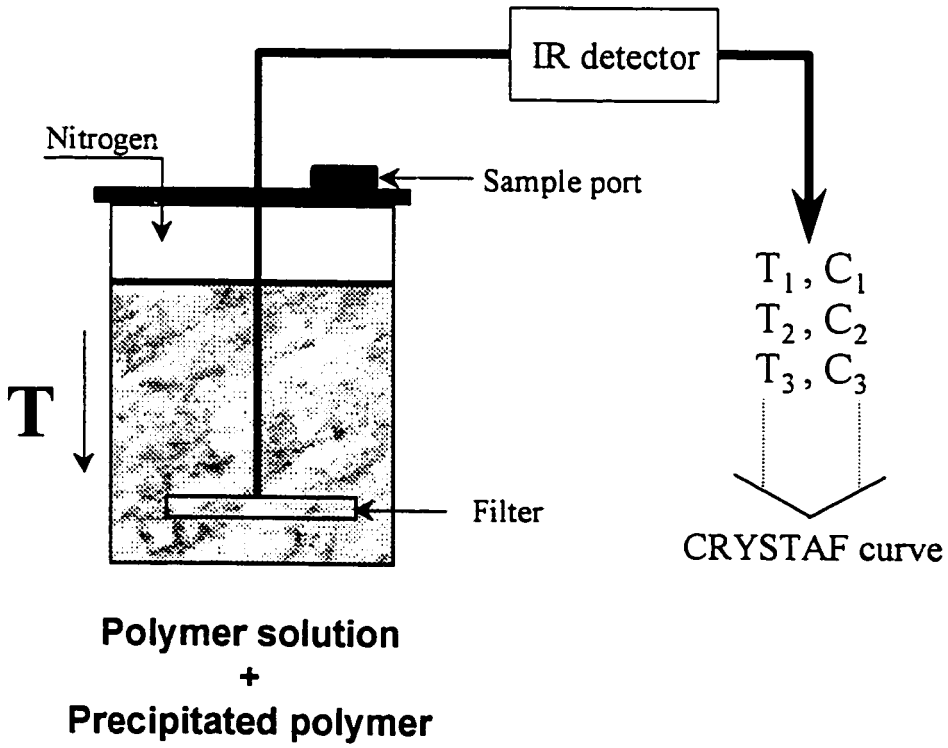

Figure 6-1- Schematic of a CRYSTAF apparatus.

A typical CRYSTAF curve for a linear-low density polyethylene sample synthesized by a multiple site-type catalyst is illustrated in Figure 6-2. The first data points, collected at temperatures above any crystallization, provide a constant concentration equal to the initial polymer solution concentration (zone 1). As temperature

decreases, the most crystalline fractions (linear chains or the ones with very few branches) will precipitate first. This results in a steep decrease in the solution concentration (zone 2). The fractionation of more-branched chains takes place at lower temperatures (zone 3). The last data point, corresponding to the lowest temperature of the crystallization cycle, represents the fraction that has not crystallized (mainly highly branched material) and remains soluble below 30 °C for this particular analysis.

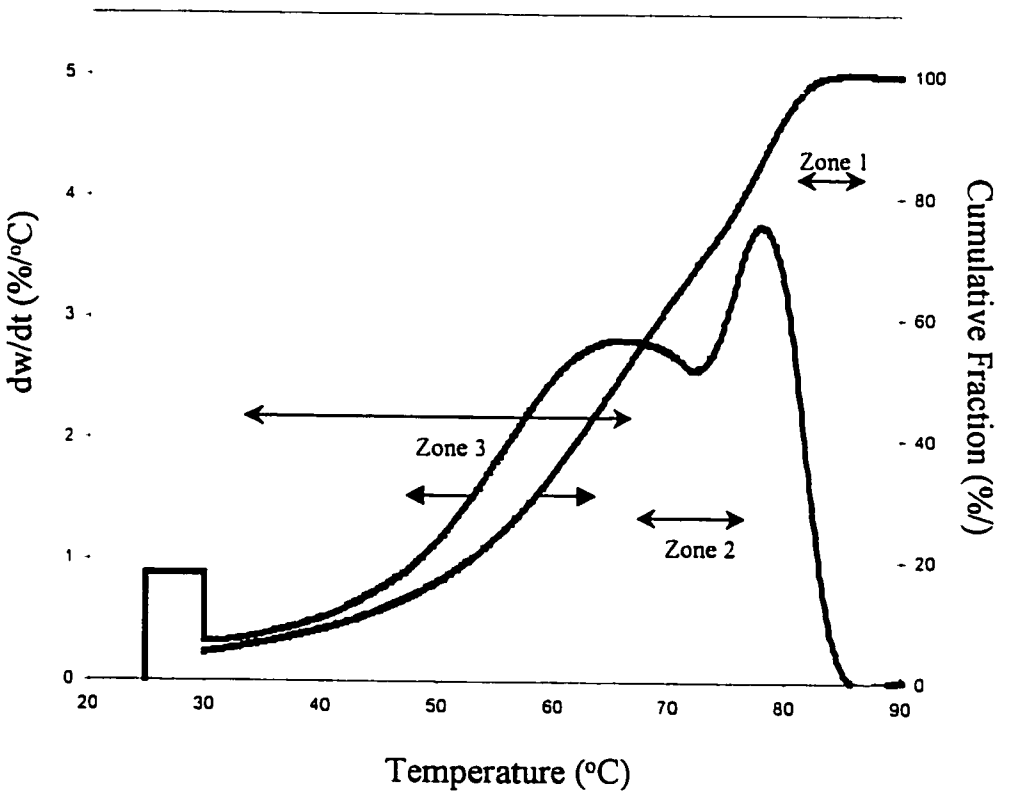

Figure 6-2- Cumulative and differential CRYSTAF profiles for LLDPE sample synthesized by a multiple site-type catalyst.

The top curve in Figure 6-2 is the cumulative CRYSTAF curve. The first derivative of this, which is very similar to TREF curves, is usually associated with the short-chain branching distribution, SCBD, (Monrabal 1994, 1996).

6-3 Fractionation Mechanism in CRYSTAF

CRYSTAF (or TREF) results are used to estimate the copolymer composition distribution (CCD) in polyolefins. However, the true relationship between CRYSTAF (or TREF) results and CCD is still to be found. Apparently, precise knowledge of the precipitation mechanism in these methods is required to relate the analysis results to the copolymer composition distribution.

In the following sections the crystallization of polymer chains from dilute solutions (similar to what takes place in CRYSTAF analysis) will be briefly reviewed. Then, based on the provided information from the crystallization kinetic studies, a mechanism for the fractionation mechanism in CRYSTAF will be proposed. Based on this proposed mechanism, CRYSTAF profiles will then be simulated and compared with experimental data.

6-3-1-Crystallization of Polymer Chains from Dilute Solutions

The thermodynamics of the crystallization of polymer chains from dilute solution have been studied by different investigators during the last fifty years. Typically, the crystals formed from dilute solutions are several microns in lateral dimensions and are of the order of 100 Å thick. This thickness is fairly uniform among the crystallites but is very sensitive to the crystallization conditions, particularly the crystallization temperature. Figure 5-3 illustrates a typical dependency of crystal thickness versus temperature (Jackson and Mandelkern 1968, Mandelkern 1970) for polyethylene. The outward appearance of a polyolefin single crystal, formed from dilute solutions, depends

on the chemical structure of the chain and crystallization conditions (temperature, nature of the solvent, cooling rate, etc.).

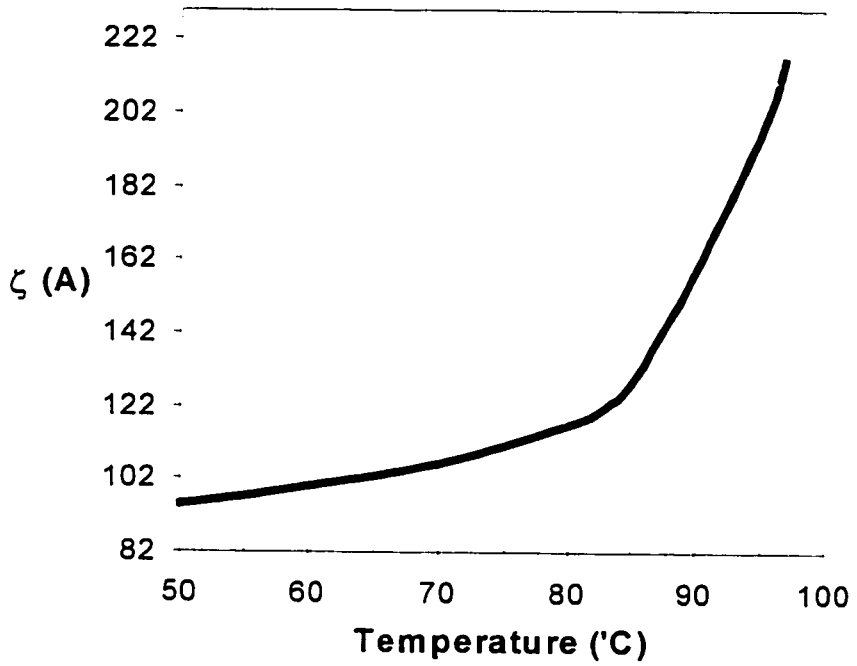

Figure 6-3- Temperature dependency of crystal thickness for polyethylene in xylene (Mandelkern 1970).

Polyolefin single crystals in their simplest form are mono-layer lamellae, which are often rhomboid (Tager 1978) (Figure 6-4). The axes *a* and *b* of a crystalline cell correspond to the long and short diagonals of a rhombus, while axis *c*, along which macromolecular chains are directed, is perpendicular to the crystal plane.

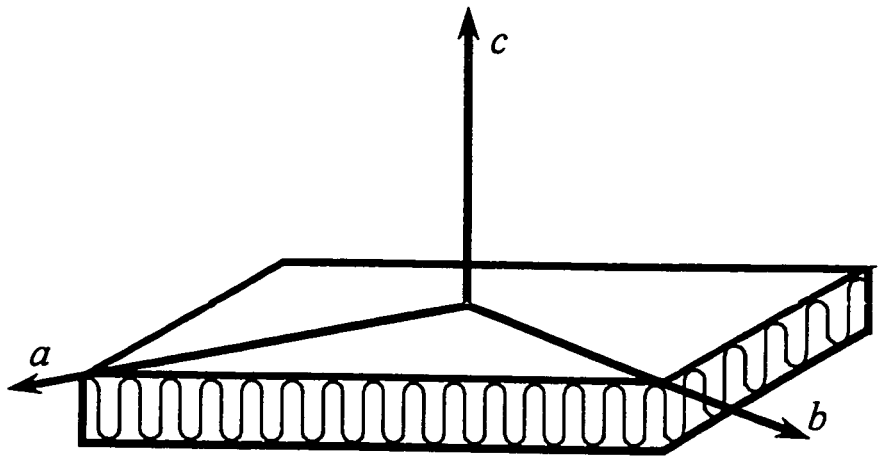

Figure 6-4- Diagram of the arrangement of crystallographic axes in lamellar crystal of polyethylene. (Tager 1978)

Since the length of macromolecules constitutes thousands of angstroms, while the thickness of a single crystal is not more than 200 Å, a chain has to fold several times to fit into the crystal. The re-entry requirement clearly demands some type of chain folding, however, the exact nature of the chain return is not obvious.

Two extreme cases can be considered which are consistent with electron microscope observation and low angle *X*-ray diffraction results (Mandelkern 1970). The first one, which is schematically illustrated in Figure 6-5, is called the regularly folded array. In this model each molecule crystallizes to the fullest extent possible. Crystallization is complete except for the number of chain elements that are required to make the fold. In this model crystalline sequences from the same molecule are adjacent to one another. In this manner it is proposed that a regularly folded interface be formed.

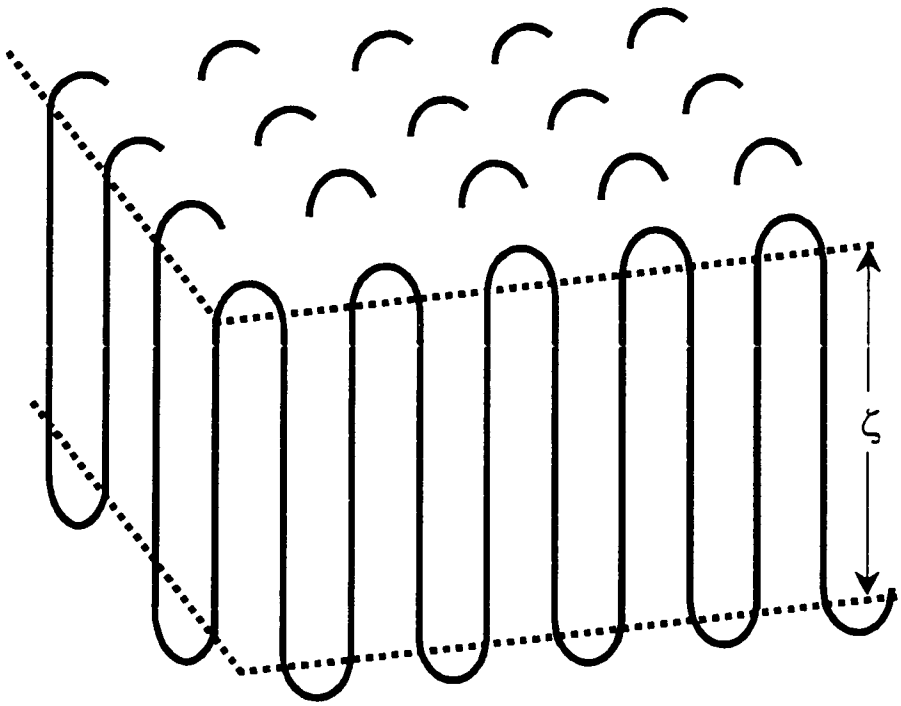

Figure 6-5- Schematic of a polyethylene single crystal with polymer chains folded regularly. (Mandelkern 1970)

Alternatively, it has been suggested that adjacent re-entry is not required (Mandelkern 1970). The crystalline sequences are thought to be connected more or less at random, with the connecting loops also being of random length. According to this model, part of the chain forms a non-ordered or amorphous top-layer before rejoining the ordered crystal lattice. A schematic representation of this model is given in Figure 6-6. The lamellar-like crystals are not completely crystalline but would deviate from the idealized situation of the first case.

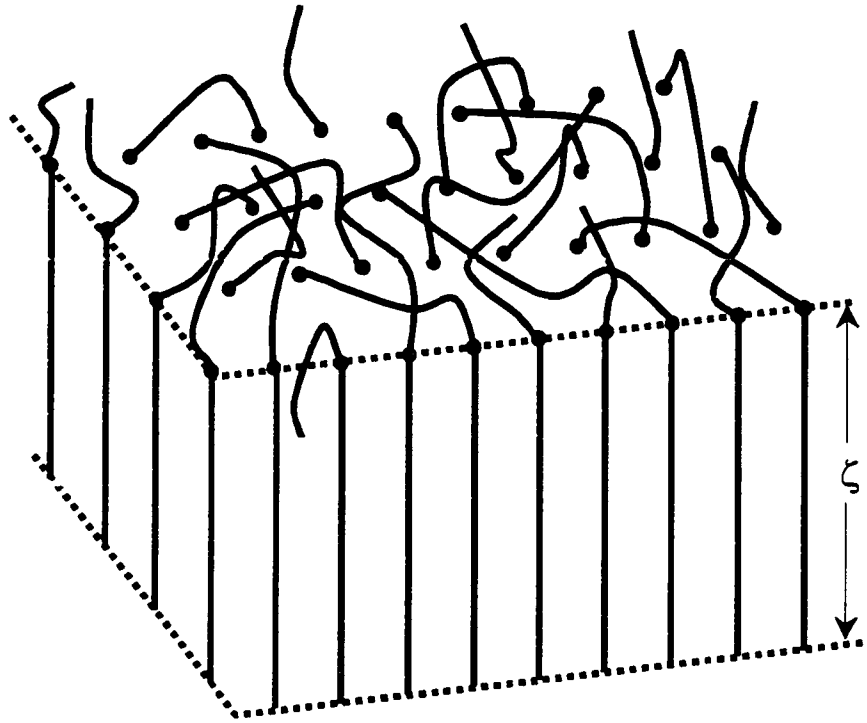

Figure 6-6- Schematic of a polyethylene single crystal with polymer chains folded irregularly. (Mandelkern 1970)

Typical crystallite sizes, ζ (in Å), as a function of the crystallization temperature T_c were illustrated in Figure 6-3 for linear polyethylene in xylene. The sizes, depending on the crystallization temperature, range from 85 Å to 190 Å and the dependency of the crystallite size on the crystallization temperature is apparent. There is a very definite change in slope of this plot, which occurs at a crystallization temperature in the vicinity of 80 °C. Curves of similar character have been obtained by many researchers for different solvents (Keller and O'Connor 1960, Price 1961, Holland and Lindenmeyer 1962).

As suggested by Mandelkern (1970), the kinetics of crystallization from dilute solutions is controlled by nucleation. This results in a very general hypothesis that the crystallite size is controlled in some manner by the critical size required for nucleation. Based on these facts and from the most general aspects of nucleation theory, it has been shown (Jackson and Mandelkern 1968, Mandelkern 1970) that the critical size of the nucleus in the chain direction, ζ^*, is inversely proportional to the free energy of fusion at the crystallization temperature. In other words:

$$\zeta^* \sim \frac{1}{\Delta f_u(v_2, T_c)} = \frac{kT_s^0}{\Delta H_u(T_s^0 - T_c)} \tag{6-1}$$

where $\Delta f_u(v_2, T_c)$ is the free energy of fusion at T_c for volume fraction of polymer v_2, and ΔH_u is the enthalpy of fusion. The proportionality, can be turned into an equation (Equation (6-1)) by the proper selection of the proportionality factor k. This factor depends on the interfacial energies involved and the specific details of the nucleation process (Mandelkern 1970). Equation 6-1 can be easily rearranged into the form

$$\frac{1}{T_c} = \frac{1}{T_s^0} + \frac{k}{\Delta H_u \zeta^* T_c} \tag{6-2}$$

This equation suggests that if ζ is identified by ζ^*, a plot of $1/T_c$ against $1/\zeta T_c$ should be linear and extrapolate to $1/T_s^0$ as ζ^* goes to infinity. Data obtained by different investigators (Nakajima et al. 1968, Jackson and Mandelkern 1968, Kawai and Keller 1965) for the crystallization of ethylene in different solvents confirm the linearity of such plots. These data also verify the fact that the intercept depends only on the solvent type. On the other hand the slope is independent of solvent type, implying that the same interfacial energy is involved in each case. It was also shown that the extrapolated T_s^0 values (crystallization temperature at which the critical nucleus size goes to infinity)

agreed with those previously obtained from the independent study of the solubility temperature of the bulk crystallized polymer. The extrapolated T_s^0 values were found to be: 113.0±1.5 for decalin; 118.6±2.0 for xylene, toluene and tetralin; 127.7±2.0 for n-octane; 133.1±2.0 and 137.4±2.5 for the two sets of n-hexadecane data. From the study of the solubility temperature of the bulk crystallized polymer, Jackson and Mandelkern (1968) found the T_s^0 values to be: 116.5±2.0 in decalin; 117.2±2 in toluene; 118.6±2 in xylene; 120.0±2 in tetralin; 126.1±2 in n-octane; 139.9±2 in n-hexadecane. The agreement obtained for the two independently determined sets of values for T_s^0 in different solvents implies that the identification of ζ with ζ^* is valid and that the crystallite thickness is controlled by a nucleation process.

The constancy of the slope for the different solvents results in a single linear relationship for the crystallite size data, independent of the crystallizing medium, by plotting ζ as a function of $T_s^0/(T_s^0-T_c)$

$$\zeta = \frac{\alpha T_s^0}{(T_s^0 - T_c)} \tag{6-3}$$

where α (slope) is equal to $k/\Delta H_u$. Equation (6-3) defines a mathematical relationship between the crystal thickness and crystallization temperature. This equation is the basis of the calculations involved in the proposed fractionation mechanism in CRYSTAF and will be discussed further in the following sections.

6-3-2- Proposed Fractionation Mechanism in CRYSTAF

In ethylene/1-octene random copolymers, the ethylene sequences form the crystallizable sections. The 1-octene portions of chains are not crystallizable because of

the bulky branches and form the amorphous sections. Since the lengths of ethylene sequences are usually much smaller than the main chain, they may not be long enough to fold several times or even once while crystallizing. However, ethylene sequences of different chains can position themselves close to each other and crystallize if their lengths are equal to or greater than the thickness of the crystallite being formed. As it is shown in Figure 6-3, the crystallite thickness is a strong function of temperature (particularly at high temperatures); therefore, at each temperature ethylene sequences having lengths equal to or greater than the crystallite thickness at that temperature will crystallize and precipitate. In the present work it has been proposed that the length of the longest ethylene sequence in the chain is the determining factor in the fractionation process in CRYSTAF.

6-4- Mathematical Modeling of CRYSTAF

In order to verify the validity of the proposed model, five different ethylene/1-octene copolymer samples, all synthesized by a single-site type catalyst were considered. Monte Carlo simulation and the crystallite thickness-temperature relationship presented in Section 6-3 are used to simulate the copolymer chains and fractionation process, respectively. The details of the copolymerization and fractionation simulations are explained in the following sections.

6-4-1- Simulation of Copolymer Chains

A Monte Carlo model was used to simulate the microstructure of the copolymer samples. The average values of the samples are tabulated in Table. 6-1.

Table 6-1- Average properties of poly(ethylene/1-octene) samples. (Soares et al. 1998)

Sample	MFI	Density	1-octene mol% (F_2)	M_n	PDI
A	3	0.902	5.64	29600	2.20
B	0.5	0.910	3.85	38000	2.21
C	1	0.910	4.00	34400	2.31
D	3.5	0.910	4.26	29300	2.15
E	6	0.911	4.16	22000	2.54

Generally, number-average molecular weight (M_n), average copolymer composition (F_2), and the values of reactivity ratios are required for the Monte Carlo simulation of copolymer chains. For the employed copolymer samples, it was proven that the catalyst system used synthesizes random copolymers (Lai et al. 1993, 1997; Swogger and Kao 1993; Sugawara 1994). This means that the product of the reactivity ratios must be equal to one (Flory 1953). This simplifies the simulation algorithm in such a way that the number-average molecular weights (M_n), and the average copolymer composition (F_2) are the only values required to determine the simulation parameters.

M_n and F_2 were determined by size exclusion chromatography and by carbon-13 nuclear magnetic resonance respectively (Soares et al. 1998),.

The number average chain length, X_n, for each sample can be easily calculated from M_n and F_2 values with the following equation:

$$X_n = \frac{M_n}{112 \times F_2 + 28 \times (1 - F_2)} \tag{6-4}$$

where 112 and 28 are the molecular weights of ethylene and 1-octene, respectively. The denominator, $112 \times F_2 + 28 \times (1\text{-}F_2)$, is the average molecular weight of the copolymer repeating unit.

The number average chain length, x_n, is related to the propagation probability, p, by the following equation (3-42):

$$X_n = \frac{1}{1-p} \tag{3-42}$$

Therefore, the propagation probability can be easily calculated by rearranging Equation (3-42) :

$$p = \frac{X_n - 1}{X_n} \tag{3-43}$$

The value of the copolymer composition (F_2) was directly used as the probability of 1-octene propagation. Table. 6-2 shows the used simulation parameters.

Table 6-2- Values of the parameters used in Monte Carlo simulation.

Sample	X_n	Propagation probability	Comonomer propagation probability
A	904.12	0.99889	0.0564
B	1216.68	0.99918	0.0385
C	1096.81	0.99909	0.04
D	927.92	0.99892	0.0426
E	698.50	0.99857	0.0416

Two hundred thousand chains were simulated for each sample. At the termination of each chain, the number average molecular weight (M_n) and the length of the longest ethylene sequence (LES) were recorded. The flowchart of the computer program is illustrated in Figure 6-7.

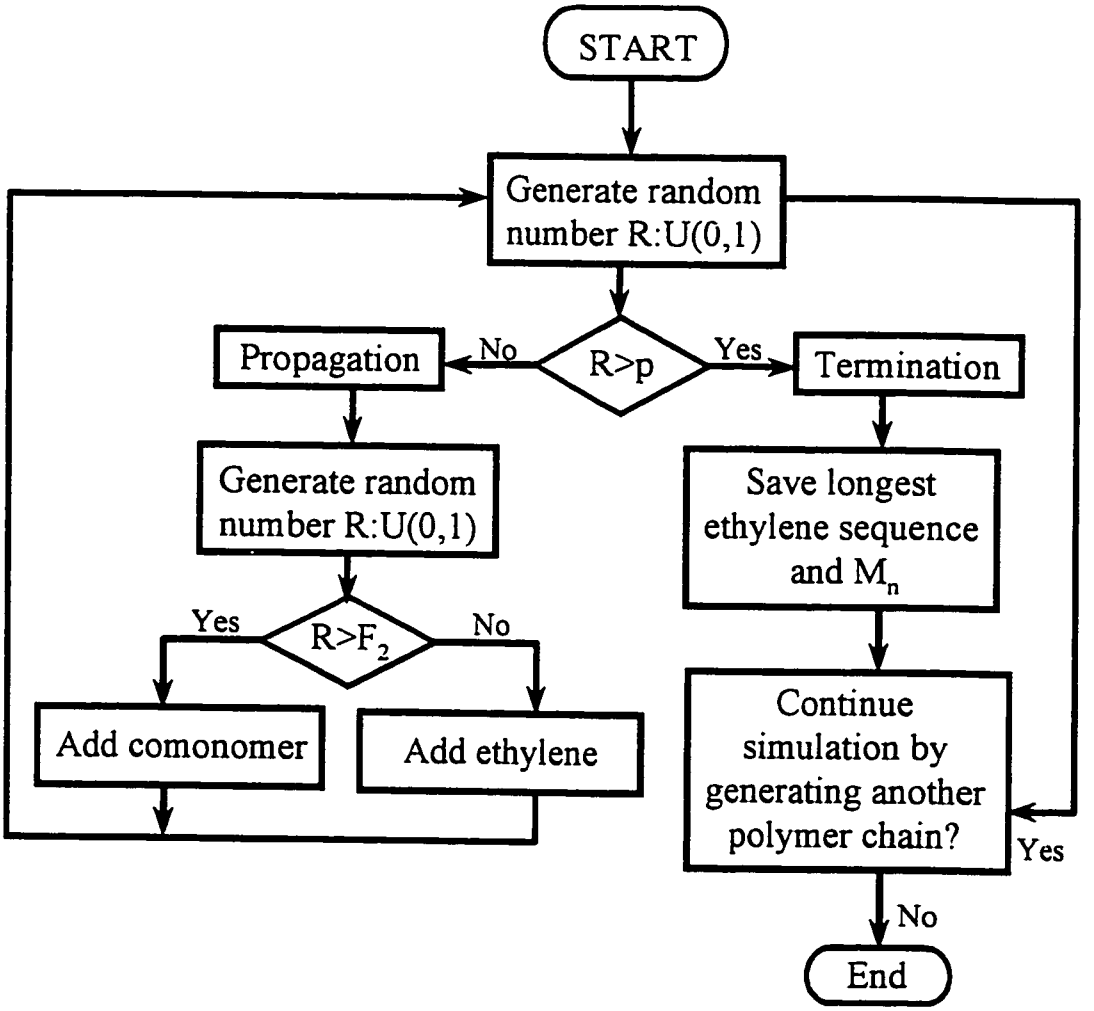

Figure 6-7- Flow chart of the computer program for the Monte Carlo model. M_n is the number average molecular weight.

6-4-2- Simulation of the Fractionation Process

For the simulation of the precipitation process in CRYSTAF, the following assumptions were made:

1. Only ethylene sequences can crystallize. This means that the chain segments containing comonomer cannot crystallize.
2. An ethylene sequence will crystallize at any temperature only if its length is equal to or greater than the crystallite thickness at that temperature.
3. With the crystallization of an ethylene sequence, the whole chain will precipitate.

It is quite obvious from Figure 6-3 that the crystallite thickness is greater at higher temperatures. Considering this fact and the above-mentioned assumptions one can easily conclude that polymer chains containing longer ethylene sequences crystallize at higher temperatures. In CRYSTAF the analysis starts at high temperatures and is continued by decreasing the temperature slowly under well-controlled conditions. Under these circumstances, it is quite reasonable to assume that the longest ethylene sequence of each chain crystallizes first (higher temperature).

The co-crystallization of the chains was then mimicked by classifying the chains according to their longest ethylene sequence (obtained from the Monte-Carlo simulation of copolymer chains). This procedure generates a weight-distribution of copolymer chains according to their longest crystallizable sequences (LES), as shown in Figure 6-8 for sample A. To convert this distribution to a CRYSTAF profile, it is necessary to relate the length of the longest ethylene sequence to the corresponding crystallization temperature.

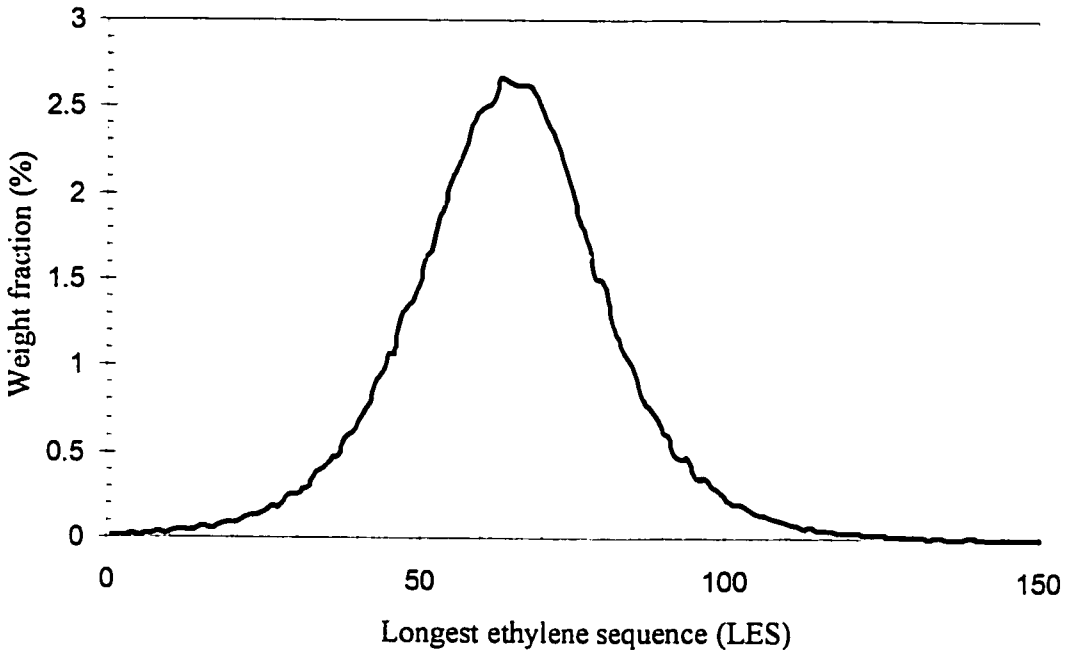

Figure 6-8- Weight fraction of polymer chains versus their longest ethylene sequence

As discussed in Section 6-3 and shown in Figure 6-3, crystallite thickness is a strong function of temperature. It was also shown the mathematical relationship between crystallite thickness and crystallization temperature can be defined by Equation (6-3).

$$\zeta = \frac{\alpha T_s^0}{(T_s^0 - T_c)} \tag{6-3}$$

Rearranging Equation (6-3) and solve for crystallization temperature, T_c, results in:

$$T_c = \frac{T_s^0(\zeta - \alpha)}{\zeta} \tag{6-5}$$

Substituting ζ by the length of the longest crystallizable sequence of each chain (LES) results in Equation (6-6):

$$T_c = \frac{T_s^0 (LES - \alpha)}{LES} \tag{6-6}$$

Britto et al. (1999) compared CRYSTAF and TREF chromatograms of the same resin and showed that they were identical except for a shift in CRYSTAF profiles to lower temperatures. They attributed the shift to the super-cooling effect, since CRYSTAF curves are measured during crystallization, while TREF ones are measured during melting/dissolution. Equation (6-6) does not account for the super-cooling effect and for the derivation of this equation, it was basically assumed that the crystallization and dissolution temperatures of a certain crystallite thickness are the same.

To account for super-cooling during crystallization, a semi-empirical parameter, β, was added to Equation (6-6) as follows (Beigzadeh et al. 2000):

$$T_c = \frac{T_s^0 (LES - \alpha)}{LES} - \beta \tag{6-7}$$

Equation (6-7) can be used to relate the length of the longest ethylene sequence to the corresponding crystallization temperature and therefore can convert the copolymer weight-distribution shown in Figure 6-8 to a CRYSTAF profile.

6-5- Results and Discussions

Monte Carlo simulation and Equation (6-7) were used to simulate the CRYSTAF chromatograms of the five ethylene/1-octene copolymers shown in Table 6-1. Equation (6-7) has three adjustable parameters to be estimated. T_s^0 is a solvent dependent parameter, α is independent of the solvent type and has to do with the interfacial energies involved in crystallization process. Therefore, it is expected that the values of these two parameters be the same for all copolymer samples.

T_s^0, the crystallization temperature of a polyethylene chain with infinite chain length in solution (infinite dilution) is a solvent property and is different from solvent to solvent. As discussed in Section 6-3-2, the values of T_s^0 for the examined solvents were found to be in the range of 110-135 °C. The most commonly employed solvent in TREF and CRYSTF is trichlorobenzene (TCB). Since TCB is a better solvent for polyethylene than the above-mentioned solvents, it is expected to have a lower T_s^0 value. DaSilva et al. (1999) reported a value of T_s^0 = 85 °C.

The values of T_s^0 and α were estimated using non-linear regression method for the CRYSTAF chromatogram of sample A and the obtained values were used for all samples. These parameters were estimated to be T_s^0 = 89 °C and α = 10, which are in complete agreement with the data obtained by Jackson and Mandelkern(1968) and DaSilva et al. (1999). The values of β, the semi-empirical intercept, were chosen by trial and error. This parameter shifts back the simulated curve to lower temperatures to account for super-cooling. The values of this parameter varied between 18-25 °C for different samples. The values of these parameters for all poly(ethylene/1-octene) samples are summarized in Table 6-3.

Table 6-3- Values of the parameters appearing in Equation (6-9) for different samples

Sample	T_s^0 (°C)	α	β (°C)
A	89	10	25
B	89	10	20.3
C	89	10	21
D	89	10	22.5
E	89	10	18

The CRYSTAF chromatograms and simulated chromatograms for the five different poly(ethylene/1-octene) samples, presented in Table 6-1, are shown in Figures 6-9 to 6-13.

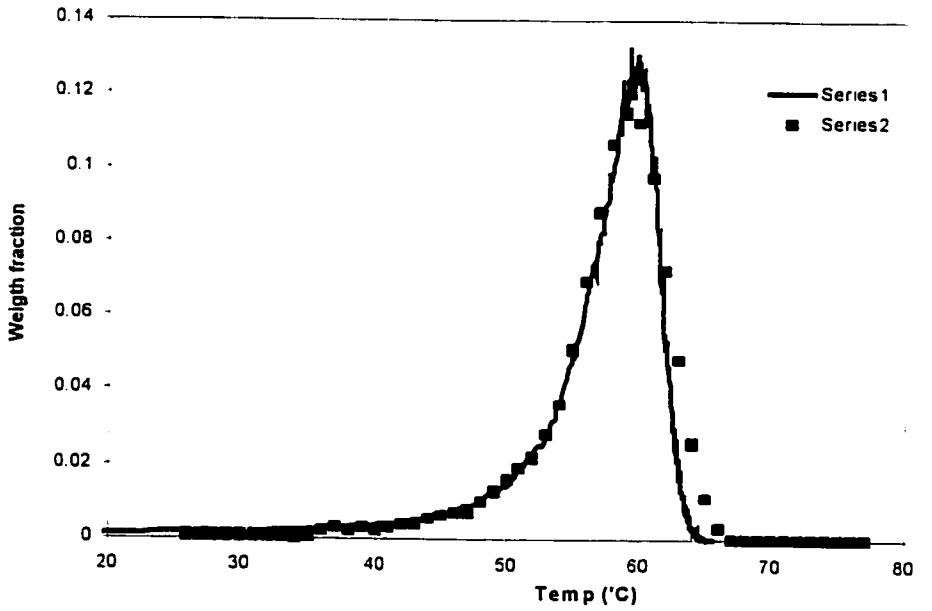

Figure 6-9- CRYSTAF and simulated chromatograms for sample A.

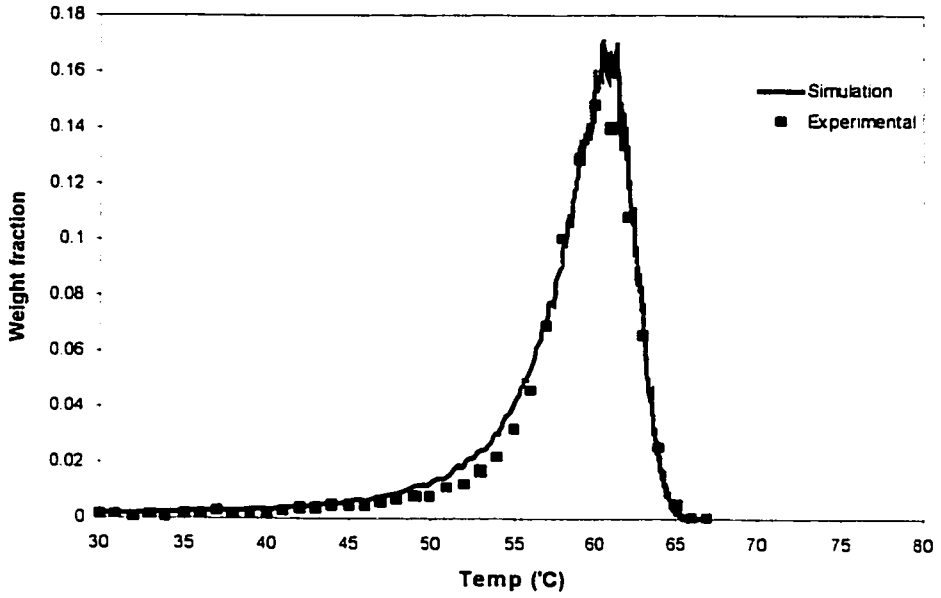

Figure 6-10- CRYSTAF and simulated chromatograms for sample B.

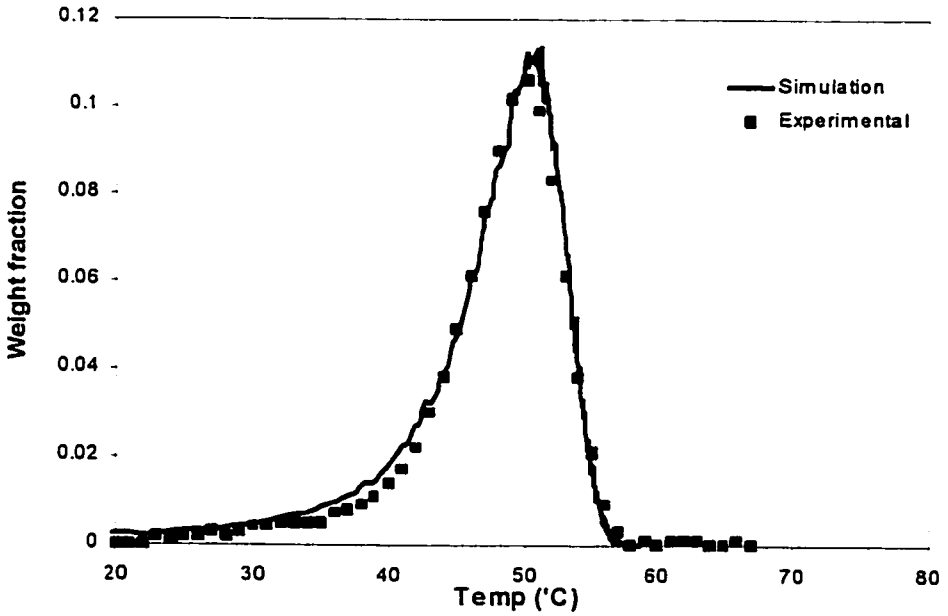

Figure 6-11- CRYSTAF and simulated chromatograms for sample C.

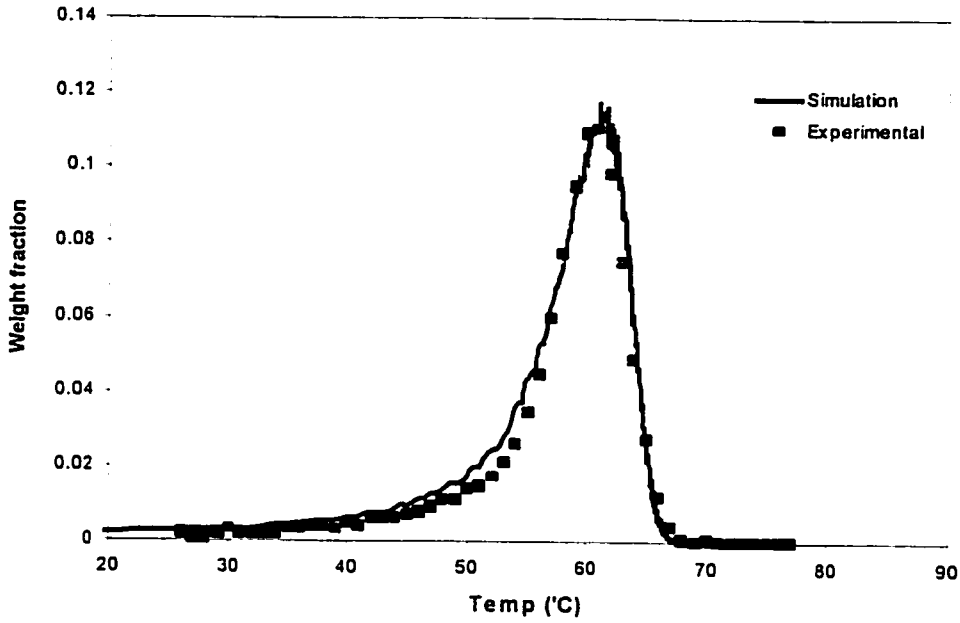

Figure 6-12- CRYSTAF and simulated chromatograms for sample D.

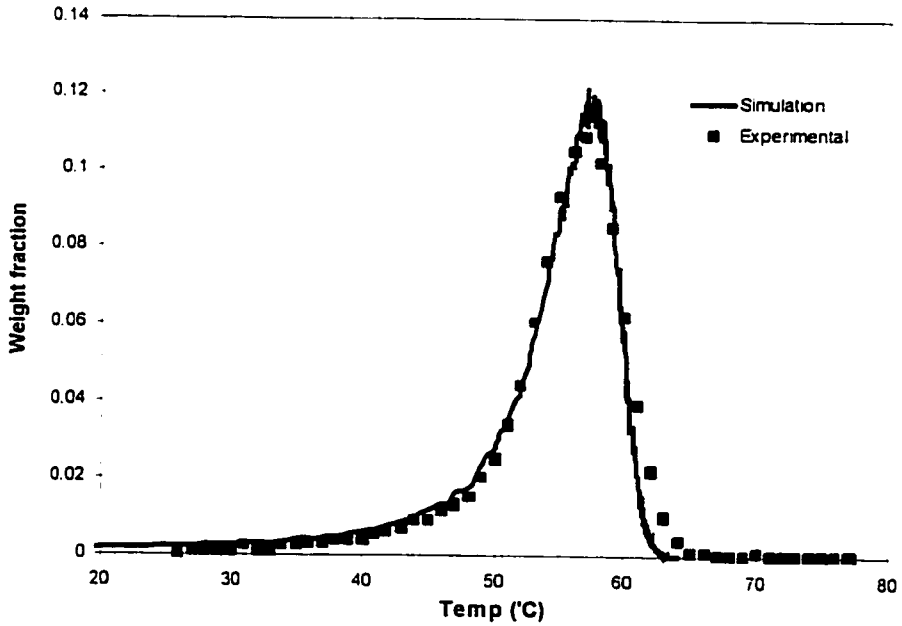

Figure 6-13- CRYSTAF and simulated chromatograms for sample E.

As can be seen in these figures the simulation results which are based on the proposed fractionation mechanism, can perfectly predict CRYSTAF chromatograms. The very good agreement between experimental and simulation results verifies the validity of the proposed fractionation mechanism (Beigzadeh et al. 2000).

6-6- Concluding Remarks

A mechanism for the fractionation of polyolefin copolymers in CRYSTAF was proposed. According to this mechanism, the length of the longest crystallizable sequence in the copolymer chain is the determining parameter in fractionation by CRYSTAF. Monte Carlo simulation was used to simulate chains of five different poly(ethylene/1-octene) samples synthesized by a single-site-type catalyst. Very good agreement between experimental and simulation results suggests that the proposed mechanism accurately describes the fractionation process in CRYSTAF.

Chapter 7

Contributions

The concept of combining two metallocene catalysts to manipulate long-chain branching (LCB) in ethylene polymerization was introduced and systematically investigated for the first time.

General dynamic and steady-state mathematical models for the homo- and co-polymerization of ethylene with other α-olefins using single or combined metallocene catalyst systems were developed. These models permit the investigation of the effects of different catalyst types, reactor types, and process conditions on chain microstructure, which help to make comprehensive conclusions about polymerization chemistry and engineering with these catalysts. An analytical expression for long-chain branch formation for ethylene homopolymerizatin using combined catalyst systems was also developed, which describes how LCB frequency varies with catalyst system

characteristics. This expression is a useful tool to quickly select a catalyst combination to produce polymer with a given LCB frequency.

Polymerization experiments were performed to validate the proposed LCB formation mechanism and modeling results. It was experimentally shown that the LCB frequency could be controlled using combined metallocene catalyst systems. Excellent agreement with model predictions was observed. The effects of cocatalyst types and amounts on the molecular weight distribution and long-chain branching frequency were also investigated. It was shown how these structural parameters could be manipulated by the proper choice of type and amount of cocatalysts.

A Monte Carlo model was developed to investigate the structure of branched polyethylene samples synthesized with mono-cyclopentadienyl metallocence catalysts. Based on the modeling results, an explanation for the melt viscosity improvements as a result of LCB formation was proposed for the first time.

The separation mechanism in Crystallization Analysis Fractionation (CRYSTAF) was investigated. In this study a mechanism for the fractionation process was proposed. Monte-Carlo simulation was used to verify the proposed mechanism. In this study copolymer chains were simulated and precipitated according to the proposed mechanism. Good agreement between experimental and simulated CRYSTAF curves was observed. This is the only mechanistic model for CRYSTAF and TREF (temperature rising elution fractionation) available in the literature.

Appendix

A- Moment Equations

Zeroth Moments

Dead chains with terminal double bonds:

$$\frac{d\lambda_0}{dt} = k_{\beta,11}\eta_0 + k_{\beta,21}\gamma_0 - (k_{LCB,11}\eta_0 + k_{LCB,21}\psi_0 + s)\lambda_0 \qquad \text{(A-1)}$$

$$\frac{d\sigma_0}{dt} = k_{\beta,12}\psi_0 + k_{\beta,22}\tau_0 - (k_{LCB,12}\eta_0 + k_{LCB,22}\psi_0 + s)\sigma_0 \qquad \text{(A-2)}$$

Dead chains with saturated chain end:

$$\begin{aligned}\frac{d\mu_0}{dt} &= (k_{CTA,11}\eta_0 + k_{CTA,12}\psi_0 + k_{CTA,21}\gamma_0 + k_{CTA,22}\tau_0)CTA \\ &\quad + k_{da,1}(\psi_0 + \eta_0) + k_{da,2}(\gamma_0 + \tau_0) - s\mu_0\end{aligned} \qquad \text{(A-3)}$$

Living chains with LCB:

$$\begin{aligned}\frac{d\eta_0}{dt} &= k_{i,11}C_1M_1 - k_{1,12}M_2\eta_0 + k_{1,21}M_1\psi_0 - k_{LCB,12}\eta_0\sigma_0 + k_{LCB,21}\psi_0\lambda_0 \\ &\quad -(k_{CTA,11}CTA + k_{\beta,11} + k_{da,1} + s)\eta_0\end{aligned} \qquad \text{(A-4)}$$

$$\begin{aligned}\frac{d\psi_0}{dt} &= k_{i,12}C_1M_2 + k_{1,12}M_2\eta_0 - k_{1,21}M_1\psi_0 + k_{LCB,12}\eta_0\sigma_0 - k_{LCB,21}\psi_0\lambda_0 \\ &\quad -(k_{CTA,12}CTA + k_{\beta,12} + k_{da,1} + s)\psi_0\end{aligned} \qquad \text{(A-5)}$$

Linear living chains:

$$\frac{d\gamma_0}{dt} = k_{i,21}C_2M_1 - k_{2,12}M_2\gamma_0 + k_{2,21}M_1\tau_0 - (k_{CTA,21}CTA + k_{\beta,21} + k_{da,2} + s)\gamma_0 \quad \text{(A-6)}$$

$$\frac{d\tau_0}{dt} = k_{i,22}C_2M_2 + k_{2,12}M_2\gamma_0 - k_{2,21}M_1\tau_0 - (k_{CTA,22}CTA + k_{\beta,22} + k_{da,2} + s)\tau_0 \quad \text{(A-7)}$$

First Moments:

Dead chains with terminal double bonds:

$$\frac{d\lambda_1}{dt} = k_{\beta,11}\eta_1 + k_{\beta,21}\gamma_1 - (k_{LCB,11}\eta_0 + k_{LCB,21}\psi_0 + s)\lambda_1 \quad \text{(A-8)}$$

$$\frac{d\sigma_1}{dt} = k_{\beta,12}\psi_1 + k_{\beta,22}\tau_1 - (k_{LCB,12}\eta_0 + k_{LCB,22}\psi_0 + s)\sigma_1 \quad \text{(A-9)}$$

Dead chains with saturated chain end:

$$\frac{d\mu_1}{dt} = (k_{CTA,11}\eta_1 + k_{CTA,12}\psi_1 + k_{CTA,21}\gamma_1 + k_{CTA,22}\tau_1)CTA + k_{da,1}(\psi_1 + \eta_1) + k_{da,2}(\gamma_1 + \tau_1) - s\mu_1 \quad \text{(A-10)}$$

Living chains with LCB:

$$\frac{d\eta_1}{dt} = k_{i,11}C_1M_1 + k_{1,11}M_1\eta_0 - k_{1,12}M_2\eta_1 + k_{1,21}M_1(\psi_1 + \psi_0) - k_{LCB,12}\eta_1\sigma_0 + k_{LCB,11}\eta_0\lambda_1 + k_{LCB,21}(\psi_1\lambda_0 + \psi_0\lambda_1) - (k_{CTA,11}CTA + k_{\beta,11} + k_{da,1} + s)\eta_1 \quad \text{(A-11)}$$

$$\frac{d\psi_1}{dt} = k_{i,12}C_1M_2 - k_{1,21}M_1\psi_1 + k_{1,22}M_2\psi_0 + k_{1,12}M_2(\eta_1 + \eta_0) - k_{LCB,21}\psi_1\lambda_0 + k_{LCB,22}\psi_0\sigma_1 + k_{LCB,12}(\eta_1\sigma_0 + \eta_0\sigma_1) - (k_{CTA,12}CTA + k_{\beta,12} + k_{da,1} + s)\psi_1 \quad \text{(A-12)}$$

Linear living chains:

$$\frac{d\gamma_1}{dt} = k_{i,21}C_2M_1 + k_{2,11}M_1\gamma_0 - k_{2,12}M_2\gamma_1 + k_{2,21}M_1(\tau_1 + \tau_0) - (k_{CTA,21}CTA + k_{\beta,21} + k_{da,2} + s)\gamma_1 \quad \text{(A-13)}$$

$$\frac{d\tau_1}{dt} = k_{i,22}C_2M_2 - k_{2,21}M_1\tau_1 + k_{2,22}M_2\tau_0 + k_{2,12}M_2(\gamma_1 + \gamma_0) - (k_{CTA,22}CTA + k_{\beta,22} + k_{da,2} + s)\tau_1 \quad \text{(A-14)}$$

Second Moments:

Dead chains with terminal double bonds:

$$\frac{d\lambda_2}{dt} = k_{\beta,11}\eta_2 + k_{\beta,21}\gamma_2 - (k_{LCB,11}\eta_0 + k_{LCB,21}\psi_0 + s)\lambda_2 \quad \text{(A-15)}$$

$$\frac{d\sigma_2}{dt} = k_{\beta,12}\psi_2 + k_{\beta,22}\tau_2 - (k_{LCB,12}\eta_0 + k_{LCB,22}\psi_0 + s)\sigma_2 \quad \text{(A-16)}$$

Dead chains with saturated chain end:

$$\frac{d\mu_2}{dt} = (k_{CTA,11}\eta_2 + k_{CTA,12}\psi_2 + k_{CTA,21}\gamma_2 + k_{CTA,22}\tau_2)CTA + k_{da,1}(\psi_2 + \eta_2) + k_{da,2}(\gamma_2 + \tau_2) - s\mu_2 \quad \text{(A-17)}$$

Living chains with LCB:

$$\frac{d\eta_2}{dt} = k_{i,11}C_1M_1 - k_{1,12}M_2\eta_2 + k_{1,11}M_1(2\eta_1 + \eta_0) + k_{1,21}M_1(\psi_2 + 2\psi_1 + \psi_0) - k_{LCB,12}\eta_2\sigma_0 + k_{LCB,11}(2\eta_1\lambda_1 + \eta_0\lambda_2) + k_{LCB,21}(\psi_2\lambda_0 + 2\psi_1\lambda_1 + \psi_0\lambda_2) - (k_{CTA,11}CTA + k_{\beta,11} + k_{da,1} + s)\eta_2 \quad \text{(A-18)}$$

$$\frac{d\psi_2}{dt} = k_{i,12}C_1M_2 - k_{1,21}M_1\psi_2 + k_{1,22}M_2(2\psi_1 + \psi_0) + k_{1,12}M_2(\eta_2 + 2\eta_1 + \eta_0) - k_{LCB,21}\psi_2\lambda_0 + k_{LCB,12}(\eta_2\sigma_0 + 2\eta_1\sigma_1 + \eta_0\sigma_2) + k_{LCB,22}(2\psi_1\sigma_1 + \psi_0\sigma_2) - (k_{CTA,12}CTA + k_{\beta,12} + k_{da,1} + s)\psi_2 \quad \text{(A-19)}$$

Linear living chains:

$$\frac{d\gamma_2}{dt} = k_{i,21}C_2M_1 - k_{2,12}M_2\gamma_2 + k_{2,11}M_1(2\gamma_1 + \gamma_0) + k_{2,21}M_1(\tau_2 + 2\tau_1 + \tau_0) - (k_{CTA,21}CTA + k_{\beta,21} + k_{da,2} + s)\gamma_2 \quad \text{(A-20)}$$

$$\frac{d\tau_2}{dt} = k_{i,22}C_2M_2 - k_{2,21}M_1\tau_2 + k_{2,22}M_2(2\tau_1 + \tau_0) + k_{2,12}M_2(\gamma_2 + 2\gamma_1 + \gamma_0) - (k_{CTA,22}CTA + k_{\beta,22} + k_{da,2} + s)\tau_2 \quad \text{(A-21)}$$

B- Polymerization Kinetic Constants

Table B-1- Kinetic constants for ethylene homopolymerization.

Kinetic Constant	Value
$k_{i,1}$ *(L/mol.s)*	3000
$k_{p,1}$ *(L/mol.s)*	4000
k_{LCB} *(L/mol.s)*	600
$k_{\beta,1}$ (s^{-1})	0.01
$k_{da,1}$ (s^{-1})	0.007
$k_{CTA,1}$ *(L/mol.s)*	0.1
$k_{i,2}$ *(L/mol.s)*	3000
$k_{p,2}$ *(L/mol.s)*	4000
$k_{\beta,2}$ (s^{-1})	0.015
$k_{da,2}$ (s^{-1})	0.003
$k_{CTA,2}$ *(L/mol.s)*	0.1

Table B-2- Kinetic constants for ethylene / 1-octene copolymerization.

Kinetic Constant	Value
$k_{i,11}$ (L/mol.s)	4000
$k_{i,12}$ (L/mol.s)	1000
$k_{i,21}$ (L/mol.s)	4000
$k_{i,22}$ (L/mol.s)	32
$k_{1,11}$ (L/mol.s)	4000
$k_{1,12}$ (L/mol.s)	1000
$k_{1,21}$ (L/mol.s)	3500
$k_{1,22}$ (L/mol.s)	875
$k_{2,11}$ (L/mol.s)	4000
$k_{2,12}$ (L/mol.s)	32
$k_{2,21}$ (L/mol.s)	3500
$k_{2,22}$ (L/mol.s)	28
$k_{LCB,11}$ (L/mol.s)	600
$k_{LCB,12}$ (L/mol.s)	450
$k_{LCB,21}$ (L/mol.s)	150
$k_{LCB,22}$ (L/mol.s)	10
$k_{\beta,11}$ (s^{-1})	0.001
$k_{\beta,12}$ (s^{-1})	0.001
$k_{da,1}$ (s^{-1})	0.007
$k_{da,2}$ (s^{-1})	0.003
$k_{CTA,11}$ (L/mol.s)	0.01
$k_{CTA,12}$ (L/mol.s)	0.01
$k_{CTA,21}$ (L/mol.s)	0.01
$k_{CTA,22}$ (L/mol.s)	0.01

C- ^{13}C-NMR analysis

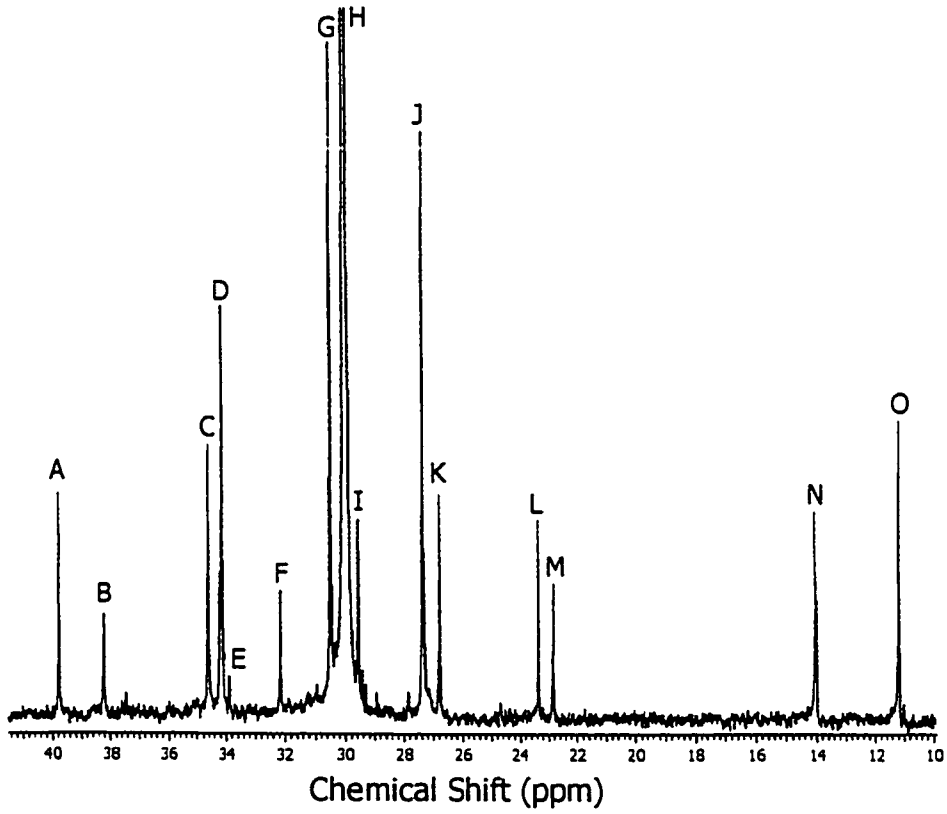

Figure C-1- ^{13}C-NMR spectrum of a polyethylene sample dissolved in ODCB. (Hansen et al. 1997)

Table C-1- ^{13}C peak assignment and chemical shift of the resonance peaks in Figure C-1.

Resonance Peak	Carbon Assignment	Chemical Shift (δ) ppm
A	Methine (B_2)	39.75
B	Methine (B_4, B_{6+})	38.24
C	$\alpha\delta^+ + 6B_6$	34.98
D	$4B_4$	34.19
E	a (allylic carbon)	33.88
F	$3s + 3B_6$	32.22
G	$\gamma\delta^+$	30.47
H	$\delta\delta^+$ (main chain)	29.99
I	$4B_6$	29.53
J	$\beta\delta^- + 5B_6$	27.31
K	$2B_2$	26.77
L	$2B_4$	23.35
M	$2s + 2B_6$	22.89
N	$1s + 1B_6$	14.17
O	$1B_2$	11.17

D- Data Required for Chao-Seader Correlation

Table D-1- Thermodynamic properties of ethylene and Isopar E.

Property		**Ethylene**	**Isopar E**
T_c (°K)		282.4	568.8
P_c (atm)		49.7	24.5
V_c (ml/gmol)		129.0	492.0
Zc		0.276	0.259
ω		0.085	0.394
Antoine's equation parameters	A	15.5368	15.9426
	B	1347.01	3120.29
	C	-18.15	-63.63
Solubility parameter (δ)		6.08	7.62
Liquid density (g/ml)		0.577	0.703
Molecular weight (g/mol)		28.054	114.232

E- Mathematical Modeling of Branch Formation in Free-Radical Polymerization

In this section a mathematical model for the free-radical polymerization of vinylic monomers with long-chain branch formation and with potential gel formation is discussed. The model uses the method of moments, but although it is based on the classical free-radical polymerization mechanism involving chain transfer to polymer as a source of branching, it is not limited to calculating the moments of the overall polymer population. Instead, it identifies a succession of branched polymer families (based on their number of branches) that evolve *en route* to gelation and are modeled individually. Gel molecules are usually thought of as polymer networks of infinite length, because of the vast difference in scale that separates them from normal sol polymer molecules. These molecules are formed as a result of the frequent growth of branched polymer molecules to higher chain lengths and higher number of branches. As a result of this growth process, higher branched families keep appearing in succession, but always in smaller amounts, since less and less of the lower branched families will be available to form them. After a number of such transitions, the resulting polymer network will be so large that the gel suddenly appears and the gel/sol transition occurs. Shortly thereafter, the newly formed gel molecules start reacting with the sol polymer, consuming the higher branching families first, since the rate of most cross-linking reactions depends on molecule size. As a result, these higher branched families are transient in nature, since they only appear shortly before the gel point is reached and are consumed soon after. This feature of the higher branched families allows to effectively approximate the gel and sol

populations without any considerable loss of information. It is generally sufficient to keep track of a finite number of branched families and consider that all higher branched molecules plus any gel formed constitute a pseudogel (Teymour and Campbell 1994). This approximation will only be in error in the immediate vicinity of the gel point. The error will be minimal if an adequate number of branched families are considered.

E-1- Kinetic Scheme

Free-radical polymerization of vinylic monomers with long chain branch formation includes steps of initiator decomposition, initiation, propagation, transfer to monomer, transfer to chain transfer agent, transfer to polymer, and termination.

Initiator decomposition:

$$I \rightarrow 2R(0,0) \qquad k_d$$

Initiation:

$$R(0,0) + M \rightarrow R(1,0) \qquad k_i$$

Propagation:

$$R(r,i) + M \rightarrow R(r+1,i) \qquad k_p$$

Transfer to monomer

$$R(r,i) + M \rightarrow P(r,i) + R(1,0) \qquad k_{tm}$$

Transfer to chain transfer agent

$$R(r,i) + CTA \rightarrow P(r,i) + R(1,0) \qquad k_{tCTA}$$

Transfer to polymer

$$R(r,i) + P(s,j) \rightarrow P(r,i) + R(s,j+1) \qquad k_{tp}$$

Termination by combination

$$R(r,i) + R(s,j) \rightarrow P(r+s, i+j) \qquad k_{tc}$$

Termination by disproportionation

$$R(r,i) + R(s,j) \rightarrow P(r,i) + P(s,j) \qquad k_{td}$$

where:

I	initiator concentration
$R(r,i)$	concentration of live polymer chains with chain length r and having i trifunctional branch points.
$P(r,i)$	concentration of dead polymer chains of chain length r and having i trifunctional branch points).
k_d	initiator decomposition rate constant
k_i	intitiation reaction rate constant
k_p	monomer propagation rate constant
k_{tm}	chain transfer to monomer rate constant
k_{tCTA}	chain transfer to chain transfer agent
k_{tp}	chain transfer to polymer rate constant
k_{tc}	termination by combination rate constant
k_{td}	termination by disproportionation rate constant

E-2- Population Balances

Linear polymer balances

According to the presented reaction mechanism, the rate of formation of linear live polymer chains can be expressed as follows:

$$\frac{dR(1,0)}{dt} = R_I + k_{tm}M\,Y_0 + k_{tCTA}CTA\,Y_0 - \left(k_pM + k_{tm}M + k_{tCTA}CTA + k_{tc}Y_0 + k_{td}Y_0 + k_{tp}Q_1\right)R(1,0) \quad \text{(E-1)}$$

$$\frac{dR(r,0)}{dt} = k_pM\,R(r-1,0) - \left(k_pM + k_{tm}M + k_{tCTA}CTA + k_{tc}Y_0 + k_{td}Y_0 + k_{tp}Q_1\right)R(r,0) \quad \text{(E-2)}$$

where:

R_I is the initiation rate and

$$Y_0 = \sum_{r=1}^{\infty}\sum_{i=0}^{\infty} R(r,i) \quad \text{(E-3)}$$

$$Q_1 = \sum_{r=1}^{\infty}\sum_{i=0}^{\infty} r\,P(r,i) \quad \text{(E-4)}$$

Application of the stationary-state hypothesis (SSH) results in:

$$\frac{dR(r,i)}{dt} = 0 \quad \Rightarrow \quad R_I = R_t \quad \Rightarrow \quad R_I = \left(k_{td} + k_{tc}\right)Y_0^2 \quad \text{(E-5)}$$

It should be mentioned that, it is assumed that a live polymer chain (polymer radical) contains only one radical center.

Substituting Equation (E-5) in Equations (E-1) and (E-2) and after some algebraic manipulations:

$$R(1,0) = (\tau + \beta)\phi\,Y_0 \quad \text{(E-6)}$$

$$R(r,0) = R(r-1,0)\phi = R(1,0)\phi^{r-1} \quad \text{(E-7)}$$

Combining Equations (E-6) and (E-7) finally results in:

$$R(r,0) = (\tau + \beta)\phi^r Y_0 \quad \text{(E-8)}$$

where:

$$\tau = \frac{k_{tm}}{k_p} + \frac{k_{tCTA} CTA}{k_p M} + \frac{k_{td} Y_0}{k_p M} \tag{E-9}$$

$$\beta = \frac{k_{tc} Y_0}{k_p M} \tag{E-10}$$

$$\gamma = \frac{k_{tp} Q_1}{k_p M} = \frac{C_p Q_1}{M} \tag{E-11}$$

$$\phi = \frac{1}{1 + \tau + \beta + \gamma} \tag{E-12}$$

Similarly, the population balance of linear dead polymer chains is as follows:

$$\frac{dP(r,0)}{dt} = k_p M Y_0 \left\{ (\tau + \beta) \frac{R(r,0)}{Y_0} + (\beta/2) \sum_{s=1}^{r-1} \frac{R(s,0)}{Y_0} \frac{R(r-s,0)}{Y_0} - \gamma r \frac{P(r,0)}{Q_1} \right\} \tag{E-13}$$

Branched polymer balances

Based on the considered polymerization kinetic scheme, the population balances for branched living and dead polymer chains can be expressed as follows:

$$\frac{dR(r,i)}{dt} = k_p M Y_0 \left\{ \frac{R(r-1,i)}{Y_0} + \gamma r \frac{P(r,i-1)}{Q_1} - (1 + \tau + \beta + \gamma) \frac{R(r,i)}{Y_0} \right\} \tag{E-14}$$

Note that: $R(r,i) = 0$ when $i \geq r$.

Application of the stationary-state hypothesis (SSH) results in:

$$R(r,i) = \phi R(r-1,i) + \frac{\gamma \phi Y_0}{Q_1} r P(r,i-1) \tag{E-15}$$

$$\frac{dP(r,i)}{dt} = k_p M Y_0 \left\{ (\tau + \gamma) \frac{R(r,i)}{Y_0} + (\beta/2) \sum_{y}^{i} \sum_{s=2}^{r-1} \frac{R(s,y)}{Y_0} \frac{R(r-s,i-y)}{Y_0} - \gamma r \frac{P(r,i)}{Q_1} \right\} \tag{E-16}$$

E-3- Moment Equations

The definition of the moments of dead and live polymer having i branch points is as follows:

$$Q_n(i) = \sum_{r=1}^{\infty} r^n P(r,i) \tag{E-17}$$

$$Y_n(i) = \sum_{r=1}^{\infty} r^n R(r,i) \tag{E-18}$$

Live polymer chains moments are obtained by applying Equation (E-18) to the population balances of the live polymer chains having different branch points and using Equations (E-19) to (E-22) to simplify the summation terms.

$$\sum_{r=1}^{\infty} \phi^r = \frac{\phi}{1-\phi} \qquad (\phi \le 1) \tag{E-19}$$

$$\sum_{r=1}^{\infty} r\phi^r = \frac{\phi}{(1-\phi)^2} \qquad (\phi \le 1) \tag{E-20}$$

$$\sum_{r=1}^{\infty} r^2\phi^r = \frac{\phi(1+\phi)}{(1-\phi)^3} \qquad (\phi \le 1) \tag{E-21}$$

Moment equations for live polymer ($i = 0$):

$$\frac{Y_0(0)}{Y_0} = \frac{(\tau+\beta)\phi}{(1-\phi)} \tag{E-22}$$

$$\frac{Y_1(0)}{Y_0} = \frac{(\tau+\beta)\phi}{(1-\phi)^2} \tag{E-23}$$

$$\frac{Y_2(0)}{Y_0} = \frac{(1+\phi)(\tau+\beta)\phi}{(1-\phi)^3} \tag{E-24}$$

Moment equations for live polymer ($i \geq 1$):

$$\frac{Y_0(i)}{Y_0} = \frac{\gamma\phi}{(1-\phi)}\frac{Q_1(i-1)}{Q_1} \tag{E-25}$$

$$\frac{Y_1(i)}{Y_0} = \frac{\gamma\phi}{(1-\phi)}\left[\frac{\phi}{1-\phi}\frac{Q_1(i-1)}{Q_1} + \frac{Q_2(i-1)}{Q_1}\right] \tag{E-26}$$

$$\frac{Y_2(i)}{Y_0} = \frac{\gamma\phi}{(1-\phi)}\left[\frac{\phi(1+\phi)}{(1-\phi)^2}\frac{Q_1(i-1)}{Q_1} + \frac{2}{1-\phi}\frac{Q_2(i-1)}{Q_1} + \frac{Q_3(i-1)}{Q_1}\right] \tag{E-27}$$

Dead polymer chains moments are calculated by applying Equation (E-17) to the population balances of the dead polymer chains having different branch points and using Equation (E-28) (Gupta and Kumar 1987) to simplify the summation terms.

$$\sum_{r=2}^{\infty} r^n \sum_{s=1}^{r-1} P_s P_{r-s} = \sum_{r=1}^{\infty} P_r \sum_{s=1}^{\infty} (r+s)^n P_s \tag{E-28}$$

Moment equations for dead polymer chains ($i = 0$)

$$\frac{dQ_0(0)}{dt} = k_p M Y_0\left\{(\tau+\gamma)\frac{Y_0(0)}{Y_0} + (\beta/2)\left(\frac{Y_0(0)}{Y_0}\right)^2 - \gamma\frac{Q_1(0)}{Q_1}\right\} \tag{E-29}$$

$$\frac{dQ_1(0)}{dt} = k_p M Y_0\left\{(\tau+\gamma)\frac{Y_1(0)}{Y_0} + \beta\frac{Y_0(0)}{Y_0}\frac{Y_1(0)}{Y_0} - \gamma\frac{Q_2(0)}{Q_1}\right\} \tag{E-30}$$

$$\frac{dQ_2(0)}{dt} = k_p M Y_0\left\{(\tau+\gamma)\frac{Y_2(0)}{Y_0} + \beta\left[\left(\frac{Y_1(0)}{Y_0}\right)^2 + \frac{Y_0(0)}{Y_0}\frac{Y_2(0)}{Y_0}\right] - \gamma\frac{Q_3(0)}{Q_1}\right\} \tag{E-31}$$

Moment equations for dead polymer chains ($i \geq 1$)

$$\frac{dQ_0(i)}{dt} = k_p M Y_0\left\{(\tau+\gamma)\frac{Y_0(i)}{Y_0} + (\beta/2)\sum_{y=0}^{i}\delta_y\frac{Y_0(i-y)}{Y_0}\frac{Y_0(y)}{Y_0} - \gamma\frac{Q_1(i)}{Q_1}\right\} \tag{E-32}$$

$$\frac{dQ_1(i)}{dt} = k_p M Y_0 \left\{ (\tau+\gamma)\frac{Y_1(i)}{Y_0} + \beta \sum_{y=0}^{i} \frac{Y_1(i-y)}{Y_0}\frac{Y_0(y)}{Y_0} - \gamma \frac{Q_2(i)}{Q_1} \right\} \quad \text{(E-33)}$$

$$\frac{dQ_2(i)}{dt} = k_p M Y_0 \left\{ (\tau+\gamma)\frac{Y_2(i)}{Y_0} + (\beta/2)\sum_{y=0}^{i} \delta_y \sum_{j=0}^{2} \frac{Y_{2-j}(i-y)}{Y_0}\frac{Y_j(y)}{Y_0} - \gamma \frac{Q_3(i)}{Q_1} \right\} \quad \text{(E-34)}$$

where:

$$\begin{Bmatrix} \delta_y = 2 & 2y = i \\ \delta_y = 1 & 2y \neq i \end{Bmatrix}$$

The derived moment equations indicate the emergence of a closure problem for the individual generation moments, since every moment depends on the next higher moment. In order to be able to solve for the moments, the usual procedure is to assume a suitable form of MWD for branched families and relate the third moment to the lower moments. Saidel and Katz (1968) used the MWD given by Schultz-Zimm equation (Billingham 1989) to relate the third moment to the lower moments. This approximation was found adequate since each branching family possesses a unimodal distribution.

$$Q_3 = 2\frac{Q_2^2}{Q_1} - \frac{Q_2 Q_1}{Q_0} \quad \text{(E-35)}$$

The model developed herein contains a set of ordinary differential equations derived for the moments of different populations (dead chains with different number of branches), complemented by a set of explicit algebraic equations for the live polymer moments. The number of equations solved depends on the number of branched families selected. For the case of *n* branched families, the model consists of (*3n+7*) ODEs and (*3n+4*) algebraic equations. These equations were solved using the method of Range-Kutta of order 6 (Gerald 1994).

The developed model was applied to an isothermal batch polymerization system where branching occurs as a result of chain transfer to polymer and where live radical termination proceeds via combination. The values of the kinetic parameters and initial conditions are given in Tables E-1 and E-2.

Table E-1- Values of the kinetic parameters used in simulation.

Kinetic Parameter	Value	
k_d	1.0E-6	(s^{-1})
k_t	1.0E-10	$(L/(mol \cdot s))$
k_p	800	$(L/(mol \cdot s))$
k_{tm}	0.09	$(L/(mol \cdot s))$
k_{tp}	0.5	$(L/(mol \cdot s))$
k_{tc}	0 - 6.0E7	$(L/(mol \cdot s))$
k_{td}	0 - 6.0E7	$(L/(mol \cdot s))$

Table E-2- Polymerization initial conditions used in simulation.

Monomer concentration	8.4 mol/l
Initiator concentration	0.005 mol/l
Initiator efficiency	0.7
Monomer density	0.9 g/ml
Polymer density	1.1 g/ml
Number of branched families considered	150

E-4- Results and Discussion

The method of overall moments tracks the evolution of the MWD moments without separating sol from gel; thus, it is limited to the calculation of the overall average molecular weights (or chain lengths), and only up to the gel point. The overall second moment (and all subsequent moments) diverges at this point, and all calculations have to be stopped. The calculation of postgel properties is impossible without the use of additional and more complicated techniques (Tobita and Hamielec 1989). In contrast, as the equations of the presented model are integrated in time, one can follow the progression of the moments of all branched families included in the model, in both pre- and postgel regimes. The dynamic behavior of these moments generally gives a good indication of the evolution of branching and gelation. If the first moment is examined, it reflects the relative amounts of polymer formed in each population, thus resulting in an estimate of level of branching. As discussed before, gel formation requires the presence of a branching mechanism and a connection mechanism. The latter is the reaction between live polymer chains (termination by combination) that results in a net decrease in the number of polymer molecules in the system. Therefore, the amount of pseudogel formed can be continuously calculated as the difference between the overall polymer first moment and the sum of the first moments of all branched families. This difference is found to be numerically equal to zero up to the gel point, where it starts increasing, marking the sol/gel transition (Figure E-1).

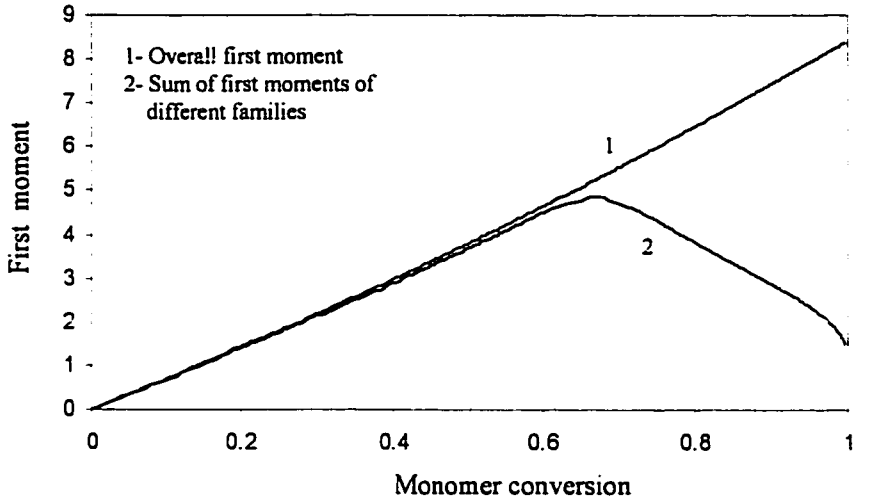

Figure E-1- Comparison of the overall first moment with the sum of the first moments of different branched families. (k_{tc} = 6.0E7, k_{td} = 0)

Figure E-2 illustrates the behavior of the first moment of the linear polymer and all branched families (up to 150 branch per chain).

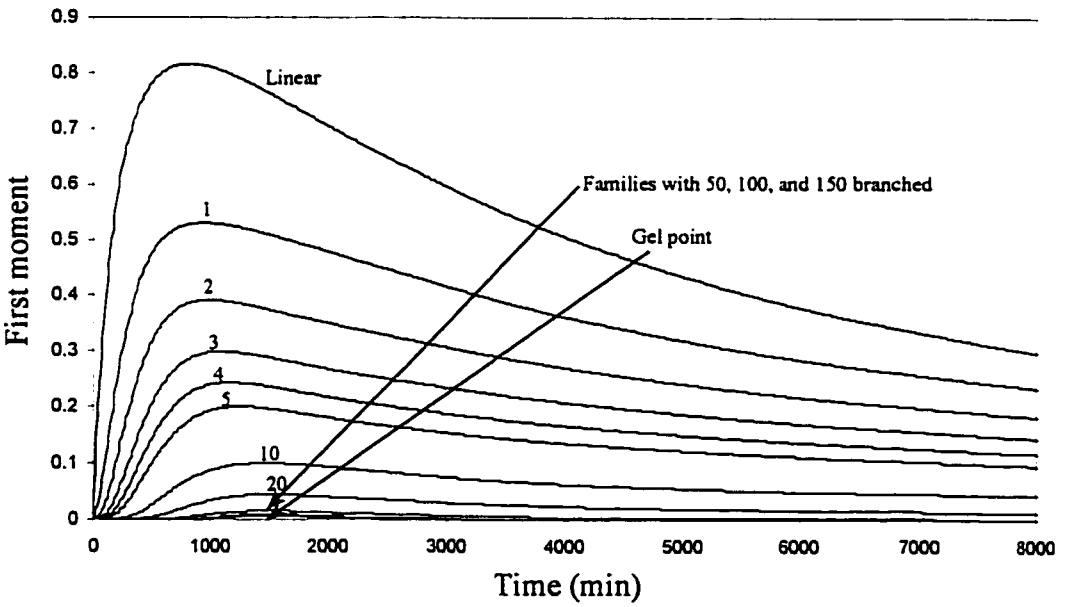

Figure E-2- Time evolution of the first moments of the linear and branched families of up to 150 branches. (k_{tc} = 6.0E7, k_{td} = 0)

It can be seen that the branched families start appearing one after the other and that each family does not start forming until enough polymer in the preceding family has been produced. This was expected, since it has already been postulated that each family is used to form the next higher family. It should also be noticed that the first moment of each family encloses the next higher (it forms before it and is consumed after it), which confirms the earlier statement about the transient nature of the higher families. It can be seen that these populations keep appearing and growing up to the gel point and then are consumed after it.

Figure E-3 presents the number- and weight-average chain lengths of the overall sol polymer versus monomer conversion. The overall sol chain length averages were calculated by summing the moments of all families and then by computing the ratio of the first to zeroth moment and the second to first moment (Equations 3-26 and 3-27).

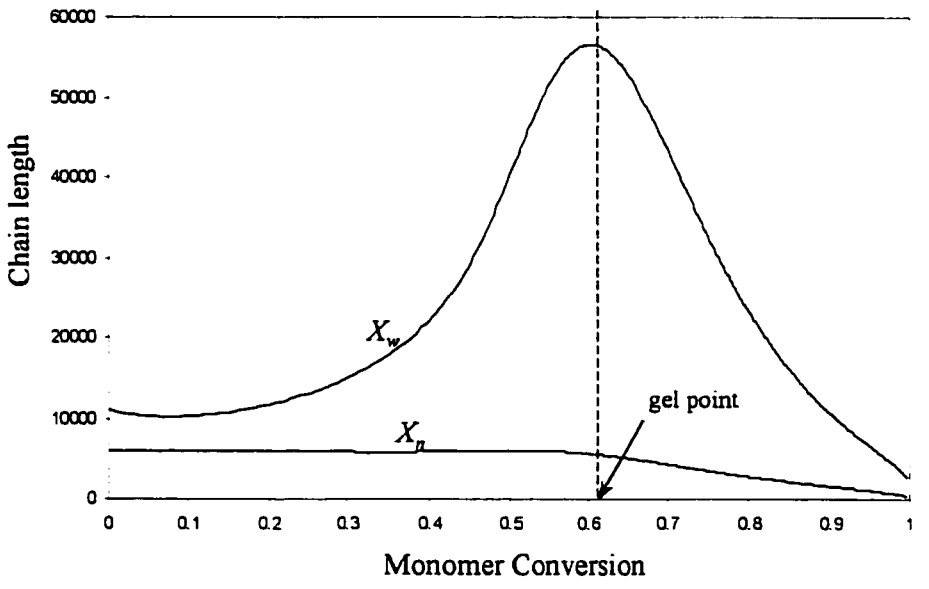

Figure E-3- Number average and weight average chain lengths of the sol polymer plotted versus monomer conversion. (k_{tc} = 6.0E7, k_{td} = 0)

The decrease in both average chain lengths after the gel point is a result of the disappearance of the higher branched families forming the high end of the MWD.

The effect of termination mechanism can also be investigated by this model. As concluded by Tobita and Hamielec (1989), live radical termination solely by disproportionation cannot result in gelation. This was verified by simulating the above mentioned system and considering that termination by combination does not occure (k_{tc} = 0). Figure E-4 illustrates the comparison between the overall first moment and the sum of first moments of all families (similar to Figure E-1) for the case that radical termination occurs only by disproportionation. As it is evident from this figure, there is no difference between the two curves, confirming that no gelation occurs in the absence of termination by combination.

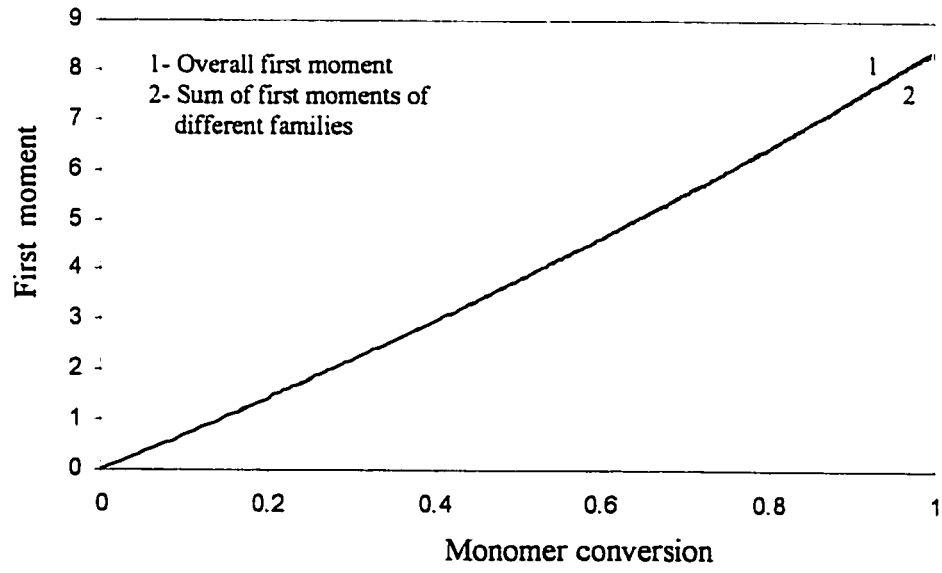

Figure E-4- Comparison of the overall first moment with the sum of the first moments of different branched families. (k_{tc} = 0, k_{td} = 6.0E7)

Figure E-5 illustrates how different families form in time, in the absence of termination by combination, by monitoring their first moments. As can be seen, unlike the previous case, the formation and disappearance of different families happens in a very wide time range and higher branched families may not even form. The comparison of this figure with Figure E-2, shows that although higher branched families form later when radical combination does not occur, they do not disappear quickly and have greater masses. This is due to the fact that in such system gelation does not occur, and therefore higher molecular weight chains are not consumed by the gel and taken away from the sol.

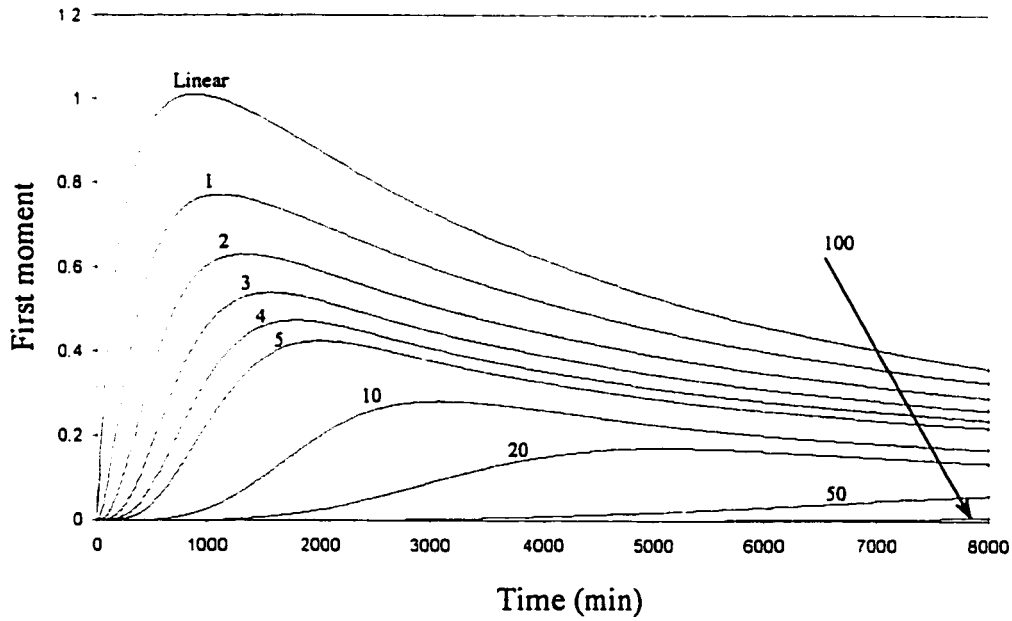

Figure E-5- Time evolution of the first moments of the linear and branched families. ($k_{tc} = 0$, $k_{td} = 6.0E7$)

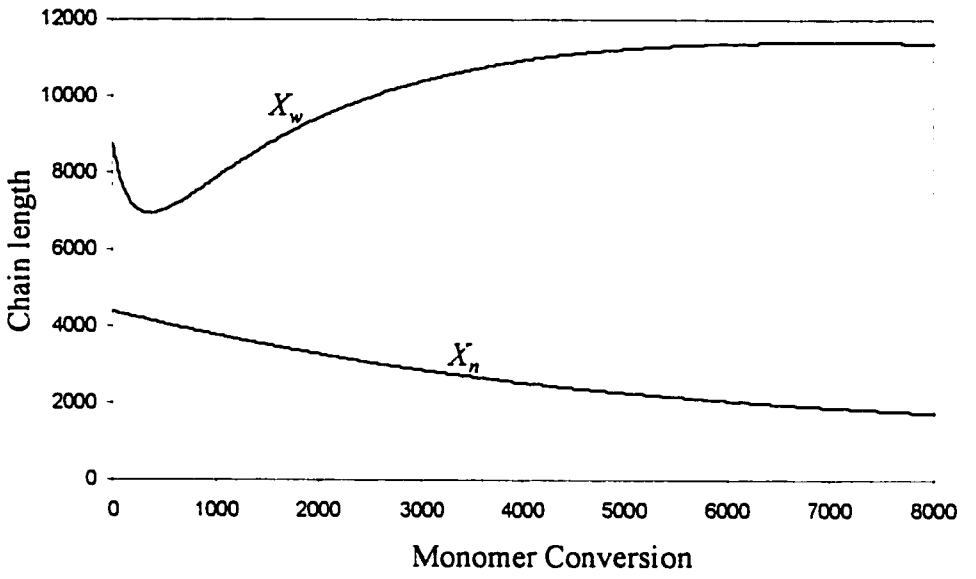

Figure E-6- Number average and weight average chain length of the sol polymer plotted versus monomer conversion. (k_{tc} = 0, k_{td} = 6.0E7)

As a consequence, the overall branching degree increases in time, resulting in a continuous increase in the weight average chain length and therefore increase in the polydispersity index. (Figure E-6)

The results presented in this appendix were to demonstrate some of the capabilities of the proposed modeling method, especially those not achieved by other methods. This method is also capable of reconstructing the sol MWD by assuming a known MWD, such as Schultz-Zimm distribution (Billingham 1989), for each branching family (Teymour and Campbell 1994). Additional effects can also be included in the model, such as dependence of rate constants on polymer structure (as reflected by the number of branches), multiple radicals on a single molecule, and diffusion limitations and

their effect on rate constants. These limitations are known to reduce the rate of termination to a larger extent than they would other reaction steps, which will greatly alter the characteristics of the sol/gel transition in any particular system.

Nomenclature

B_n	average number of LCB per polymer chain.
c	concentration of solute in solution.
C	total catalyst concentration
C_i	catalyst site type i.
C_L	linear catalyst.
C_{LCB}	LCB catalyst.
CTA	chain transfer agent.
$D^=$	macromonomer concentration.
$D^=_{m,r,i}$	dead polymer of chain length r containing i long chain branches and terminal unsaturation, ended with monomer m (m = 1 or 2).
DC	dead catalyst site (or inactive).
$D_{r,i}$	dead polymer of chain length r containing i long chain branches and a saturated chain-end.
F_i	cumulative copolymer composition of monomer i.
I	initiator concentration.
i	number of trifunctional branch points.
k	proportionality factor.
$k_{CTA,jq}$	transfer rate constant for a living chain made on catalyst site type j ended with monomer q.
k_d	initiator decomposition rate constant.
$k_{da,j}$	deactivation rate constant for catalyst site type j.

k_{fmi} transfer to monomer rate constant for site-type i.

k_i initiation reaction rate constant.

$k_{i,jq}$ initiation rate constant for catalyst site type j reacting with monomer q.

$k_{j,mq}$ propagation rate constant for incorporation of monomer q to a chain made on catalyst site type j ended with monomer m.

k_{LCB} long-chain branch formation rate constant.

$k_{LCB,jm}$ propagation rate constant for incorporation of macromonomers ended with monomer m to a living chain ended with monomer j.

k_p monomer propagation rate constant.

k_{pi} propagation rate constant for site-type i.

k_{tc} termination by combination rate constant

k_{trCTA} chain transfer to chain transfer agent rate constant.

k_{td} termination by disproportionation rate constant.

k_{tm} chain transfer to monomer rate constant

k_{tp} chain transfer to polymer rate constant.

$k_{\beta i}$ β-hydride elimination rate constant for site-type i.

$k_{\beta,jq}$ β-hydride elimination rate constant of a living chain made on catalyst site type j ended with monomer q.

M monomer concentration.

M_1, M_2 monomers 1 and 2.

M_l ethylene concentration in liquid phase.

M_n number-average molecular weight.

M_w	weight-average molecular weight.
n_i	number of LCBs per molecule for the chains having chain length of i.
P	CGC active sites concentration.
p	propagation probability.
$P(r,i)$	concentration of dead polymer chains of chain length r and having i trifunctional branch points).
$P_{r,1}$	living polymer of chain length r containing i long chain branches made on catalyst site type 1 ending with monomer 1.
Q	linear catalyst active sites concentration.
Q_r	linear living polymer of chain length r made on catalyst site type 2 ending with monomer 1.
r	chain length, mole fraction of CGC in catalyst mixture.
R_β	rate of β-hydride elimination reaction.
$R(r,i)$	concentration of live polymer chains with chain length r and having i trifunctional branch points.
R_{cf}	net rate of dead polymer chain formation.
R_{CTA}	rate of transfer reaction.
R_{da}	rate of deactivation reaction.
R_{LCB}	rate of macromonomer propagation.
RT	mean residence time in the reactor.
s	reciprocal of the mean residence time in the reactor.
$S_{r,1}$	living polymer of chain length r containing i long chain branches made on catalyst site type 1 ending with monomer 2.

t	time.
T_c	crystallization tempreature.
T_r	linear living polymer of chain length r made on catalyst site type 2 ending with monomer 2.
T_s^0	crystallization temperature when the critical nucleus size goes to infinity.
V	retention volume.
w_i	weight fraction of chains having chain lengths i.
X_n	number-average chain length.
X_w	weight-average chain length.
Δf_u	free energy of fusion.
ΔH_u	enthalpy of fusion.

Greek letters

γ_j	jth moment of living polymer chains made on the linear catalyst, ended with monomer 1.
τ_j	jth moment of living polymer chains made on the linear catalyst, ended with monomer 2.
σ_j	jth moment of the dead polymers with terminal double-bond ended with monomer 2.
ψ_j	jth moment of the living polymer chains made on the LCB catalyst ended with monomer 2.
$[\eta]$	intrinsic viscosity.
β	semi-empirical intercept.

η_j *j*th moment of the living polymer chains made on the LCB catalyst ended with monomer 1.

λ_j *j*th moment of the dead polymers with terminal double-bond ended with monomer 1.

λ_n instantaneous number of branches per 1000 carbon atoms.

μ_j *j*th moment of the dead polymers with saturated chain-end.

ζ crystallite size.

ζ^* critical size of the nucleus in the chain direction.

Abbreviations

^{13}C-NMR carbon-13 nuclear magnetic resonance.

^{1}H-NMR proton nuclear magnetic resonance.

CCD copolymer composition distribution.

CGC constrained geometry catalyst.

CGC-Ti titanium-based constrained geometry catalyst.

CRYSTAF crystallization analysis fractionation.

CTA chain transfer agent.

GPC gel permeation chromatography.

HDPE high-density polyethylene.

LCB long-chain branching.

LDPE low-density polyethylene.

LES longest ethylene sequence.

LLDPE linear low-density polyethylene.

MAO	methylaluminoxane.
MW	molecular weight.
PDI	polydispersity index.
PE	polyethylene.
SCBD	short-chain branching distribution.
SEC	size exclusion chromatography.
TCB	1,2,4-trichlorobenzene.
TIBA	tri(isobutyl)aluminum.
TMA	trimethylaluminum.
TMS	tetramethylsilane.
TPFB	tris(pentafluorophenyl)borane.
TREF	temperature rising elution fractionation.

References

Beigzadeh D., J. Soares, T.A. Duever, **Combined Metallocene Catalysts: an efficient technique to manipulate long-chain branching frequency of polyethylene**, *Macromol. Rapid Commun.*, **v.20**, n.10, p.541, 1999

Beigzadeh D., J. Soares, T.A. Duever. **Modeling of fractionation in CRYSTAF using Monte Carlo simulation of crystallizable sequence lengths: ethylene/1-octene copolymers synthesized with single-site-type catalysts,** *J. Appl. Polym. Sci.*, in print (2000).

Beigzadeh D., J.B.P. Soares, A.E. Hamielec, **Recipes for synthesizing polyolefins with tailor-made molecular weight, polydispersity index, long-chain branching frequencies, and chemical composition using combined metallocene catalyst systems in a CSTR at steady-state**, *J. Appl. Polym. Sci.*, **v.71**, p.1753, 1999a.

Beigzadeh D., J.B.P. Soares, A.E. Hamielec, **Study of long-chain branching in ethylene polymerization**, *Polym. React. Eng. J.*, **v.5**, n.3, p.141, 1997.

Beigzadeh D., J.B.P. Soares, T.A. Duever, **Analysis of branching structure in polyethylene resins synthesized with constrained geometry catalyst systems, using Monte Carlo simulation**, *Polym. React. Eng. J.*, **v.7**, n.2, 1999b.

Billingham N.C., **Molecular weight distributions**, *Comp. Polym. Sci.*, **v.3**, Sir Geoffrey Allen, Frs, Ed., Pergamon Press, Oxford, 1989.

Box E.P., W.G. Hunter, J.S. Hunter, *Statistics for Experimenters*, John Wiley & Sons, New York, 1978

Brant, P., J.A.M. Canich, **Ethylene/longer α-olefin copolymers,** U.S.Patent 5,475,075, 1995.

Brant, P., J.A.M. Canich, N.A. Merrill, **Ethylene/branched olefin copolymers.** U.S.Patent 5,444,145, 1995.

Britto L.J.D., J.B.P. Soares, A. Penlidis, B. Monrabal, **Pololefin analysis by single-step crystallization fractionation,** *J. Polym. Sci., Part B: polym. Phys.*, **v.37**, p.539, 1999.

Carman C.J., C.E. Wilkes, **Monomer sequence distribution in ethylene propylene elastomers. I. Measurement by carbon-13 nuclear magnetic resonance spectroscopy,** *Rubber Chem. Tech.*; **v.44**, p781, 1971.

Chum, P.S., C.I. Kao, G.W. Knight, **Structure/property relationships in polyolefins made by constrained geometry catalyst technology**. *Plastic Eng.*, **v.51**, n.6, p.21, 1995.

De Pooter M., P.B. Smith, K.K. Dohrer, K.F. Bennett, M.D. Meadows, C.G. Smith, H.P. Schouwenaars, R.A. Geerards, **Determination of the composition of common linear low density polyethylene copolymers by ^{13}C-NMR spectroscopy,** *J. Appl. Polym. Sci.*, **v.42**, p.399, 1991.

Elicabe G., C. Cordon, J. Carella, **Modeling the fractionation process in TREF systems. II. Numerical Analysis,** *J. Polym. Sci., Part B: Polym. Phys.*, **v.34**, p.527, 1996a.

Elicabe G., C. Cordon, J. Carella, **Modeling the fractionation process in TREF systems. III. Model validation with low molecular weight homopolymers,** *J. Polym. Sci., Part B: Polym. Phys.*, **v.34**, p.1147, 1996b.

Forlini F., Z. Fan, **Metallocene-catalyzed propene/1-hexene copolymerization: influence of amount and bulkiness of cocatalyst and of solvent polarity**, *Macromol. Chem. Phys.*, **v.198**, p.2397, 1997.

Gerald, C.F., *Applied Numerical Analysis*, 5th edition. Addison-Welsley Pub.Co, 1994.

Glockner G, **Polymer Characterization by Liquid Chromatography**, *Journal of Chromatography Library*, **v. 34**, Elsevier, Amsterdam 1987

Grubisic Z., Remmp P., Benoit H., **A universal calibration for gel permeation chromatography**, *J. Polym. Sci., Part B*, **v.5**, p.753, 1967.

Gupta S.K., A. Kumar, *Reaction Engineering of Step Growth Polymerization*, Plenum Press, New York, 1987.

Hamielec, A.E., J.F. MacGregor and A. Penlidis. **Multicomponent free-radical polymerization in batch, semi-batch and continuous reactors**. *Makromol. Chem., Macromol. Symp.*, **v.10/11**, p.521, 1987.

Hansen E.W., R. Blom, O.M. Bade, **NMR characterization of polyethylene with emphasis on internal consistency of peak intensities and estimation of uncertainties in derived branch distribution numbers**, *Polymer*, **v.38**, n.17, p.4295, 1977.

Holland V.F., P.H. Lindenmeyer, **Morphology and crystal growth rate of polyethylene crystalline complexes**, *J. Polym. Sci.*, **v.57**, p.589, 1962.

Huang J., G.L. Rempel, **Ziegler-Natta catalysts for olefin polymerization: mechanistic insights from metallocene systems**, *Prog. Polym. Sci.*, **v.20**, p.459, 1995.

Hulbert H.M., Katz S., **Some problems in particle technology; A statistical mechanical formulation,** *Chem. Eng. Sci.*, **v.19**, p.555, 1964.
J. McMurry; *Organic Chemistry*; Brooks/Cole Publishing Co.; 3rd Ed., 1992.

Jackson J.F., Mandelkern L., **Solubility of crystalline polymers. II. Polyethylene fractions crystallized from dilute solutions,** *Macromolecules*, **v.1**, n.6, 1968.

Jin C., Q. Guo, **A new method for rapid evaluation of long-chain branching in polymers,** *J. Appl. Polym. Sci.*, **v.41**, p.2383, 1990.

Kawai T., A. Keller, *Phil. Mag.*, **v.11**, p.1165, 1965.

Keller A., A. O'Connor, **A study on the relation between chain folding and chain length in polyethylene,** *Polymer*, **v.1**, p.163, 1960.

Khadir A., M. Gauthier (a), **Highly branched (arborescent) polymers as melt processing additives**. *Annu. Tech. Conf. -- Soc. Plast. Eng.*, **v.55**, p.3732, 1997.

Khadir A., M. Gauthier (b), **Arborescent polymers as rheological modifiers for linear polymers**. *Polym. Mater. Sci. Eng.*, **v.77**, p.174, 1997.

Kim J.D, J.B.P. Soares, G.L. Rempel, **Synthesis of tailor-made polyethylene through the control of polymerization conditions using selectively combined metallocene catalysts in a supported system,** *J. Polym. Sci.,: Part A, Polym. Chem.*, **v.37**, p.331, 1999.

Kim J.D, J.B.P. Soares, G.L. Rempel, **Use of hydrogen for the tailoring of the molecular weight distribution of polyethylene in bimetallic supported metallocene catalyst system,** *Macromol Rapid Commun.*, **v.19**, p.197, 1998.

Kim, Y.H., **Hyperbranched Polymers 10 years After**. *J. Polym. Sci.: Part A: Polymer Chemistry*, **v.36**, p.1685, 1998.

Kimura K., S. Yuasa, Y. Maru, **Carbon-13 nuclear magnetic resonance study of ethylene-1-octene and ethylene-4-methyle-1-pentene copolymers**, *Polymer*, **v. 25**, p.441, 1984.

Knight, G.W., S. Lai, **New rules for ethylene α-olefins interpolymers - unique structure and property relationships.** In "Polyolefins VIII", Technical Paper, Reg. Tech. Conf. - Soc. Plast. Eng., 28-40, 1993.

Kroshwitz J.I., *Polymers: Polymer Characterization and Analysis*, John Wiley and Sons, New York 1990.

Lai, S.Y., J.R. Wilson, G.W. Knight, J.C. Stevens, P.W.S. Chum. **Elastic substantially linear olefin polymers,** U.S.Patent 5,272,236, 1993.

Lai, S.Y., J.R. Wilson, G.W. Knight, J.C. Stevens. **Elastic substantially linear olefin polymers**. U.S. Patent 5,665,800, 1997.

Lecacheux D., J. Lesec, and C. Quivoron, **High-temperature coupling of high-speed GPC with continuous viscometry. I. Long-chain branching in polyethylene**. *J. Appl. Polym. Sci.*, **v.27**, p.4867, 1982.

Lindeman L.P., J.Q. Adams, **Carbon-13 nuclear magnetic resonance spectroscopy**, *Analytical Chemistry*, **v.43**, n.10, p.1245, 1971.

Liu W., D.G. Ray III, P.L. Rinaldi, **Resolution of signals from long-chain branching in polyehtylene by ^{13} NMR at 188.6 MHz,** *Macromolecules*, **v.32**, p.3817, 1999.

Lovell P.A., *Comprehensive Polymer Science*, (Ed. G. Allen), Pergamon Press, Oxford, **v. 1**, ch. 9, 1989.

Malmberg A., E. Kokko, P. Lehmus, B. Lofgren, J.V. Seppala, **Long-chain branched polyethene polymerized by metallocene catalysts Et[Ind]$_2$ZrCl$_2$/MAO and Et[IndH$_4$]$_2$ZrCl$_2$/MAO**, *Macromolecules*, **v.31**, p.8448, 1998.

Mandelkern L., **Thermodynamic and physical properties of polymer crystals formed from dilute solution**, *Progress in Polymer Science*, **v.2**, p.165, 1970.

Meira G.R.; *Modern Methods of Polymer Characterization*; chapter 2; John Wiley and Sons, New York, 1991.

Michiels W., A.M. Escalona, **Mixed cocatalyst systems in metallocene ethylene polymerization**, *Mocromol. Symp.*, **v.97**, p.171, 1995.

Mirabella F.M., L. Wild, **Determination of long-chain branching distribution of polyethylenes**, *Advances in Chemistry Series No. 227, Polymer characterization: Physical Property, Spectroscopic, and Chromatographic Methods*. American Chemical Society, 1990.

Mirabella, F.M., Proceedings of international GPC symposium 87, Itasca, IL, p.180, May 1987.

Mitchell J., *Applied Polymer Analysis and Characterization*, Hanser Publisher, Munich 1987.

Monrabal B., CRYSTAF: **Crystallization analysis fractionation. A new approach to the composition analysis of semicrystalline polymers**, *Macromol. Symp.*, **v.110**, p.81, 1996.

Monrabal B., **Crystallization analysis fractionation: A new technique for the analysis of branching distribution in polyolefins,** *J. Appl. Polym. Sci.*, **v.52**, p.491, 1994.

Monrabal B., J. Blanco, J. Nieto, J.B.P. Soares, **Characterization of homogeneous ethylene/1-octene copolymers made with a single-site catalyst. CRYSTAF analysis and calibration,** *J. Polym. Sci., Part A: Polym. Chem.*, **v.37**, p.89, 1999.

Morrison R.T., R.N. Boyd; *Organic Chemistry*; Allyn and Bacon Inc.; 4th Ed., 1983.

Nakijama A., S. Hayashi, T. Korenaya, T. Sumida, **Effect of solvent on single crystal formation from dilute polyethylene solution,** *Kolloid-Z*, **v.222**, p.124, 1968.

Olabisi O., Atiqullah M., W. Kaminsky, **Group 4 metallocene: supported and unsupported,** *J. M. S.- Rev. Macromol. Chem. Phys.*, **C37(3)**, p.519, 1997.

Price F.P., **Markoff chain model for growth of polymer single crystals,** *J. Chem. Phys.*, **v.35**, n.5, 1961.

Ram A., and Miltz J., **New method for MWD determination in branched polymers,** *J. Appl. Polym. Sci.*, **v.15**, p. 2639, 1971.

Randall J.C., **A review of high resolution liquid ^{13}C nuclear magnetic resonance of ethylene-based polymers,** *J. Macromol. Sci., Rev. Macromol. Chem. Phys.*; **C29 (2&3)**, p201, 1989.

Randall J.C., **Carbon-13 NMR of ethylene-1-olefin copolymers: Extension to the short-chain branch distribution in a low-density polyethylene,** *J. Polym. Sci.,, Polym. Phys. Ed.*; **v.11**, p.275, 1973.

Randall J.C., *Polymer Sequence Determination, Carbon-13 NMR Method*; Academic Press; 1977.

Reddy S.S., S. Sivaram, **Homogeneous metallocene-methylaluminoxane catalyst systems for ethylene polymerization**, *Prog. Polym. Sci.*, **v.20**, p.309, 1995.

Saidel G.M., Katz S., *J. Polym. Sci., Polym. Phys. Ed.*, **v.6**, p.1149, 1968.

Seo Y., K.U. Kim, **A new model for rapid evaluation of the degree of long-chain branching in polymers**, *Polymer*, **v.35**, n.19, p.4163, 1994.

Shiono T., Y. Moroki, T. Ikeda, **Copolymerization of poly(propylene) macromonomer with ethylene by (tert-butanamide)dimethyl(tetramethyle-η^5-cyclopentadienyl)silanetitanium dichloride/methylaluminoxane catalyst**, *Macromol. Chem. Phys.*, **v.198**, p.3229, 1997.

Shiono, T., Y. Moriki and K. Soga. **Copolymerization of poly(propylene) macromonomer and ethylene with metallocene catalysts**. *Macromol. Symp.*, **v.97**, p.161, 1995.

Silverstein R.M., G.C. Bassler, T.C. Morrill, *Spectrometric Identification of Organic Compounds*, John Wiley & Sons, New York, 1991.

Small P.A., **Long-chain branching in polymers**, *Adv. Polym. Sci.*, **v.18**, p.1, 1975.

Smith J.M., H.C. Van Ness, *Introduction to Chemical Engineering Thermodynamics*, McGraw-Hill Book Company, New York, 1975.

Soares J.B.P., A.E. Hamielec, **Temperature rising elution fractionation of linear polyolefins**, *Polymer*, **v.36**, n.8, 1995.

Soares J.B.P., A.E. Hamielec, **Temperature rising elution fractionation,** *Modern Techniques for Polymer Caracterization*, edited by: R.A. Pethrick and J.V. Dawkins, John Wiley & Sons, 1999.

Soares J.B.P., B. Monrabal, J. Nieto, J. Blanco, **Crystallization analysis fractionation (CRYSTAF) of poly(ethylene-co-1-octene) made with single-site-type catalysts: A mathematical model for the dependence of composition distribution on molecular weight,** *Macromol. Chem. Phys.*, **v.199**, p.1917, 1998.

Soares, J.B.P., A.E. Hamielec, **Bivariate chain length and long chain branching distribution for copolymerization of olefins and polyolefin chains containing terminal double-bonds,** *Macromol. Theory Simul.*, **v.5**, p.547, 1996.

Soares, J.B.P., A.E. Hamielec, **The chemical composition component of the distribution of chain length and long chain branching for copolymerization of olefins and polyolefin chains containing terminal double-bonds,** *Macromol. Theory Simul.*, v.6, p.591, 1997.

Soares, J.B.P., J.D. Kim, G.R. Rempel, **Analysis and control of the molecular weight and chemical composition distribution of polyolefins made with metallocene and Ziegler-Natta catalysts,** *Industrial & Engineering Chemistry Research*, **v.36**, n.4, p.1144, 1997.

Soga K., M. Kamanika, **Copolymerization of olefins with SiO_2-, Al_2O_3-, and $MgCl_2$-supported metallocene catalysts activated by trialkylaluminums,** *Macromol. Chem. Phys.*, **v.195**, p.1369, 1994.

Soga K., T. Uozumi, S. Nakamura, T. Toneri, **Structure of polyethylene and copolymers of ethylene with 1-octene and oligoethylene produced with Cp_2ZrCl_2 and $[(C_5Me_4)SiMe_2N(t\text{-}Bu)]TiCl_2$ catalysts**, *Macromol. Chem. Phys.*, **v.197**, p.4237, 1996.

Stockmayer W.H., **Distribution of chain length and compositions in copolymers**, *J. Chem. Phys.*, **v.13**, n.6, 1945.

Sugawara, M., **Branching structure and performances of metallocene-based copolymers**. Proceedings of the 4th International Business Forum on Specialty Polyolefins, Houston, Texas, U.S.A., p.37, 1994.

Swogger, K.W. and C.I. Kao, **Process technology for unique polymer design using Dow Constrained Geometry Catalyst**. In "Polyolefins VIII", Technical Paper, Reg. Tech. Conf. - Soc. Plast. Eng., p.13-20, 1993.

Swogger, K.W. and C.I.Kao (1993). **Process technology for unique polymer design using Dow Constrained Geometry Catalyst**. In "Polyolefins VIII", Technical Paper, Reg. Tech. Conf. - Soc. Plast. Eng., p.13, 1993.

Tager A. *Physical Chemistry of Polymers*, Mir Publisher, Moscow, 1978.

Teymour F., J.D. Campbell, **Analysis of the dynamics of gelation in polymerization reactors using the "Numerixal Fractionation" technique**, *Macromolecules*, **v.27**, p.2460, 1994.

Tobita H., A.E. Hamielec, **Modeling of network formation in free radical polymerization**, *Macromolecules*, **v.22**, p.3098, 1989.

Van Krevelen D.W.; *Properties of Polymers*; 3rd ed., Elsevier Science, Amsterdam, 1990.

Wang W.J., Dajing Yan, S. Zhu, A.E. Hamielec, **Long-chain branching in ethylene polymerization using binary homogeneous metallocene catalyst system**, *Polym. React. Eng. J.*, **v.7**, n.3, p.327, 1999b.

Wang W.J., E. Kolodka, S. Zhu, A.E. Hamielec, **Continuous solution copolymerization of ethylene and 1-octene with constrained geometry metallocene catalyst**, *J. Polym. Sci., Part A: Polym. Chem.*, **v.37**, p.2949, 1999a.

Zhu S., D. Li, **Molecular weight distribution of metallocene polymerization with long chain branching using a binary catalyst system**, *Macromol. Theory Simul.*, **v.6**, p.793, 1997.

Zimm B.H., R.W. Kilb, **Dynamics of branched polymer molecules in dilute solution**, *J. Polym. Sci.*, **v.37**, p.19, 1959.

Zimm B.H., W.H. Stockmayer, **The dimensions of chain molecules containing branches and rings**, *J. Chem. Phys.*; **v.17**, p.1301, 1949.